The Electronic Spectrum of Selenium Dioxide

A thesis submitted for the degree of Doctor of Philosophy at the University of Oxford

Sarah Anne Crowther

Corpus Christi College

Hilary Term 2003

Abstract

The Electronic Spectrum of Selenium Dioxide

A thesis submitted for the degree of Doctor of Philosophy at the University of Oxford.

Sarah Anne Crowther, Corpus Christi College, Hilary Term 2003.

The $\tilde{\mathrm{C}}^1B_2 \leftarrow \tilde{\mathrm{X}}^1A_1$ electronic transition of SeO_2 has been investigated under high resolution, at a rotational temperature of around 10 K, using the technique of Laser Excitation Spectroscopy. The vibrationally-resolved survey spectrum contained around 100 new bands in addition to the bands which had been reported in a previous study of the same region (G.W. King and P.R. McLean, *J. Mol. Spec.* **51**, 1974). In the light of this new spectrum a number of bands have been reassigned, most significantly the 0_0^0 band, and a number of progressions have been extended. This led to a revised determination of the vibrational constants of the excited state, and a more acceptable estimate of ν_3' than was suggested in the previous work. These reassignments and extensions of existing assignments accounted for only a small fraction of the newly observed bands; those remaining are thought to be due to a different electronic transition which lies in the same region as the $\tilde{\mathrm{C}}^1B_2 \leftarrow \tilde{\mathrm{X}}^1A_1$ transition. The 1_0^3, 1_0^2 and 1_0^1 bands of the $\tilde{\mathrm{C}}^1B_2 \leftarrow \tilde{\mathrm{X}}^1A_1$ transition were also recorded at rotational resolution and analysed using the method of ground state combination differences. The 1_0^3 band was found to be perturbed, which was one of the major factors which prompted the survey study described above. From the analysis of these bands the rotational constants of the excited state were determined and hence the geometry of the SeO_2 molecule in the given vibrational levels of the $^1B_2$ excited state was calculated. This in turn enabled the rotational constants and the geometry of the (000) vibrational level of the excited state to be estimated. This work confirms that the symmetry of the excited state is $^1B_2$ and the transition studied is $\tilde{\mathrm{C}}^1B_2 \leftarrow \tilde{\mathrm{X}}^1A_1$. An additional band around 31957 cm^{-1} was also recorded at rotational resolution, which was initially though to be the 0_0^0 band, on the basis of King and McLean's assignments. However in the light of the reassignments the nature of this band is not known, and attempts to assign it as a vibrationally cold band of the $\tilde{\mathrm{C}}^1B_2 \leftarrow \tilde{\mathrm{X}}^1A_1$ transition were unsuccessful, implying that it is probably either a hot band of the $\tilde{\mathrm{C}}^1B_2 \leftarrow \tilde{\mathrm{X}}^1A_1$ transition or a band belonging to different electronic transition.

Acknowledgements

Firstly, I would like to thank my supervisor, Prof. John Brown for all his help and encouragement over the past four years. It has been a pleasure to work with him and be a member of his research group. I would also like to thank Prof. Ian Beattie for his help and advice at various points.

This work has been made possible by the numerous technical and support staff of the PTCL. In particular, I would like to thank Paul Mitchell from lab services for his good humour and all his excellent work, especially his lab moving skills and ability to shout at builders!

I am also grateful to the EPSRC for financial support, and to Corpus Christi College for providing funds for me to attend various conferences.

I have been lucky to work with many friendly and talented people. The various members of the group, both past and present, have made the past four years very enjoyable, as well as providing a useful source of knowledge. These members of the group include Christian Hill, Catherine Wilson, Stephen Kermode, Philip Hodges, Sara Beaton, and the numerous Part II's, in particular Anup Mistry, whose hard work on parts of the spectrum of SeO_2 for his Part II project proved to be particularly useful. Other Part II's include Helen Cooke, Lynsey Serrage, Clare Nash, Amy Pilkington, Alex McIntosh, Tom Gray and Gavin Little. Many other members of the department have also provided much helpful advice, and in the case of Dave and Pat much entertainment as well.

I would also like to thank all my friends outside of the department for the fun we've had over the years.

Finally I would like to thank all my family, especially my parents, for their love and support.

Contents

Chapter 1

Introduction

Selenium dioxide, SeO_2, is a small, closed shell molecule. Selenium is in group 16 of the periodic table, so SeO_2 is isoelectronic with O_3, SO_2 and TeO_2. At room temperature SeO_2 is a pale pink solid, and it sublimes at about 350 °C. The physical properties of the group 16 dioxides change regularly down the group, as would be expected. O_3 and SO_2 are gases at room temperature, but TeO_2, which is heavier than SeO_2, is a solid. These physical properties are summarised in Table 1.1.

Table 1.1: Physical properties of the group 16 dioxides.

Molecule	Melting point / °C	Boiling point / °C
O_3	- 192.7	- 111.9
SO_2	- 72.7	- 10
SeO_2	Sublimes $\sim$ 350	
TeO_2	733	1245

SeO_2 is an asymmetric top molecule with C_{2v} symmetry. This makes the rotational spectrum very complicated. There are a large number of allowed transitions, but since the two oxygen atoms are identical, nuclear spin statistics have the effect of removing half the possible energy levels which helps to simplify the spectrum, as will be explained later.

This work describes the recording and analysis of part of the electronic spectrum of SeO_2 in the gas phase. The electronic spectra of polyatomic molecules provide us with a very useful source of information about the electronically excited states of the molecules.

Whereas the ground states of such molecules can be studied by various methods (microwave, infrared and Raman spectroscopy, and electron and X-ray diffraction), electronic spectroscopy is the only method suitable for looking at the excited states. To obtain values for the bond angles and bond lengths of these molecules in their excited states it is necessary to look at the rotational structure of the electronic bands. The spectra observed can be very complex, and hence such analysis is usually limited to small polyatomic molecules. With only three atoms, SeO_2 is sufficiently small that it should be possible to resolve and understand the rotational structure of the electronic transitions.

1.1 Motivation for this Work

The main reason for studying SeO_2 was to assist in the study of TeO_2. Although the electronic spectrum of rotationally cold TeO_2 has been recorded at high resolution [1, 2], it was only possible to analyse the vibrational structure of the spectrum. A successful analysis of the rotational structure has not yet been achieved. Similar to SeO_2, TeO_2 is a closed shell molecule with C_{2v} symmetry. However there are eight isotopes of Te, many of which have a significant natural abundance, as shown in Table 1.2. This large number of isotopes

Table 1.2: Te isotopes and their natural abundances.

Isotope	Atomic Mass (u)	Natural Abundance (%)
^{120}Te	119.9040	0.096
^{122}Te	121.9031	2.60
^{123}Te	122.9043	0.908
^{124}Te	123.9028	4.816
^{125}Te	124.9044	7.14
^{126}Te	125.9033	18.95
^{128}Te	127.9045	31.69
^{130}Te	129.9063	33.80

greatly complicates the spectrum of a naturally occurring sample of TeO_2. In particular, the approximate 2:3:3 ratio for ^{126}Te:^{128}Te:^{130}Te leads to a large number of strong lines in the spectrum. Very little previous work had been done on TeO_2, more specifically the

microwave spectrum has not been charactersied, so the ground state rotational constants are not known. This made attempts to analyse the electronic spectrum almost impossible.

In contrast, the microwave spectrum of SeO_2 has been well characterised (see Section 1.2.1), which significantly helped in the analysis of the electronic spectrum of SeO_2. There are also fewer isotopes of Se, as shown in Table 1.3, and only ^{78}Se and ^{80}Se have significant abundances, with an approximate ratio of 1:2. By studying the same electronic transition of SeO_2 as was investigated for TeO_2, it is hoped that the analysis of SeO_2 can be extrapolated to TeO_2, and so assist in the analysis of the recorded bands of TeO_2.

Table 1.3: Se isotopes and their natural abundances.

Isotope	Atomic Mass (u)	Natural Abundance (%)
^{74}Se	73.9225	0.9
^{76}Se	75.9192	9.0
^{77}Se	76.9199	7.6
^{78}Se	77.9173	23.6
^{80}Se	79.9165	49.7
^{82}Se	81.9167	9.2

The initial motivation to study TeO_2 came from the importance of the molecule in the technology of nuclear reactors. ^{131}Te and ^{132}Te are by-products of the fission process that occurs in nuclear reactors. They then continue the fission process by decaying to iodine atoms, by the emission of β particles. For ^{131}Te the fission process is as follows:

$$^{131}\mathrm{In} \xrightarrow{t_{1/2}=29\mathrm{secs}} {}^{131}\mathrm{Sn} \xrightarrow{t_{1/2}=63\mathrm{secs}} {}^{131}\mathrm{Sb} \xrightarrow{t_{1/2}=23\mathrm{mins}} {}^{131}\mathrm{Te} \xrightarrow{t_{1/2}=25\mathrm{mins}} {}^{131}\mathrm{I} \qquad (1.1)$$

A similar process occurs for the ^{132}Te isotope. At the high temperatures and pressures present in a nuclear reactor Te atoms will be in the gas phase (b.p. 989.8 °C). In the event of an accident, with the fission reaction running out of control, the gaseous Te would be likely to react with any oxygen and water present, so it is necessary to be able to simulate the transport mechanisms of such radioactive isotopes into the atmosphere. Characterising the products of the reaction between Te and water at high temperatures can help with this simulation. Studying the electronic spectrum of TeO_2 is a starting point for characterising

the products of the reactions between Te or TeO_2 and water at high temperatures:

$$\begin{aligned} &Te + H_2O \\ &TeO_2 \ + H_2O. \end{aligned}$$

The study of SeO_2 also provides an interesting comparison with O_3 and SO_2, both of which are important atmospheric molecules. The electronic and microwave spectra of these two molecules have both been well characterised in other works [3, 4, 5, 6].

1.2 Previous Work on the Spectrum of SeO_2

1.2.1 The Microwave Spectrum

The microwave spectrum of SeO_2 was first observed by Takeo *et al.* in 1970 [7]. They recorded around 90 transitions in the 8 - 36 GHz region, for the five most abundant isotopomers of SeO_2 in the ground state and in the first excited states of all three normal vibrations for $^{80}SeO_2$ and $^{78}SeO_2$. The transitions observed obeyed the *B*-type selection rules (see Section 3.5), which is consistent with the molecule being of C_{2v} symmetry and the 2-fold top axis coinciding with the *b*-axis of the molecule. Analysis of the data allowed them to calculate all three rotational constants (A, B and C) for the ground vibrational state and the first excited state of each vibration, for both $^{80}SeO_2$ and $^{78}SeO_2$. The centrifugal distortion constants were also determined for the ground state of $^{80}SeO_2$, and values for $^{78}SeO_2$ were then calculated from the $^{80}SeO_2$ values. These constants for the ground state are given in Table 1.4, for both $^{80}SeO_2$ and $^{78}SeO_2$. From this data Takeo determined that the equilibrium structure of SeO_2 has a Se−O bond length of 160.76 ± 0.06 pm, and an O−Se−O bond angle of 113.833 ± 0.083 °.

Further work on the microwave spectrum of SeO_2 was published by Takeo *et al.* in 1972 [8]. They recalculated the third-order potential constants of SeO_2 using vibrational frequencies reported from matrix-isolation studies of SeO_2. In their previous paper, Takeo *et al.* calculated the potential function of SeO_2 in the gas phase using the vibration-rotation interaction constants obtained from microwave spectroscopy. To perform this calculation it was necessary to use all the normal vibrational frequencies of the molecule. The bending

Table 1.4: Rotational constants for the ground vibrational state for $^{80}SeO_2$ and $^{78}SeO_2$, as calculated by Takeo *et al.* [7].

Rotational Parameter	$^{78}SeO_2$ / MHz	$^{80}SeO_2$ / MHz
A	29037.7 ± 0.27[a]	28825.2 ± 0.27
B	8676.52 ± 0.09	8676.56 ± 0.09
C	6663.11 ± 0.06	6651.89 ± 0.06
τ_{aaaa}	-2.22[b]	-2.19 ± 0.03
τ_{bbbb}	-0.043[b]	-0.043 ± 0.006
τ_{aabb}	0.22[b]	0.22 ± 0.017
τ_{abab}	-0.03[b]	-0.03 ± 0.011

[a] Three times the standard deviation.
[b] Calculated from the $^{80}SeO_2$ values.

vibration, ν_2, had not been measured by infrared spectroscopy and so was estimated. In addition, the symmetric stretching vibration, ν_1, was heavily overlapped by the stronger absorption of the asymmetric stretching vibration, ν_3. Therefore when Cesaro *et al.* [9] recorded a spectrum of $^{80}Se^{16}O_2$ isolated in an argon matrix, Takeo considered it to be worthwhile to recalculate the third order potential. The values for the two calculations are given in Table 1.5. Takeo also made a more accurate measurement of the dipole moment. The dipole moment was calculated from the Stark shifts of several spectral lines, the average value being 2.62 ± 0.05 D.

Table 1.5: Third order potentials for SeO_2, as calculated by Takeo *et al.* [8].

Vibrational parameter	Takeo's first study / cm^{-1}	Recalculation / cm^{-1}
ω_1	910	922.0
ω_2	362	372.5
ω_3	967	965.6

No further work was done on the microwave spectrum of SeO_2 until 1997, when Alekseev *et al.* [10] recorded about 650 transitions in the 70 - 650 GHz region. They recorded transitions in the ground state for all six isotopomers of SeO_2, transitions in the first excited state of the bending vibration ($v_2 = 1$) for the five most abundant isotopomers, and

transitions in the second excited state of the bending vibration ($v_2 = 2$) for $^{80}SeO_2$. Using the A-reduced form of Watson's Hamiltonian [11], Alekseev was able to derive rotational and centrifugal distortion constants (including the octic ones) for all the states studied. The values for $^{80}SeO_2$ and $^{78}SeO_2$ in the ground vibrational state are given in Table 1.6. From

Table 1.6: Rotational constants of the ground vibrational level of $^{78}SeO_2$ and $^{80}SeO_2$, as calculated by Alekseev [10]. The numbers in brackets represent 1 standard deviation in the units of the last digit given.

Rotational Parameter	$^{78}SeO_2$ / cm^{-1}	$^{80}SeO_2$ / cm^{-1}
A	0.968602592(87)	0.961549416(50)
B	0.289420969(26)	0.289423056(14)
C	0.222257444(28)	0.221883458(14)
$\Delta_J \times 10^7$	2.06354(30)	2.06021(15)
$\Delta_{JK} \times 10^6$	-1.95932(14)	-1.93941(8)
$\Delta_K \times 10^5$	2.03736(14)	2.00821(5)
$\delta_J \times 10^8$	7.35205(63)	7.36526(47)
$\delta_K \times 10^7$	371781(217)	3.66524(170)

these values it is possible to determine more accurate values for the ground state structural parameters. The Se−O bond length of the (000) vibrational level has been determined to be 160.8779532(40) pm, and the O−Se−O bond angle to be 114.0153684(26) ^{o} for $^{80}SeO_2$. These are slightly larger than the equilibrium values calculated by Takeo *et al.* (160.76 pm and 113.833 ^{o}) [7], as would be expected due to the effects of anharmonicity.

1.2.2 The Electronic Spectrum

The first published work on the electronic spectrum of SeO_2 was by Asundi *et al.* in 1936 [12]. They studied the absorption spectrum between about 241 and 316 nm, and observed almost 90 bands. Their preferred method of assignment was to select the 0_0^0 transition first, and then try to find regular progressions which fitted with this assignment of the origin band. To select the origin band they considered two factors. Firstly, a comparison of the relative intensities of the origin band and another band originating from a higher vibrational level of the ground state should show that at higher temperatures the latter gains in intensity relative to the origin band. Secondly, considering the energy of excitation

of the SeO_2 molecule enabled them to find an approximate position for the origin band. The energies of excitation and the bond energies are known to decrease with increasing mass of the molecule, and therefore the origin of the SeO_2 band system was expected to be shifted slightly towards longer wavelengths than that of SO_2. So they assigned the 0_0^0 transition to a band at 32560 $cm^{-1}$and subsequently assigned the other bands using the selection rules for vibrational transitions deduced by Herzberg and Teller [13]. They assigned progressions in the symmetric stretching vibration and the asymmetric stretching vibration in both the ground and excited states, the values for which are given in Table 1.7. It is important to note that in accordance with the notation used by Asundi *et al.*, in this

Table 1.7: Vibrational constants for SeO_2, as calculated by Asundi *et al.* [12].

Vibrational parameter	Value / cm^{-1}
ν_2'' [a]	901
ν_3''	1189
ν_2' [a]	663
ν_3'	790

[a] ν_2 is the symmetric stretching vibration.

data ν_1 refers to the bending vibration, ν_2 to the symmetric stretching vibration and ν_3 to the asymmetric stretching vibration. It is now the convention to always label the symmetric stretching vibration as ν_1 and the bending vibration as ν_2. No bands were observed with quanta of the bending vibration excited, in either the ground or excited electronic states, a fact which Asundi claimed "indicates a principal deficiency of the theory". In contrast, they believed that their analysis with respect to the asymmetric stretching vibration was a very good confirmation of Herzberg and Teller's selection rules.

A couple of years later, Choong Shin-Piaw [14] discovered a number of systems of absorption bands of both SeO_2 and TeO_2 in the ultraviolet and visible regions of the electromagnetic spectrum. He classified the bands of SeO_2 into three main systems - the A system between about 206.9 and 220.5 nm, the B system between about 221.1 and 338.3 nm, and the C system above 340.4 nm. The B system, which is the same system as that studied by Asundi, was by far the most extensive of these, consisting of a large number of

bands. The 0_0^0 transition was assigned to a peak at 35082 cm^{-1}, and the majority of the lines in the central region of the system were assigned, along with some of the bands at the extremities. Vibrational constants were obtained for all three normal vibrations in the excited state, and for two vibrations in the ground state, as given in Table 1.8. Again, ν_1 is the bending vibration, ν_2 is the symmetric stretching vibration and ν_3 is the asymmetric stretching vibration.

Table 1.8: Vibrational constants for SeO_2, as calculated by Choong Shin-Piaw [14].

Vibrational constant	Value / cm^{-1}
ν_2'' [a]	917
ν_3''	173.2
ν_1' [b]	247.9
ν_2' [a]	657.9
ν_3'	781.8

[a] ν_2 is the symmetric stretching vibration.
[b] ν_1 is the bending vibration.

The differences between these two studies prompted Duchesne and Rosen [15] to do further work on the absorption spectrum of SeO_2 in 1941. They attempted to analyse approximately 125 bands in the B system using the Herzberg-Teller selection rules. The dominant feature in their spectrum was a long progression in approximately 650 cm^{-1}, which they identified as the totally symmetric stretching frequency in the excited state, ν_1'. They assigned the 0_0^0 transition to a peak with its band head at 33323 cm^{-1} and point of maximum intensity at 33330 cm^{-1}. They also assigned an interval of approximately 900 cm^{-1} to the symmetric stretching frequency in the ground state, ν_1''. Further work by King and McLean, as will be discussed below, later showed that this was a missassignment. When comparing their results with those of Choong Shin-Piaw, Duchesne and Rosen claimed that Choong Shin-Piaw had completely disregarded the Herzberg-Teller selection rules. Although Choong Shin-Piaw assigned approximately twice as many bands as Duchesne and Rosen, the comparision showed that Choong Shin-Piaw did not always pick out the heads of distinct bands but rather may have thought that the complex structure of

one band was due to a number of different bands. Duchesne and Rosen believed that the measurements of Asundi in the region 31600 to 41400 cm^{-1} agreed fairly well with their measurements.

In 1961 Haranath and Sivaramumurty [16] reported the emission spectrum of SeO_2 in the region 270 to 470 nm from SeO_2 vapour excited in a high frequency discharge. The band heads seen in the region 320 - 470 nm appeared to be diffuse, whereas those between 270 and 320 nm appeared sharp and red degraded. They assigned the bands below 320 nm as belonging to the B system seen in absorption by Duchesne and Rosen. However approximately 100 bands above 320 nm could not be assigned as an extension of this B system, or as part of the C system. Therefore these bands were assigned as belonging to two new overlapping systems, to each of which alternate bands belong. Bands in these two systems arise from transitions between symmetric stretching vibrational levels in the lower state and bending vibrational levels in the excited state, i.e. $1^0_{v''_1} 2^{v'_2}_0$ transitions. The origins of these two systems are 93 cm^{-1} apart, and within about 200 cm^{-1} of the origin of the B system. The symmetric stretching frequency in the lower state was found to be 910 cm^{-1} for both of these systems. Similarly, the frequency of the bending vibration was found to be 182 cm^{-1} in both systems. Since the average value for the symmetric stretching frequency in the lower state was the same in both cases, Haranath and Sivaramumurty considered the two systems as having a common lower state. However, since these systems were not observed in the absorption spectra they could not say whether this was the normal ground state of SeO_2.

In 1974, King and McLean [17] carried out further analysis of the vibrational band structure of the absorption spectrum for the electronic transition from the ground $^1A_1$ state to the so-called B system, in the region 230 - 340 nm. They produced SeO_2 vapour by heating the absorption cell to temperatures between 120 and 200 °C. A section of their spectrum is shown in Figure 1.1. As can be seen from the picture, the heads of most of the bands are poorly defined. King and McLean had problems establishing the wavenumber of the band heads, and this was further complicated by the large amount of overlap they observed between adjacent bands. Hence the frequencies they quote for the various bands are only accurate to ± 10 cm^{-1}. In spite of these difficulties, we can place more confidence

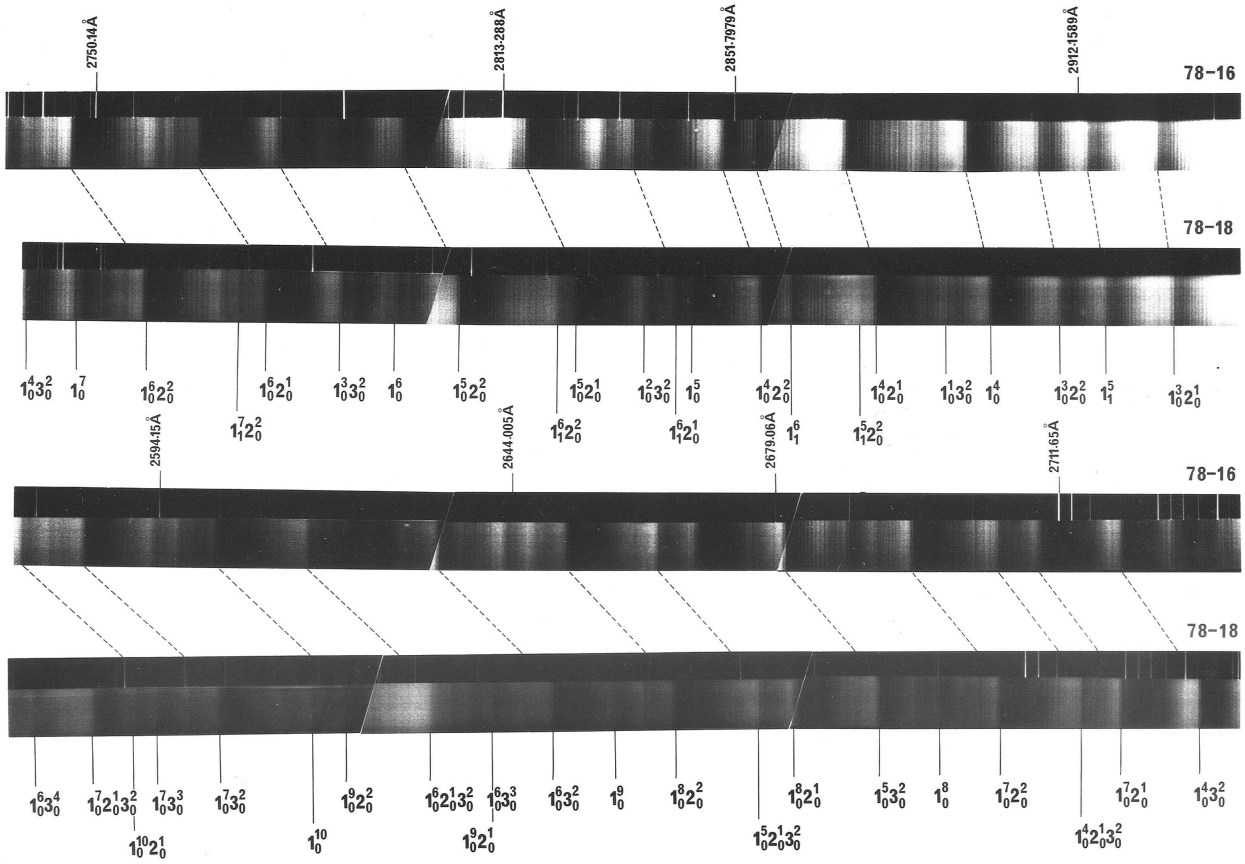

Figure 1.1: A section of the absorption spectrum of $^{78}Se^{16}O_2$ and $^{78}Se^{18}O_2$ recorded by King and McLean [17].

in their assignments that in any of the previous assignments discussed due to the fact that King and McLean used isotopically enriched samples of SeO_2, whereas all the previous workers used naturally occurring samples. They used three different isotopic species - $^{78}Se^{16}O_2$, $^{80}Se^{16}O_2$ and $^{78}Se^{18}O_2$. We would expect the origin band to be unchanged on isotopic substitution, and for there then to be a regular, linear isotopic shift through the different progressions in ν_1 and ν_2. In reality, the 0_0^0 band is at 31955.0, 31957.4 and 31963.9 cm^{-1} respectively for the different isotopic species, and hence the isotopic splitting is -2.4 cm^{-1} on substitution of ^{80}Se by ^{78}Se. The splitting was found to be 1.5 cm^{-1} per quanta of ν_1 excited. This study revealed the values for the symmetric stretching vibration and the bending vibration in both the ground and excited electronic states, as quoted in Table 1.9.

Table 1.9: Vibrational constants for $^{78}SeO_2$ and $^{80}SeO_2$, as calculated by King and McLean [17].

Vibrational constant	$^{78}SeO_2$/ cm^{-1}	$^{80}SeO_2$/ cm^{-1}
ν_1''	923	922.6
ν_2''	373	372
ν_1'	650.2	648.8
ν_2'	260	258

The individual bands can also be seen to show some coarse rotational structure converging towards the higher frequency end of the bands, although this is not fully resolved and hence can not be used to carry out a full rotational analysis. This spectrum also showed additional sharp peaks about 78 cm^{-1} above the origin band and many of the hot bands, for each isotope. This separation could not be explained by combinations of ν_1 and ν_2. In addition, the fact that this separation is not dependent on isotopic substitution does not support such a vibrational interpretation. King and McLean explained the presence of these bands as being due to a double-minimum potential in the excited state with respect to the normal coordinate Q_3', and that the first quantum of the asymmetric stretching vibration, ν_3', is 78 cm^{-1}.

Further to their vibrational analysis of the B-system, King and McLean went on to study the rotational band contour of the absorption peak at 294.9 nm [18]. In their vibrational analysis they had assigned this band as being due to the 1_0^3 transition. This band was chosen because it was strong, relatively free from overlap, and showed no obvious perturbations, and hence was the most suitable band closest to the origin. The 0_0^0 band, in contrast, was weak and strongly overlapped by other bands. The spectrum they obtained showed a series of strong K sub-bands converging to heads. Although the heads of these K sub-bands were not well defined, they were still suitable to be used in conjunction with the ground state rotational parameters from Takeo's work and a simulation program to obtain values for the rotational constants in the excited electronic state. The computer program was used to generate type A, B and C band contours for excited state rotational constants corresponding to bond angles over the range 94 - 104 $^{\circ}$ and bond lengths over

the range 161 - 175 pm. Only one of the excited state parameters was varied in practice, $(A' - \bar{B}')$. The best agreement between the simulated and observed contours was obtained for an A-type transition with the excited state constants corresponding to a bond length of 174 pm and bond angle of 101.0 ^{o} for both $^{78}SeO_2$ and $^{80}SeO_2$. The rotational constants obtained from these parameters are given in Table 1.10, along with the band origins. The

Table 1.10: Rotational constants for the $^1B_2$ excited state of $^{78}SeO_2$ and $^{80}SeO_2$, as calculated by King and McLean [18].

Constant	$^{78}SeO_2$/ cm^{-1}	$^{80}SeO_2$/ cm^{-1}
ν_0	33896.7	338905.1
A	0.60657	0.60215
B	0.29221	0.29221
C	0.19721	0.19674

calculated A-type contours using these rotational constants reproduced the overall intensity distribution and pattern of the observed profiles well, although the wavenumber agreement of the K-heads was rather poor. Calculated B- or C-type band contours did not resemble the observed one as they did not show any prominent K-structure but instead consisted of a jumble of lines. Therefore King and McLean concluded that the 1_0^3 band, and hence the 0_0^0 band must be parallel, A-type transitions. This implies that the symmetry of the excited state is $^1B_2$, and the electronic transition to be $\tilde{C}^1B_2 \leftarrow \tilde{X}^1A_1$. On excitation the O−Se−O bond angle decreases slightly and the O−Se bond length increases, as would be expected for a $\tilde{C}^1B_2 \leftarrow \tilde{X}^1A_1$ transition. Further evidence for this being the correct assignment of the electronic transition comes from the analogous system of SO_2 in the 180 - 235 nm region. The origin band of this system occurs at 42573.450 cm^{-1}and has been rotationally analysed as an A-type transition, and the electronic nature of this transition has been identified as $\tilde{C}^1B_2 \leftarrow \tilde{X}^1A_1$ [19].

1.2.3 The Infrared Spectrum

The infrared spectrum of SeO_2 was most recently studied by Konings *et al.* in 1998 [20]. All three normal vibrational modes of SeO_2 are infrared and Raman active. In the ground

electronic state the symmetric stretching and bending vibrations (ν_1 and ν_2 respectively) are *B*-type bands, whereas the asymmetric stretching vibration (ν_3) is an *A*-type band. In the gas-phase infrared spectrum of SeO_2 Konings observed two intense absorption bands at 364 and 968 cm^{-1}, which are attributed to ν_2'' and ν_3'' respectively. There was a weak shoulder on the low frequency side of the asymmetric stretching band which probably represents the symmetric stretching mode, since this vibration is expected to have a small intensity in the infrared. They also assigned a weak absorption band at 1869 cm^{-1} to the $\nu_3'' + \nu_1''$ combination band. The results are in good agreement with previous data obtained in the gas phase.

1.2.4 Lifetime Measurements

Miziolek measured the radiative liefetime of SeO_2 vapour excited at 288.8 nm, in the $\tilde{C}^1B_2 \leftarrow \tilde{X}^1A_1$ transition [21]. This wavelength corresponds to the 1_0^4 transition assigned by King and McLean, and was chosen because it is one of the strongest absorption bands. A solid sample of SeO_2 was placed in a chamber at room temperature and allowed to reach its vapour pressure of 9.1×10^{-8} Torr, i.e. the lifetime was measured under collision-free conditions. The results indicated the lifetime to be $\tau_r = 36.1 \pm 2.5$ μs.

1.2.5 *Ab Initio* Calculations

Recent calculations carried out for SeO_2 using density functional theory (DFT) [22] provide further information which should be helpful in our analysis of the electronic spectrum. The results of these calculations are shown below. Table 1.11 contains information about the relative energies of the two states of interest ($^1A_1$ and $^1B_2$), along with the bond length and bond angle of the molecule in these two states. Table 1.12 contains information about the vibrational frequencies. The results labelled ADF-V were preformed using triple-ζ Slater type orbitals including d and f polarization functions, n-2 frozen cores for Se, 1s frozen cores for O and the ZORA relativistic approach. These calculations have been preformed using local (LDA) and non-local (Becke-Perdew 1986 or BP86) functionals, the latter in principal being of higher quality. The results labelled TZVP / B3LYP were performed with

Table 1.11: Relative energies and geometries from DFT calculations [22].

Calculation level	State	Bond length / pm	Bond angle / °	Relative energy / cm
ADF-V / LDA	$^1A_1$	161.6	113.8	0
ADF-V / BP86		163.6	113.8	0
TZVP / B3LYP		163.0	114.0	0
ADF-V / LDA	$^1B_2$	171.0	102.6	22190
ADF-V / BP86		173.0	102.1	22920
TZVP / B3LYP		172.9	101.6	23420

Table 1.12: Vibrational frequencies from DFT calculations [22].

Calculation level	Electronic state	ν_1 / cm^{-1}	ν_2 / cm^{-1}	ν_3 / cm^{-1}
ADF-V / LDA	$^1A_1$	942	356	978
ADF-V / BP86		898	349	932
TZVP / B3LYP		932	355	961
TZVP / B3LYP	$^1B_2$	793	299	843

triple-ζ Gaussian type orbitals including d polarized functions and the hybrid functional B3LYP. The calculated bond angles and bond lengths for the ground state all agree fairly well with the experimental data, although the best agreement for the bond angle is at the TZVP / B3LYP level of calculation whereas the best agreement for the bond length is at the ADF-V / LDA level. The calculated vibrational frequencies are also in fairly good agreement with the experimentally determined values, with the TZVP / B3LYP level again giving the best agreement. The comparison between the calculated values in the $^1B_2$ excited electronic state and the experimental determination of these parameters by King and McLean is not quite so favourable, however hopefully this work will be able to improve that comparison. It is worth noting that these calculations do not predict a double-minimum potential in the excited state, and that the calculated value for ν_3' is considerably different from that determined by King and McLean.

Bibliography

[1] D.F. Hullah and J.M. Brown. The Electronic Spectrum of Tellurium Dioxide. *Journal of Molecular Spectroscopy*, **200**(2), 2000.

[2] D.F. Hullah. *The Electronic Spectra of FeH and TeO_2*. D.Phil thesis, University of Oxford, 1999.

[3] F.J. Lovas. Microwave Spectral Tables III. Triatomic Molecules. *Journal of Physical and Chemical Reference Data*, **7**, 1978.

[4] Joens J.A. An assignment of the structural features in the Hartley band absorption spectrum of ozone. *Journal of Chemical Physics*, **100**(5), 1994.

[5] F.J. Lovas. Microwave Spectra of Molecules of Astrophysical Interest 22. Sulfur Dioxide (SO_2). *Journal of Physical and Chemical Reference Data*, **14**(2), 1985.

[6] K. Yamanouchi, M. Okunishi, Y. Endo, and S. Tsuchiya. Laser Induced Fluorescence Spectroscopy of the $\tilde{C}^1B_2$- $^1A_1$ band of jet-cooled SO_2: Rotational and Vibrational Analyses in the 235 - 210 nm region. *Journal of Molecular Structure*, **352/353**(Com), 1995.

[7] H. Takeo, E. Hirota, and Y. Morino. Equilibrium Structure and Potential Function of Selenium Dioxide by Microwave Spectroscopy. *Journal of Molecular Spectroscopy*, **34**, 1970.

[8] H. Takeo, E. Hirota, and Y. Morino. Third-order Potential Constants and Dipole Moment of SeO_2 by Microwave Spectroscopy. *Journal of Molecular Spectroscopy*, **41**, 1972.

[9] S.N. Cesaro, M. Spoliti, A.J. Hinchcliffe, and S.J. Ogden. Infrared spectrum and thermodynamic functions of matrix isolated selenium dioxide. *Journal of Chemical Physics*, **55**(12), 1971.

[10] E.A. Alekseev, O.I. Baskakov, and S.F. Dyubko. Microwave Spectrum of Selenium Dioxide. *Proceedings of SPIE - International Society of Optical Engineers*, **3090** (High Resolution Molecular Spectroscopy), 1997.

[11] J.K.G. Watson. *Aspects of Quartic and Sextic Centrifugal Effects on Rotational Energy Levels*, Volume 6, chapter 1 of *Vibrational Spectra and Structure*. Elsevier, 1977.

[12] R.K. Asundi, M. Jan-Khan, and R. Samuel. Spectra of SeO and SeO_2. *Proceedings of The Royal Society*, **157**, 1936.

[13] G. Herzberg and E. Teller. Schwingungsstruktur der Elektronenübergänge bei mehratomigen Molekülen. *Zeitschrift für Physikalisch Chemie*, **B21**, 1933.

[14] P. Choong Shin-Piaw. Spectres de bandes du sélénium, du tellure et de leurs oxydes dans l'ultra-violet. *Annales de Physique*, 1938.

[15] J. Duchesne and B. Rosen. Recherches sur le spectre d'apsorption de la molecule SeO_2. *Physika*, **8**(6), 1941.

[16] P.B.V. Haranath and V. Sivaramumurthy. Emission band spectrum of SeO_2 molecule. *Indian Journal of Physics*, **35**, 1961.

[17] G.W. King and P.R. McLean. Selenium Dioxide: Vibrational Analysis of the 3130 Å $^1B_2$ - $^1A_1$ Absorption System. *Journal of Molecular Spectroscopy*, **51**, 1974.

[18] G.W. King and P.R. McLean. Selenium Dioxide: Rotational Analysis and Franck-Condon Calculations for the 3130 Å $^1B_2$ - $^1A_1$ Absorption System. *Journal of Molecular Spectroscopy*, **52**, 1974.

[19] J.C.D. Brand, P.H. Chiu, A.R. Hoy, and H.D. Bist. Sulfur Dioxide: Rotational Constants and Asymmetric Structure of the $\tilde{C}^1B_2$ State. *Journal of Molecular Spectroscopy*, **60**, 1976.

[20] R.J.M. Konings, A.S. Booij, and A. Kovács. The Infrared Spectra of SeO_2 and TeO_2 in the Gas Phase. *Chemical Physics Letters*, **292**, 1998.

[21] A.W. Miziolek. Radiative Lifetime and Quenching Rates of SeO_2 Vapor. *Chemical Physics Letters*, **74**(1), 1980.

[22] A.J. Bridgeman. Private communication. 2001.

Chapter 2

Experimental Methods

2.1 Introduction

The electronic spectrum of rotationally and vibrationally cold SeO_2 was studied in the gas phase using the technique of Laser Induced Fluorescence (LIF). A tunable laser source is used to irradiate the sample molecules, which absorb a photon when the frequency of the laser is resonant with a transition in the molecule. The resulting fluorescence is recorded as a function of the laser frequency. This technique is more sensitive than absorption - it is, in principal, a zero background technique, as fluorescence can only occur when the laser frequency is resonant with a transition. This makes the detection of weak features much easier than in absorption experiments.

Two separate experiments have been carried out during this study:

1. A pulsed dye laser was used to study the broad-band, vibrationally resolved spectrum between about 292 and 327 nm.

2. A ring dye laser was used to record a number of the individual vibrational bands at higher, rotational resolution.

2.2 The Heated Nozzle

The gas phase SeO_2 molecules used in this work were produced in a heated nozzle, which leads to a free-jet expansion, and rotationally cold molecules. The nozzles used are constructed from alumina tubes (400 mm long, 10 mm OD, 7 mm ID), closed at one end, with a 250 μm hole drilled in the closed end. The alumina tube contains a small crucible of SeO_2 powder at the closed end, as illustrated in Figure 2.1. The tube is electrically

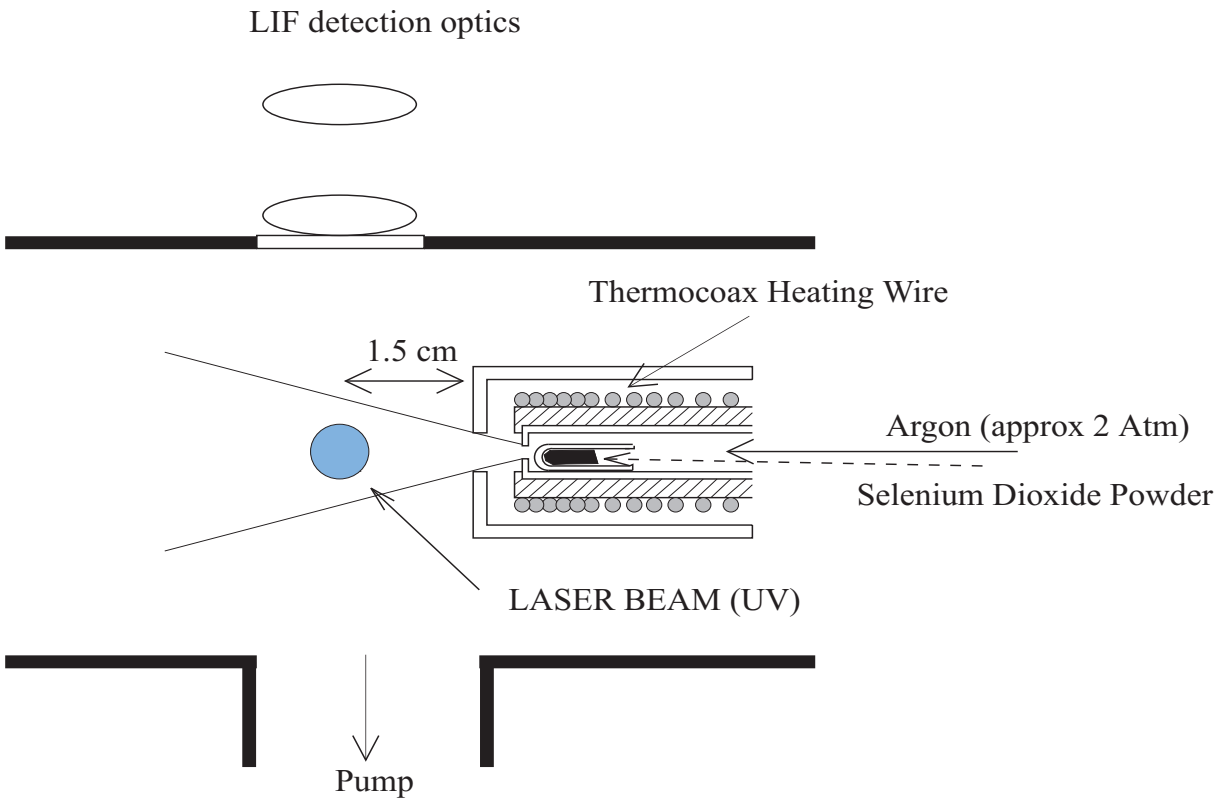

Figure 2.1: The heated nozzle.

heated using a Phillips 1NcAc15 Thermocoax heating wire. The temperature is controlled using a 'Variac' power supply, and measured using a K type thermocouple placed under the heating wires at the end of the nozzle. It is possible to obtain temperatures up to about 1000 °C using this Thermocoax, although it was only necessary to heat the sample up to between 300 and 320 °C in this work. At this temperature the vapour pressure of SeO_2 is high enough to give a good signal-to-noise ratio, but the temperature is also low

enough not to immediately sublime the sample and so it lasts a good working day. The nozzle is surrounded by a metal shroud, to reduce the amount of black body radiation in the chamber, and the detection optics are also shielded to prevent black body radiation from reaching the Photomultiplier Tube (PMT) detector. The heated nozzle is surrounded by a water jacket, to keep the rest of the chamber as cold as possible. A stream of argon at 3.5 bar pressure is passed continuously over the SeO_2, and carries the gas molecules into the chamber. In some of the survey experiments this pressure was dropped to 2 bar to promote the intensity of hot bands.

The chamber is cubic in shape, with two long arms on either side, as illustrated in Figure 2.2. These two arms are for the input and output of the laser radiation to and

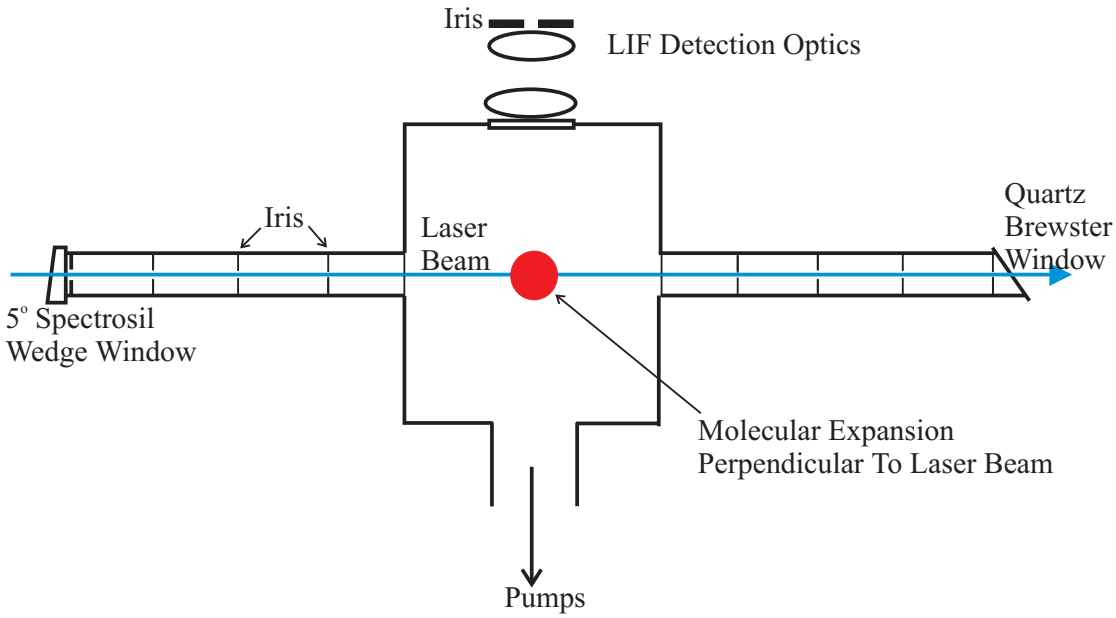

Figure 2.2: The reaction chamber.

from the chamber. They contain an number of baffles and irises to ensure that the light travels straight through them, and hence the amount of scattered light in the chamber is reduced; they also reduce the amount of light scattered by the windows reaching the PMT. Thus the light beam intersects the centre of the beam of molecules perpendicularly. The fluorescence is detected from above, so the detection is mutually perpendicular to both the molecular beam and the laser beam. On the input arm there is a 5 ° wedge window, and

on the output arm there is a Brewster window, both of which also help reduce the amount of scattered light in the chamber.

The chamber is pumped using a two-stage Leybold Trivac mechanical pump and an Edwards Roots blower mechanical pump. The pressure in the chamber is measured with a Pirani gauge, and an ultimate pressure of 5 mTorr can be obtained. The backing pressure of the Ar behind the nozzle is usually 3.5 bar, which leads to a pressure under load of around 85 mTorr at 320 °C.

The nozzle is mounted on bellows, which allow its position relative to the laser beam to be adjusted to maximise the intensity of the fluorescence seen.

The fluorescence is detected using a Phillips XP2020Q uv sensitive PMT. An iris is placed between the focussing lenses and the PMT for the high resolution experiments. This reduces the volume of the expansion from which fluorescence is detected, and hence reduces the Doppler line width of the individual rotationally resolved peaks. It was possible to get a good signal to noise ratio with an iris as small as 1 mm diameter, which significantly reduced the width of the peaks to a FWHM of 0.015 cm^{-1}.

2.3 Expansion Conditions from the Nozzle

A free-jet molecular beam is a neutral beam extracted from an underexpanded, supersonic, continuum jet expansion from a high pressure gas source into a low pressure background. This is the same type of expansion that occurs from converging-diverging supersonic rocket nozzles, although the diverging part is not required - hence the term 'free'-jet.

The features of a free-jet expansion are shown in Figure 2.3 [1]. The gas starts at a negligibly small velocity in the nozzle, called the stagnation state, at a pressure of P_0 and temperature of T_0. The background pressure in the chamber is given by P_b, and hence a pressure difference of $(P_0 - P_b)$ is imposed. The mean velocity of the gas is equal to the local speed of sound, or the Mach number (M) is equal to 1, if the ratio of P_0/P_b equals a critical value G, where

$$G = \left(\frac{\gamma + 1}{2}\right)^{\frac{\gamma}{\gamma - 1}} . \tag{2.1}$$

γ is the ratio of the heat capacity at constant pressure to that at constant volume (= $\frac{5}{3}$

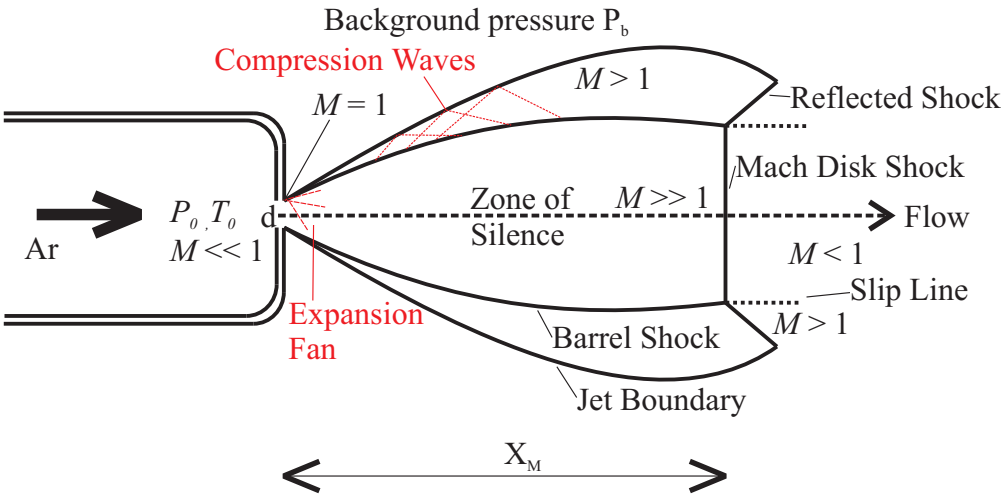

Figure 2.3: Features of a free jet expansion [1].

for a perfect, monatomic gas), hence G is less than 2.1 for all gases. If the pressure ratio at the exit of the nozzle is less than G, then the flow of the gas is subsonic, and no further expansion occurs. However as P_0/P_b increases, M is equal to 1 at the exit of the nozzle. The pressure at the exit of the nozzle becomes independent of P_b, and equal to $P_0/G \approx P_0/2$. Since the pressure at the exit of the nozzle is now greater than P_b, the gas is said to be 'underexpanded'. Subsequently, expansion occurs as the gas flow attempts to meet the necessary boundary condition impossed by the background pressure P_b. The velocity of the flow, or M increases with the flow area, and hence M is greater than 1 beyond the exit of the nozzle.

The expansion is ignorant of the conditions further downstream, and so overexpands. It then needs to be recompressed by a system of shockwaves, the barrel shock at the sides, and the Mach disk shock normal to the centerline, as illustrated in Figure 2.3. The location of the Mach disk relative to the nozzle is given by

$$x_M = 0.67d\sqrt{\left(\frac{P_0}{P_b}\right)}. \tag{2.2}$$

The location of this disk turns out to be insensitive to γ. The diameter of the barrel shock and Mach disk are of the order of $0.75x_M$ and $0.5x_M$ respectively. The region between the

nozzle and the Mach disk is called the 'zone of silence', and is the portion of the molecular beam that is studied. So in this work, where P_0 is about 3.5 bar and P_b about 85 mTorr, the Mach disk is located about 30 mm beyond the nozzle.

This expansion to supersonic velocities leads to translationally cold Ar atoms, and the SeO_2 molecules can then be cooled by energy transfer. Collisions with the Ar atoms lead to rotational and vibrational cooling of the SeO_2 molecules. Typically 100 - 1000 collisions will occur between a SeO_2 molecule and the Ar atoms in the zone of silence. Only 10 - 100 collisions are required to cool the rotational temperature of SeO_2 down to between 10 and 15 K. Vibrational cooling is less efficient, requiring at least 1000 collisions to completely cool down the molecules, and so only partial vibrational cooling to around 100 K can occur before the Mach disk is reached. Beyond the Mach disk, the temperature rapidly rises to that of the surrounding region.

2.4 The Laser Systems

2.4.1 Principles of Laser Operation

Laser radiation is particularly useful for spectroscopic experiments for a number of reasons: it has a high power, it is highly collimated, it is monochromatic with a narrow linewidth, and it is spatially and temporally coherent.

Dye lasers are widely used in spectroscopy because they can be tuned over large wavelength ranges, and have fairly high power outputs. The dyes used are usually large planar polyatomic organic molecules, in which there is extensive delocalisation of the electrons. A non-linear molecule with N atoms has (3N-6) different vibrational modes, each of which has many rotational levels. In solution the frequency of collisions is sufficiently high that each level is broadened by its short lifetime, and the energy levels overlap to form a continuum of levels in the different electronic states. A fixed frequency pump laser excites the dye from the singlet S_0 ground state up to the first excited singlet state, S_1, as illustrated in Figure 2.4. Collisions between the vibrational and rotational levels which are very close in energy lead to a very rapid, non radiative, relaxation to the lower levels of the S_1 state.

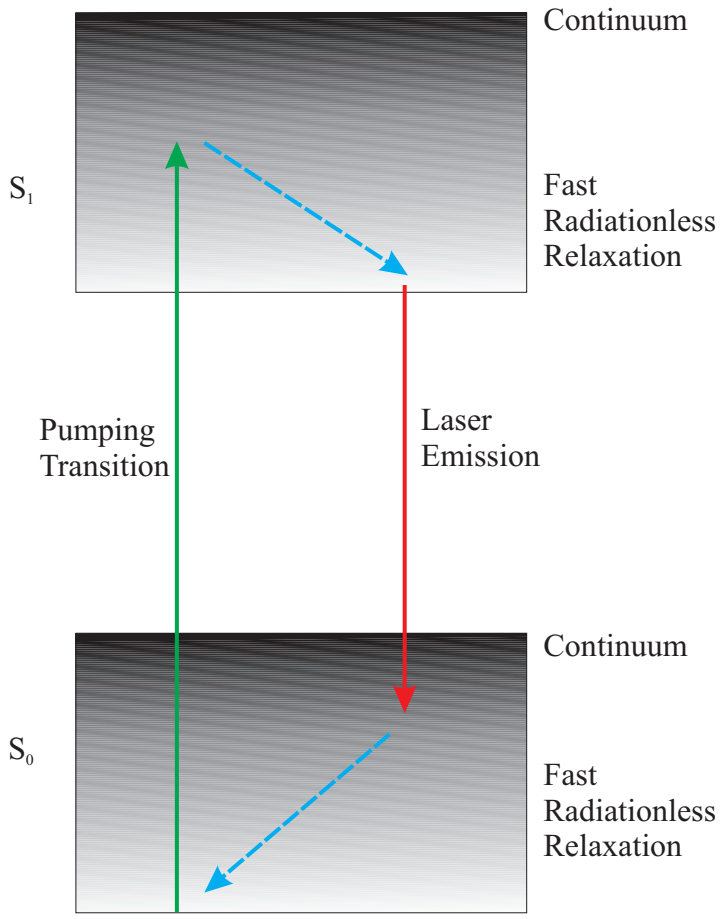

Figure 2.4: The mechanism of laser action in a dye laser.

Fluorescence, which is the basis of the laser action, occurs when the molecules relax back to the higher vibrational levels of the S_0 state. This is then followed by a further radiationless transition back to the lower energy levels of the S_0 state, leaving the molecules ready to be re-excited by the pump laser and hence the required population inversion can be maintained.

2.4.2 The Pulsed Laser System

The broad band spectrum of SeO_2 was recorded using a Lambda Physik FL3002 pulsed dye laser pumped by a Lambda Physik 205i excimer laser, operating with XeCl at 308 nm. Rhodamine 6G, Rhodamine B and DCM dyes were all used, dissolved in methanol. The

output was frequency doubled using a β-Barium Borate (BBO) crystal.

The excimer was triggered by the dye laser at 10 Hz, and the excess radiation from the pump beam was directed on to a photodiode, and used as a trigger pulse for the data collection system.

The wavelength is varied by simultaneously stepping the diffraction grating and rotating the doubling crystal of the dye laser. The grating and the crystal move a fixed amount in each step, the smallest size of which used in these experiments of 0.001 nm. The laser is internally calibrated, but as there is a slight offset of the grating (about 0.02 nm of frequency doubled light) the scans were independently calibrated from the positions of well known features in the spectrum (Section 4.2.1).

2.4.3 The Continuous Wave Laser System

The rotationally resolved spectrum of SeO_2 was recorded using a Coherent 899-21 continuous wave ring dye laser, pumped by a Coherent Innova 100 argon ion (Ar^+) laser, operating at 514 nm. Rhodamine 6G and Sulphurrhodamine B (Kiton Red) dyes were used, this time dissolved in ethylene glycol. Again the output was frequency doubled, this time using a KDP (potassium dihydrogen phosphate or KH_2PO_4) crystal with the Rhodamine 6G dye, and a lithium iodate ($LiIO_3$) crystal with the Sulphurrhodamine B dye.

2.4.4 The Ring Dye Laser

A schematic of the ring dye laser is shown in Figure 2.5.

Ring dye lasers have the advantage over linear lasers that they produce a travelling wave inside the laser cavity rather than a standing wave. This means that the whole of the dye jet is used, whereas in a linear laser nodes form in the dye jet, hence a ring laser gives considerable higher power.

The resonance cavity of the laser is defined by a series of highly reflective mirrors, which are coated to reflect specific wavelength ranges. Light leaves the laser cavity through the output coupler, which is slightly transmitting. When doubled radiation is required a more reflective output coupler is used, giving higher power in the cavity. The KDP or $LiIO_3$

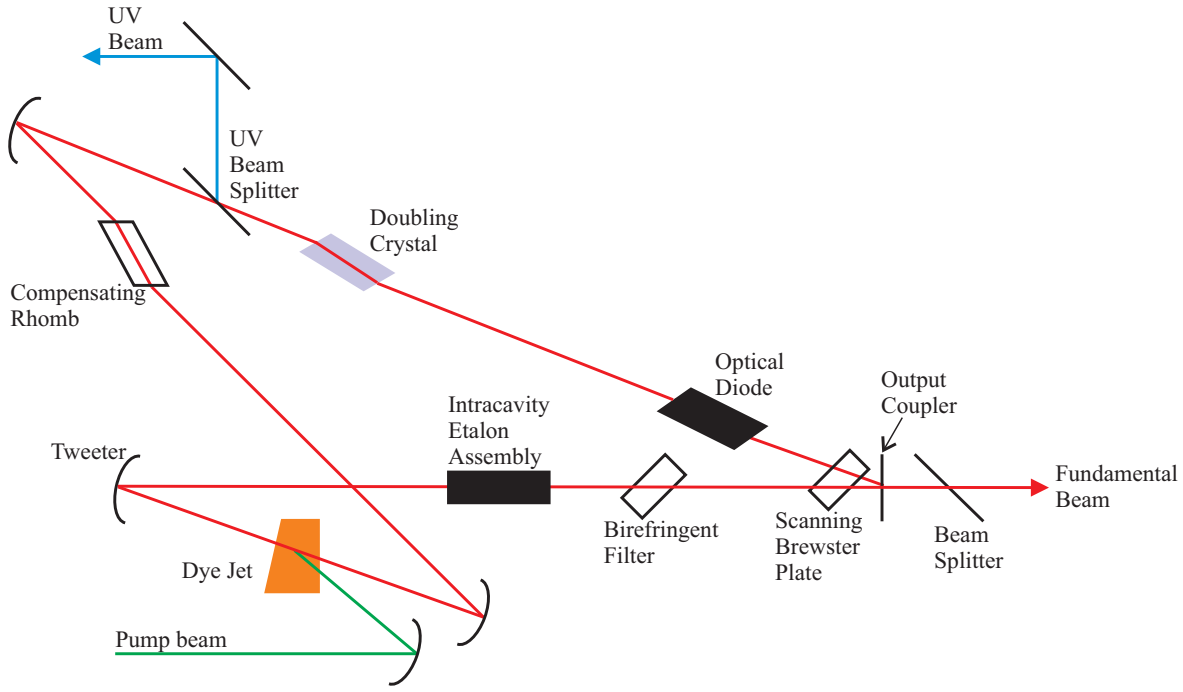

Figure 2.5: A schematic of the Coherent 899-21 ring dye laser.

doubling crystal is placed in the upper section of the laser ring. Frequency doubling, or second harmonic generation, is dependent on the laser intensity, although in a non-linear fashion, hence the more highly reflective output coupler used improves the power output of the doubled light. The crystal can be rotated according to the frequency of the fundamental light, allowing the whole range of wavelengths to be doubled.

The laser cavity also contains a number of other components to characterise the properties of the beam. An optical diode consisting of a Faraday rotator and an optical rotator restricts the light to travelling in only one direction in the cavity. The birefringent filter reduces the laser linewidth to approximately 0.5 cm^{-1}, and is used for manual broadband tuning of the laser to the nearest 7 cm^{-1}. An intracavity assembly (ICA), consisting of a thick étalon (with a free spectral range of 10 GHz) and a thin étalon (with a free spectral range of 240 MHz), together with a scanning Brewster plate, reduces the linewidth to about 10 MHz ($\sim$ 0 003 cm^{-1}). Active stabilisation (which locks the laser to a specific frequency) is achieved using a passive reference cavity, which also contains a scanning Brewster plate

and étalons, outside the main laser cavity. Any deviations in the laser frequency (due to vibrations, turbulence in the dye jet, etc.) generate an error signal which is fed to the 'tweeter'. The tweeter is on a piezoelectric mount, so can correct for fast cavity length variation. Another part of the error signal is fed to the Brewster plate to correct for slower cavity changes. This reduces the laser line width to 500 kHz ($\sim$ 0.00002 cm^{-1}), which is considerably less than the Doppler linewidth of the experiment. The frequency of the laser is scanned by rotating the galvo-mounted Brewster plate in the reference cavity. The laser then corrects the positions of the étalons and intracavity Brewster plate, to allow scans of up to 30 GHz (1 cm^{-1}) of the fundamental wavelength or 60 GHz of frequency doubled light.

2.5 Low Resolution Experimental Setup

Figure 2.6 shows the arrangement of the apparatus in the low resolution experiment.

The dye laser triggers the excimer, which in turn triggers the boxcar, as explained above. The fluorescence is detected on the PMT, and fed to a Stanford Research Systems SR250 boxcar. After a delay of 3 ns from receiving the trigger pulse, the boxcar integrates the voltage it receives from the PMT during a gate of 50 ns. This is then averaged over 30 pulses at a fixed wavelength, and sent via a SR245 interface to the computer. The laser is scanned in 'burst mode' - the grating and crystal stay fixed in one position for the 30 pulses, and then moves onto the next position before the next set of 30 pulses begins.

Using the excimer light to trigger the boxcar means that any problems due to 'jitter' of the laser are removed. For example, if the boxcar was triggered by the dye laser, and there was a delay between the dye laser sending a signal to the excimer and when it actually fired, this could cause problems. However since the boxcar is triggered by the excimer, the delay time and gate are entirely relative to when the excimer actually fires.

2.6 High Resolution Experimental Setup

The apparatus used in the high resolution set up is shown in Figure 2.7.

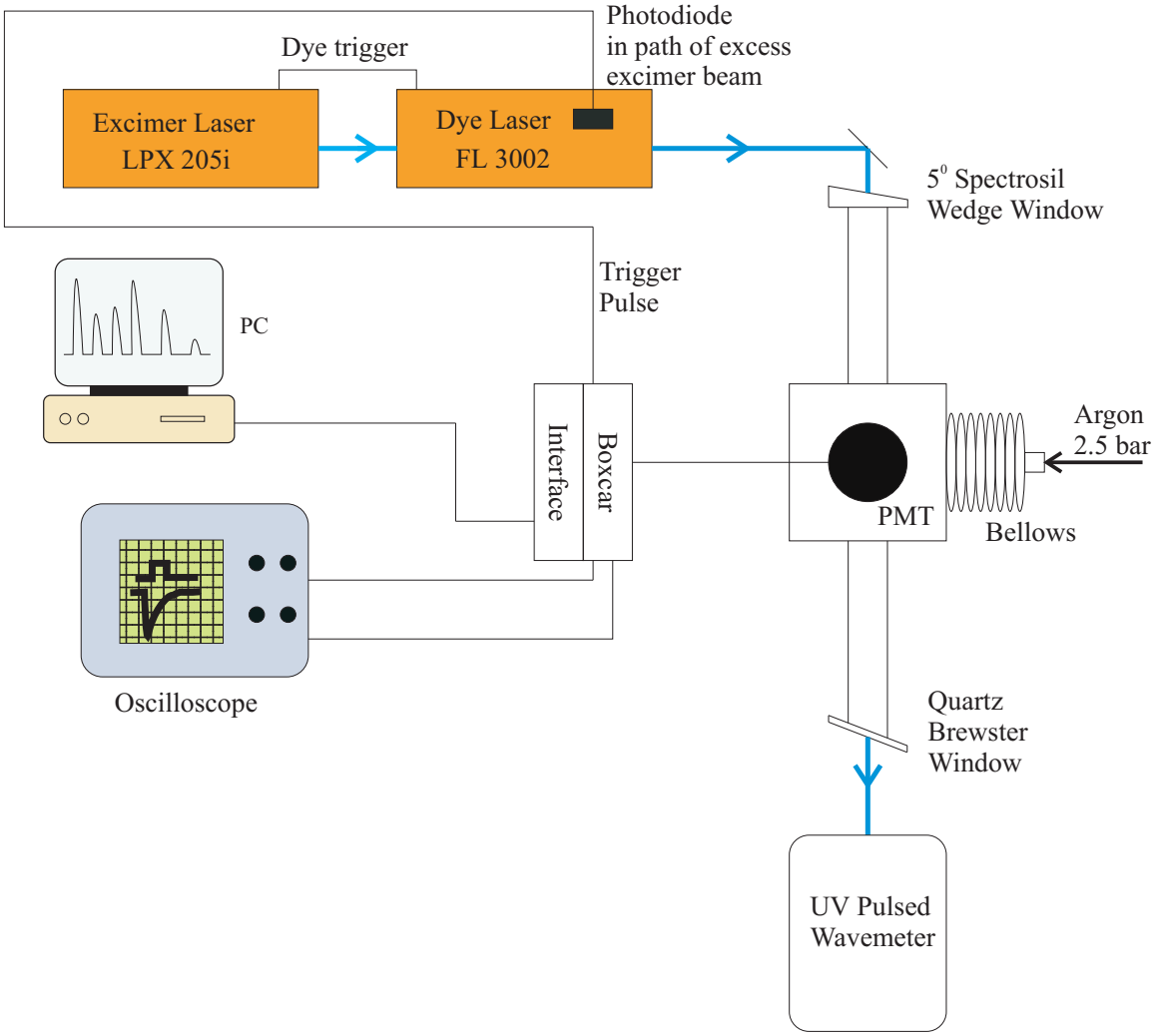

Figure 2.6: Experimental setup for the low resolutions scans.

The fundamental frequency light from the laser is used for calibration. As can be seen in Figure 2.7, this beam is split into three portions, which are passed through an iodine cell, a 1 m confocal étalon with a free spectral range of 75 MHz, and a Burleigh uv pulsed wavemeter. The wavemeter is used for rough calibration to $\pm$ 0.02 cm^{-1}. The spectrum of iodine has been well characterised [2], and can be used in conjunction with the étalon for absolute calibration of the spectra. The fringes from the étalon allow accurate interpolation between the calibration peaks from the iodine absorption spectrum and the peaks seen from the sample.

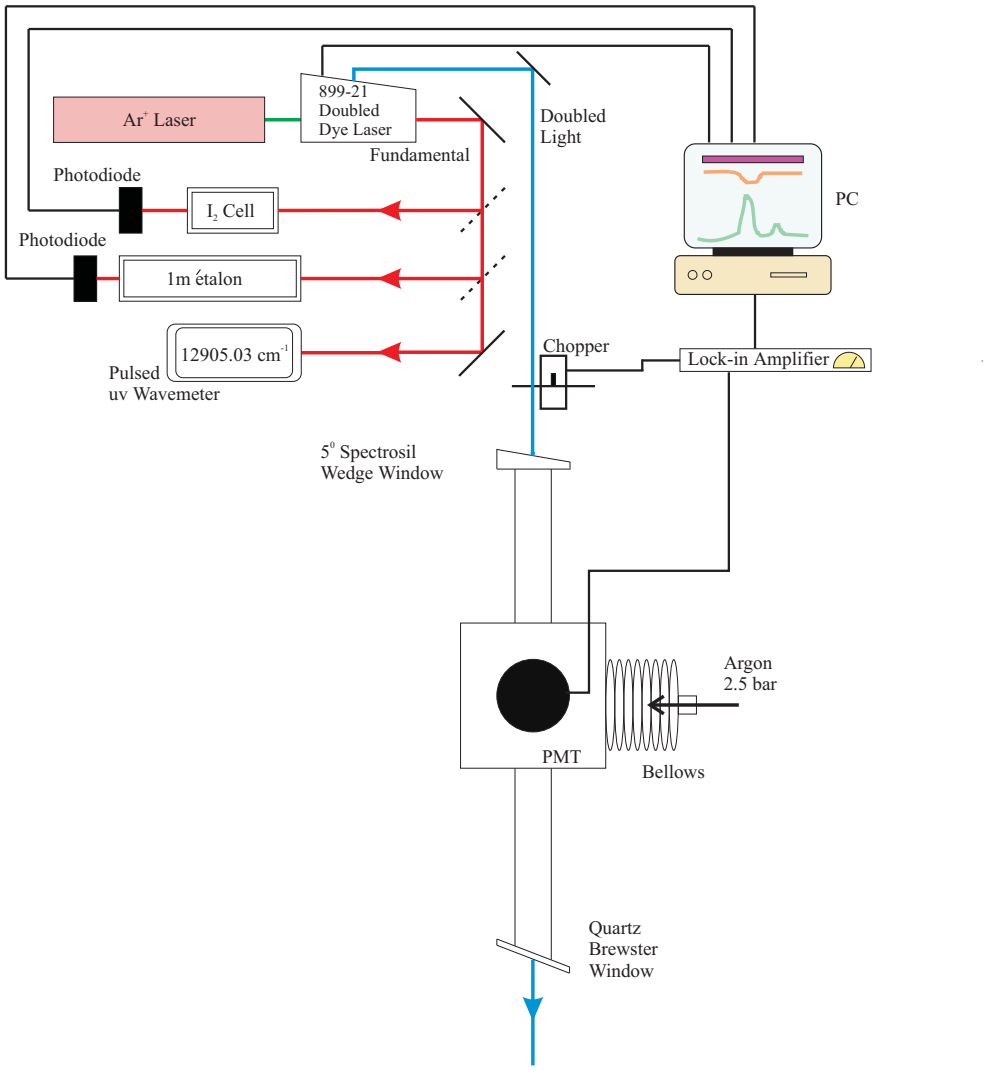

Figure 2.7: Experimental setup for the high resolution scans.

The voltage from the PMT is the input for a Brookdeal 9508 lock-in amplifier. The laser beam is mechanically chopped at 1 kHz before it enters the reaction chamber, and a reference signal from the chopper is also fed to the lock-in amplifier. This allows for phase-sensitive detection. Continuous detection tends to give a poor signal-to-noise ratio due to random $1/f$ noise. Chopping the laser beam converts this d.c voltage signal into one of sufficiently high frequency that a.c. amplification can be used. This has the effect of greatly reducing the $1/f$ noise below 1 kHz, i.e. the random noise is reduced because the signal is only sampled when the laser beam is known to be allowed into the chamber.

2.7 Experimental Accuracy

A strong spectral line can generally be measured to 1/10 of its Full Width Half Maximum (FWHM). The FWHM of a typical SeO_2 line in this study is found to be 0.016 cm^{-1} or approximately 450 MHz. The iodine lines typically have a FWHM of 0.02 cm^{-1}. Hence the errors in measuring the SeO_2 and I_2 lines are $\pm$ 0.0016 and $\pm$ 0.002 cm^{-1} respectively. Therefore, the internal consistency, or precision with which a line can be measured is given by $\sqrt{(0.0016)^2 + (0.002)^2} = 0.0026$ cm^{-1}. The peaks in the iodine spectrum are quoted to an accuracy of $\pm$ 0.002 cm^{-1}, which leads to an absolute accuracy of $\sqrt{(0.0026)^2 + (0.002)^2}$ = 0.0032 cm^{-1}. The free spectral range of the étalon is known to within 0.01 MHz, which does not contribute significantly to the error of the experiment. The accuracy calculated here is for strong, unblended lines, hence the positions of weaker or overlapped lines can not be determined as accurately.

Bibliography

[1] D.R. Miller. *Atomic and Molecular Beam Methods.* Oxford University Press, 1988.

[2] S. Gerstenkorn and P. Luc. *Atlas du Spectre de la Molecule d'Iode.* Center National de la Recherche Scientifique II, Orsay, France, 1978.

Chapter 3

Theory

3.1 Molecular Orbital Description of SeO_2

SeO_2 has 18 valence electrons, and so has an electronic structure analogous to that of O_3 and SO_2. The ground state confirmations of these molecules are described as ... $(a_2'')^2$ $(b_2')^2$ $(\bar{a}_1' s_A)^2$ [1]. The electronic states of polyatomic molecules are classified according to the resultant electron spin and the symmetry of the molecule. As can be seen from the electronic configuration given above, SeO_2 has no unpaired electrons in the ground state and so the multiplicity $(2S+1)$ is 1, i.e. it is a singlet state. The symmetry of this configuration is seen to be A_1 and hence the ground state is denoted as $^1A_1$.

The lowest excited states of SeO_2 are usually obtained by promotion of one of the $(\bar{a}_1' s_A)^2$ electrons, although this is not always the case. The electronic configurations of these states, and their terms, are given below in order of increasing energy above the ground state:

$$\ldots \quad (a_2'')^2(b_2')^2(\bar{a}_1' s_A)(\bar{b}_1'') \quad {}^{1,3}B_1 \tag{3.1}$$

$$\ldots \quad (a_2'')^2(b_2')^2(\bar{a}_1' s_A)^0(\bar{b}_1'')^2 \quad {}^1A_1 \tag{3.2}$$

$$\ldots \quad (a_2'')^2(b_2')(\bar{a}_1' s_A)^2(\bar{b}_1'') \quad {}^{1,3}A_2 \tag{3.3}$$

$$\ldots \quad (a_2'')^2(b_2')(\bar{a}_1' s_A)(\bar{b}_1'')^2 \quad {}^{1,3}B_2 \tag{3.4}$$

$$\ldots \quad (a_2'')(b_2')^2(\bar{a}_1' s_A)^2(\bar{b}_1'') \quad {}^{1,3}B_2 \tag{3.5}$$

$$\ldots \quad (a_2'')(b_2')^2(\bar{a}_1' s_A)(\bar{b}_1'')^2 \quad {}^{1,3}A_2 \tag{3.6}$$

3.2 Electronic Transitions and Selection Rules

In order for any transition to take place, whether it be electronic, vibrational or rotational, the transition must be allowed by the selection rules for that type of transition.

The first selection rule to consider for electronic transitions is that the change in spin must be equal to zero, i.e.

$$\Delta S = 0 \tag{3.7}$$

In other words, only states of the same multiplicity can combine with each other. This rule is held fairly rigorously, although transitions between states of different multiplicity are sometimes seen, usually with very weak intensity or in heavier molecules. Considering the electronic configurations and states given above for SeO_2, transitions from the singlet ground state to any of the triplet states are are formally forbidden, although such transitions are probably weakly allowed because SeO_2 is a fairly heavy molecule.

The probability of an electronic transition between two states depends on the square of the matrix elements of the dipole moment:

$$\left| \int \Psi_e'^* M \Psi_e'' d\tau_e \right|^2 \tag{3.8}$$

where M is the dipole moment of the molecule. In order for a transition to take place this integral must be non-zero, and it can be shown that this is only the case when the direct product of the symmetry species transforms like one of the components of M. The magnitude of this integral, and hence that of the electronic transition, is largest when the electronic configuration of the two states concerned differ by only one electron. Transitions involving the change of more than one electron usually have very low probabilities, and although they may be formally allowed, they are very weak and can almost be treated as forbidden transitions. Considering the possible electronic configurations for SeO_2 given

above, transitions from the ground state to the states labelled 3.3 and 3.6 are forbidden because, in the C_{2v} symmetry group, the direct product $A_1 \times A_2 = A_2$ does not contain a component of M. Transitions to 3.2 and 3.4 are formally allowed, but will be very weak due to more than one electron being excited. This only leaves transitions to the $^1B_1$ (3.1) and $^1B_2$ (3.5) states which are allowed and have an appreciable intensity. This work considers transitions to an excited state thought to be the $^1B_2$ state.

Electronic transitions often lead to a large change in the geometry of the molecule. Walsh [2] proposed two principles which can be used to estimate the variation of the binding energies of orbitals with the bond angle:

1. Whether or not an orbital becomes more tightly bound with change in angle is determined primarily by whether or not it changes from being built from a p-orbital of A to be being built from an s-orbital of A,

2. If the orbital is antibonding between the end atoms it is most tightly bound when the later are are as far as part as possible (i.e. in the linear molecule); if it is bonding between the end atoms it is most tightly bound when the atoms are as near together as possible (i.e. at 90 °),

where A is the central atom in an AB_2 molecule such as SeO_2. By considering the changes in binding energies of the different orbitals with bond angle it is possible to construct a Walsh diagram, from which we can then see what structures are most favoured by different electronic configurations. The $\tilde{C}^1B_2 \leftarrow \tilde{X}^1A_1$ transition, which is the one studied here, involves promotion of an electron from the (a_2'') orbital, which is localised on the oxygen atom and is weakly antibonding, to the $(\bar{b}_1'')$ orbital, which has a bonding component between the oxygen atoms and an antibonding component between the selenium and each oxygen atom. Hence this electronic transition should be accompanied by a small decrease in the bond angle and a moderate increase in the bond length in the excited state compared with the ground state. The $^1B_1 \leftarrow \tilde{X}^1A_1$ transition, on the other hand, should involve a moderate increase in the bond angle and a small increase of the bond length on excitation.

Because of the large change in geometric structure on excitation, the electronic transition is expected to consist of a large number of vibrational bands.

3.3 Vibrational Structure and Selection Rules

According to the formula that non-linear polyatomic molecules have (3N-6) normal vibrational modes, SeO_2 has three normal vibrations. These are a symmetric stretching vibration (ν_1), a bending vibration (ν_2) and an asymmetric stretching vibration (ν_3). These three modes are illustrated in Figure 3.1. In the C_{2v} point group these vibrations transform as A_1, A_1 and B_2 respectively, when the x- or c-axis is the axis perpendicular to the plain of the molecule, as illustrated in Figure 3.2.

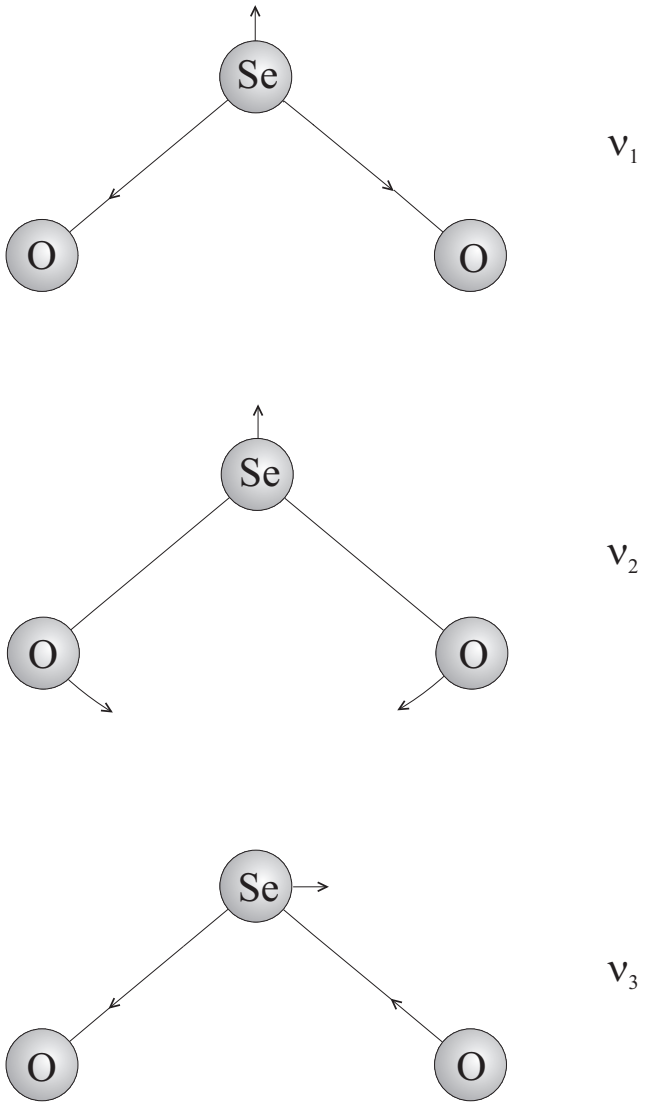

Figure 3.1: The vibrational modes of SeO_2.

The frequencies of the band origins of the vibrational transitions are given by

$$\nu = \nu_e + G'(v_1', v_2', v_3') - G''(v_1'', v_2'', v_3'') \tag{3.9}$$

which is commonly expressed in cm^{-1}, a quantity widely used in spectroscopy as it is directly proportional to the energy. ν_e is the origin of the electronic transition. $G'(v_1', v_2', v_3')$ and $G''(v_1'', v_2'', v_3'')$ are the vibrational term values for the upper and lower electronic states respectively. To a first approximation, neglecting the effects of anharmonicity, these can be expressed as

$$G(v_1, v_2, v_3) = \sum_i \nu_i \left(v_i + \frac{d_i}{2} \right) \tag{3.10}$$

where d_i is the degeneracy of the vibration, which is always 1 in the case of SeO_2. The more complex expression, including the anharmonicity of the vibrations is

$$G(v_1, v_2, v_3) = \sum_i \omega_i \left(v_i + \frac{d_i}{2} \right) + \sum_i \sum_{k \geq i} x_{ik} \left(v_i + \frac{d_i}{2} \right) \left(v_k + \frac{d_k}{2} \right) + \sum_i \sum_{k \geq i} g_{ik} l_i l_k \ldots \tag{3.11}$$

where ω_i is the zero-order frequency and x_{ik} is the anharmonicity constant. The final term is a small correction applied if one or more degenerate vibrations are excited.

3.3.1 The Franck-Condon Principle

The intensity of a vibrational band in an electronic transition can be determined from the Franck-Condon principle. The intensity of a transition is proportional to the square of the matrix elements:

$$\left| \int \int \Psi_e'^* \Psi_v'^* M \Psi_e'' \Psi_v'' d\tau_e d\tau_v \right|^2 . \tag{3.12}$$

Assuming that the probability of the electronic transition does not vary appreciably during a vibration, this equation can be factorised as

$$\left| \int \Psi_e'^* M \Psi_e'' d\tau_e \right|^2 \left| \int \Psi_v'^* \Psi_v'' d\tau_v \right|^2 . \tag{3.13}$$

Hence the intensity of the vibrational transition is given simply by

$$\left| \int \Psi_v'^* \Psi_v'' d\tau_v \right|^2 \tag{3.14}$$

which is known as the overlap integral. Summed over all vibrational levels this overlap integral is equal to one, hence the intensity of an electronic transition summed over all vibrational bands depends only on the probability of the electronic transition, as was previously discussed.

In order for a vibrational transition to be allowed, the symmetries of both vibrational wavefunctions must be the same. Then the overlap integral, which is also known as the Franck-Condon intensity, is non-zero.

3.3.2 Vibrational Selection Rules

Vibrational selection rules are derived from the integral

$$\int \Psi_v'^* \Psi_v'' d\tau_v. \tag{3.15}$$

For vibrations which are symmetric with respect to all the symmetry elements in the molecule, the vibrational quantum number may change by any amount (governed only by the Franck-Condon principle). However vibrations which are antisymmetric with respect to some symmetry operation may only change by even number increments of the vibrational quantum number. As mentioned above, in SeO_2 the symmetric stretching vibration and the bending vibration are symmetric, however the antisymmetric stretching vibration is not symmetric. So the selection rules for SeO_2 are

$$\Delta v_1 = 0, \pm 1, \pm 2, \ldots \tag{3.16}$$

$$\Delta v_2 = 0, \pm 1, \pm 2, \ldots$$

$$\Delta v_3 = 0, \pm 2, \pm 4, \ldots$$

For small changes in geometry, transitions with $\Delta v = 0$ are expected to be stronger than those with $\Delta v \neq 0$. However if there is a large change in the geometry of the molecule, as is the case with SeO_2, transitions with $\Delta v = 0$ are not necessarily the strongest.

3.4 Properties of an Asymmetric Rotor

As previously mentioned, SeO_2 has C_{2v} symmetry and so is an asymmetric rotor. Therefore, the three moments of inertia about the three mutually perpendicular axis are all different, and hence the three rotational constants (A, B and C) which are derived from the moments of inertia are also all different. The rotational axes of SeO_2 are shown below in Figure 3.2.

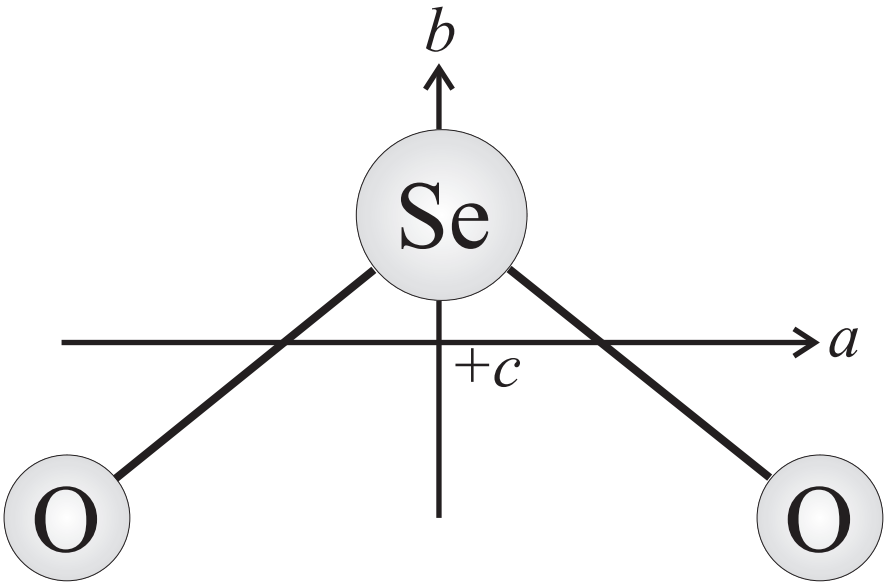

Figure 3.2: The rotational axes of the SeO_2 molecule.

Note that all three of the axes pass through the centre of mass of the molecule, which is on the C_{2v} axis, and close to the Se atom. The moments of inertia about the axes are related to the rotational constants (in cm^{-1}) as follows:

$$A = \frac{\hbar}{4\pi c I_a}, \quad B = \frac{\hbar}{4\pi c I_b}, \quad C = \frac{\hbar}{4\pi c I_c}. \tag{3.17}$$

The moment of inertia, I, is the sum of the mass of each molecule multiplied by its squared perpendicular distance from the axis of rotation, $I = \sum_i m_i r_i^2$. Conventionally, $A > B > C$ and hence $I_a < I_b < I_c$. We can treat SeO_2 using the rigid-rotor approximation, in which the bonds between the nuclei are assumed to be rigid and of fixed length. Although this is not strictly true as the bonds do actually change length due to the vibrational motion, it turns out to be a very good approximation.

In some cases it is possible to approximate asymmetric tops to either prolate or oblate symmetric tops depending of the value of Ray's asymmetry parameter. Ray's asymmetry parameter is a measure of the asymmetry of a molecule, and is given by

$$\kappa = \frac{2B - A - C}{A - C}. \tag{3.18}$$

In the case of a prolate top $\kappa = -1$, and for an oblate top $\kappa = 1$. Using the ground state rotational constants determined by Alekseev [3] given in Table 1.6 and the constants for the excited state calculated by King and McLean [4] as given in Table 1.10, the values of κ for the ground and excited states of $^{80}SeO_2$ are $\kappa'' = -0.82$ and $\kappa' = -0.53$ respectively. Hence SeO_2 is strongly asymmetric in both the ground and excited state, and it is not appropriate to use a prolate top approximation.

3.4.1 Rotational Energy Levels

As with any molecule, in order to calculate the rotational energy levels of an asymmetric top it is necessary to solve the Schrödinger equation [5]:

$$H|\Psi\rangle = E|\Psi\rangle \tag{3.19}$$

where H is the complete Hamiltonian for the molecule, containing the kinetic energy and Coulomb potential of the electrons, along with the vibrational and rotational kinetic energy terms:

$$H = H_{el} + H_{vib} + H_{rot}. \tag{3.20}$$

It is necessary to consider the rotational part of this Hamiltonian, H_{rot}, in more detail.

In the case of an asymmetric molecule it is not possible to rearrange H_{rot} so that it only contains J^2 and one component of J. H_{rot} is given by

$$H_{rot} = AJ_a^2 + BJ_b^2 + CJ_c^2 \tag{3.21}$$

where J_a, J_b and J_c are the components of the total angular momentum, J, along the a, b and c axes respectively (as shown in Figure 3.2).

To obtain expressions for the rotational energy levels it is necessary to solve the eigenvalue equation

$$H_{rot}|JK\rangle = E_{rot}|JK\rangle \tag{3.22}$$

where $|JK\rangle$ are the basis set functions used to set up the matrix H_{rot}. K is another quantum number, which is the projection of J onto the top axis of the molecule, in this case the a-axis. To set up the matrix of H_{rot} we have to generate the complete set of elements $\langle J'K'|H_{rot}|J''K''\rangle$ for any given J. Since it is not possible to rearrange H_{rot} to comprise of only J^2 and one component of J, H_{rot} will not be diagonal in K. Therefore it is necessary to find a new set of functions, $|J\Gamma\rangle$, in which H_{rot} is diagonal. This new set of functions is a linear combination of the original basis functions:

$$|J\Gamma\rangle = \sum_K a_K^J |JK\rangle \tag{3.23}$$

such that

$$H|J\Gamma\rangle = E(J\Gamma)|J\Gamma\rangle \tag{3.24}$$

where $E(J\Gamma)$ is the energy of the rotational state $|J\Gamma\rangle$.

It turns out to be convenient to rearrange H_{rot} in the same representation as is used for a symmetric top molecule:

$$H_{rot} = \frac{1}{2}(B+C)\left(J_b^2 + J_c^2\right) + AJ_a^2 + \frac{1}{2}(B-C)\left(J_b^2 - J_c^2\right) \tag{3.25}$$

$$= \alpha J^2 + \beta J_a^2 + \gamma\left(J_+^2 + J_-^2\right) \tag{3.26}$$

where

$$\alpha = \frac{1}{2}(B+C), \quad \beta = A - \frac{1}{2}(B+C), \quad \gamma = \frac{1}{4}(B-C). \tag{3.27}$$

It is the asymmetric term γ that tends to spoil the symmetric top form of Equation 3.26, and the ratio of γ to one of the other constants, usually β, is used as a measure of how asymmetric a molecule really is - in other words κ can be rewritten in terms of α, β and γ.

In order to continue with setting up the matrix of H_{rot}, the following non-vanishing matrix elements are required:

$$\langle JK|J^2|JK\rangle = J(J+1) \tag{3.28}$$

$$\langle JK|J_a^2|JK\rangle = K^2 \tag{3.29}$$

$$\begin{aligned} \langle JK+2|J_-J_-|JK\rangle &= \langle JK|J_+J_+|JK+2\rangle \\ &= \sqrt{(J-K)(J+K+1)(J-K-1)(J+K+2)} \end{aligned} \tag{3.30}$$

$$\begin{aligned} \langle JK-2|J_+J_+|JK\rangle &= \langle JK|J_-J_-|JK-2\rangle \\ &= \sqrt{(J+K)(J-K+1)(J+K-1)(J-K+2)}. \end{aligned} \tag{3.31}$$

Now we can try to solve H_{rot}. For low values of J is it possible to do this algebraically, as will be discussed below. For larger values of J, above about 5, the problem rapidly becomes much more complicated and a computer is required to diagonalise the large matrices involved. The Hamiltonian matrix is diagonal in J, and so reduces to a set of blocks of differing J. The dimension of each of these blocks is $(2J+1) \times (2J+1)$, which is equal to the range of K for any given J value.

If we now consider the case of $J = 2$ by way of an example, we get a 5×5 matrix

representation of H_{rot}, which is given by

$$\begin{pmatrix} 6\alpha+4\beta & 0 & \gamma\sqrt{24} & 0 & 0 \\ 0 & 6\alpha+\beta & 0 & 6\gamma & 0 \\ \gamma\sqrt{24} & 0 & 6\alpha & 0 & \gamma\sqrt{24} \\ 0 & 6\gamma & 0 & 6\alpha+\beta & 0 \\ 0 & 0 & \gamma\sqrt{24} & 0 & 6\alpha+4\beta \end{pmatrix} \tag{3.32}$$

The columns of this matrix are labelled $|K\rangle = |-2\rangle, |-1\rangle, \ldots |+2\rangle$ from left to right, and the rows $\langle K| = \langle -2|, \langle -1|, \ldots \langle +2|$ from top to bottom, as is the usual convention. A transformation is required to diagonalise the matrix, and this is found to be a basis function of the type

$$\frac{1}{\sqrt{2}}\{|J+K\rangle \pm |J-K\rangle\}. \tag{3.33}$$

This transformation is carried out using the Wang matrix, U_J, which has dimensions of $(2J+1)\times(2J+1)$, and has the form

$$U_J = \frac{1}{\sqrt{2}} \begin{pmatrix} \ddots & & & & & & \\ & -1 & 0 & 0 & 0 & 1 & \\ & 0 & -1 & 0 & 1 & 0 & \\ & 0 & 0 & \sqrt{2} & 0 & 0 & \\ & 0 & 1 & 0 & 1 & 0 & \\ & 1 & 0 & 0 & 0 & 1 & \\ & & & & & & \ddots \end{pmatrix} \tag{3.34}$$

The matrix is transformed according to

$$U_J H_{rot} U_J = \tilde{H}_{rot}. \tag{3.35}$$

When this transformation is carried out on the matrix representation for $J = 2$, the new

matrix is given by

$$\begin{pmatrix} 6\alpha+4\beta & 0 & 0 & 0 & 0 \\ 0 & 6\alpha+\beta-6\gamma & 0 & 0 & 0 \\ 0 & 0 & 6\alpha & 0 & \gamma\sqrt{48} \\ 0 & 0 & 0 & 6\alpha+\beta+6\gamma & 0 \\ 0 & 0 & \gamma\sqrt{48} & 0 & 6\alpha+4\beta \end{pmatrix} \tag{3.36}$$

This matrix then needs to be made into three 1×1 blocks and one 2×2 block, by swapping the appropriate rows and columns, in order to complete the diagonalisation:

$$\begin{pmatrix} 6\alpha+4\beta & 0 & 0 & 0 & 0 \\ 0 & 6\alpha+\beta-6\gamma & 0 & 0 & 0 \\ 0 & 0 & 6\alpha & \gamma\sqrt{48} & 0 \\ 0 & 0 & \gamma\sqrt{48} & 6\alpha+4\beta & 0 \\ 0 & 0 & 0 & 0 & 6\alpha+\beta+6\gamma \end{pmatrix} \tag{3.37}$$

It is now possible to solve this matrix for H_{rot} and determine expressions for the rotational energy levels when $J=2$:

$$E_{rot}(2_{20}) = 2A+2B+2C+2\sqrt{(B-C)^2+(A-C)(A-B)} \tag{3.38}$$

$$E_{rot}(2_{21}) = 4A+B+C \tag{3.39}$$

$$E_{rot}(2_{11}) = A+4B+C \tag{3.40}$$

$$E_{rot}(2_{12}) = A+B+4C \tag{3.41}$$

$$E_{rot}(2_{02}) = 2A+2B+2C-2\sqrt{(B-C)^2+(A-C)(A-B)} \tag{3.42}$$

using the notation $E_{rot}(J_{K_aK_c})$. K_a is the projection of J onto the a axis, and is the value of $|K|$ for the limiting case of a prolate symmetric top. Similarly, K_c is the projection of J onto the c axis, and is the value of $|K|$ for the limiting case of an oblate top.

3.5 Rotational Selection Rules

As with all molecules, the dipole selection rule that

$$\Delta J = 0, \pm 1 \text{ with the restriction that } J = 0 \nleftrightarrow J = 0 \tag{3.43}$$

applies to SeO_2. The total value of K ($K = K_a + K_c$) must obey the condition that

$$K = J \text{ or } J + 1. \tag{3.44}$$

Further restrictions apply to K_a and K_c depending on which axis the transition moment lies along. If the transition moment lies along the a-axis it is known as an A-type transition, and the selection rules for K_a and K_c are

$$\Delta K_a = 0, \pm 2, \ldots \quad \Delta K_c = \pm 1, \pm 3, \ldots \tag{3.45}$$

A B-type transition, with the transition moment lying along the b-axis, has the selection rules

$$\Delta K_a = \pm 1, \pm 3, \ldots \quad \Delta K_c = \pm 1, \pm 3, \ldots \tag{3.46}$$

and a C-type transition, which has the transition moment lying along the c-axis, obeys the following selection rules

$$\Delta K_a = \pm 1, \pm 3, \ldots \quad \Delta K_c = 0, \pm 2, \ldots \tag{3.47}$$

The transitions studied here are thought to be A-type, and it will be possible to confirm or reject this by the nature of the rotational transitions observed. Obviously the transitions with $\Delta K_a = 0$ and $\Delta K_c = \pm 1$ will be expected to be much stronger that those with the more relaxed selection rules ($\Delta K_a = \pm 2$ etc); however these transitions are allowed due to the mixing of the basis states.

3.6 Nuclear Spin Statistics

Nuclear spin statistics play an important role when studying the spectrum of SeO_2, and have a dramatic effect on the appearance of the rotational structure of the spectrum. The two oxygen nuclei in SeO_2 are identical. A ^{16}O nucleus has a nuclear spin, I, of zero, which make it a Boson. This means that the overall wavefunction, Ψ_{tot}, must be symmetric with respect to interchange of these two identical nuclei.

According to the Born-Oppenheimer approximation, the total wavefunction can be rewritten as the product of the electronic, vibrational, rotational and nuclear spin components:

$$\Psi_{tot} = \Psi_{el}\Psi_{vib}\Psi_{rot}\Psi_{ns}. \tag{3.48}$$

Hence the symmetry of the total wavefunction is the product of the symmetries of its individual components.

It is now necessary to consider the symmetries of the individual components in turn. The nuclear spin wavefunction, Ψ_{ns}, must by symmetric with respect to interchange of the two identical O nuclei (P_{12}) because the combination of two Bosons will only allow this result. It can also be shown that the vibrational wavefunctions, Ψ_{vib}, of the ground and excited states being studied are also symmetric. This leaves us with the electronic and rotational wavefunctions, Ψ_{el} and Ψ_{rot}, the product of which will have to be symmetric in order to keep the overall product and hence the total wavefunction symmetric. As previously discussed, the ground electronic state has been determined as $^1A_1$ [6] which is totally symmetric, hence the rotational wavefunction of the ground state must also be symmetric with respect to P_{12}. The excited electronic state is believed to be $^1B_2$ [7, 4], which is antisymmetric, and so in this case the rotational wavefunction must also be antisymmetric.

The symmetry of the rotational wavefunction of an asymmetric top with respect to P_{12} is determined by the values of the quantum numbers K_a and K_c. This rotational wavefunction is symmetric if K_a and K_c are either both odd or both even (often denoted ee or oo). It is antisymmetric if K_a is even and K_c odd, or vice versa (denoted eo or oe). So if we consider, for example, the energy level 2_{12}, it is forbidden in the $^1A_1$ ground state

but is allowed in the $^1B_2$ excited state. The result of this is that half the rotational energy levels are missing in both the ground and excited states, and hence no asymmetry doublets are observed in practice. Figure 3.3 shows all the possible energy levels for the first few J values, in K_a stacks. In the ground state only those levels shown in red are allowed, and those in black are forbidden. In contrast, in the $^1B_2$ excited state only the levels shown in black are allowed and those in red are forbidden.

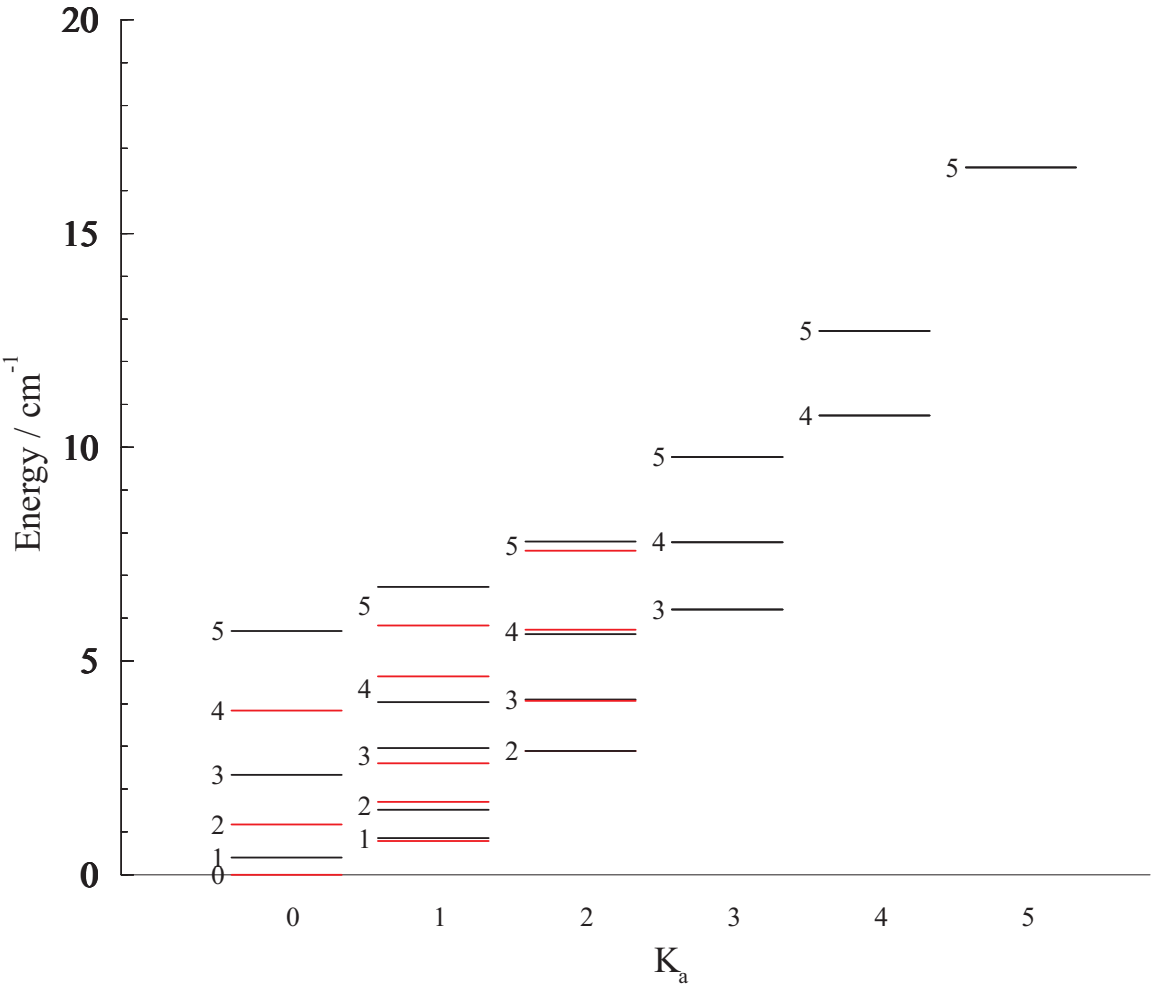

Figure 3.3: The rotational energy levels of an asymmetric top. The levels are represented in stacks with a given K_a value and the values of J is to the left. Note that the asymmetry splitting decreased with K_a and increases with J. For a given J value the energy increases with increasing $\tau = K_a - K_c$.

Bibliography

[1] D.A. Ramsey. *Electronic Spectra of Polyatomic Molecules and the Configuration of Molecules in Excited Electronic States*, Volume 2, chapter 4 of *Determination of Organic Structures by Physical Methods*. Academic Press Inc., New York, 1962.

[2] A.D. Walsh. The Electronic Orbitals, Shapes, and Spectra of Polyatomic Molecules. Part I. AH_2 Molecules. *Journal of the Chemical Society*, 1953.

[3] E.A. Alekseev, O.I. Baskakov, and S.F. Dyubko. Microwave Spectrum of Selenium Dioxide. *Proceedings of SPIE - International Society of Optical Engineers*, **3090** (High Resolution Molecular Spectroscopy), 1997.

[4] G.W. King and P.R. McLean. Selenium Dioxide: Rotational Analysis and Franck-Condon Calculations for the 3130 Å $^1B_2$ - $^1A_1$ Absorption System. *Journal of Molecular Spectroscopy*, **52**, 1974.

[5] H.W. Kroto. *Molecular Rotation Spectra*. Dover Publications, Inc., 1992.

[6] H. Takeo, E. Hirota, and Y. Morino. Equilibrium Structure and Potential Function of Selenium Dioxide by Microwave Spectroscopy. *Journal of Molecular Spectroscopy*, **34**, 1970.

[7] G.W. King and P.R. McLean. Selenium Dioxide: Vibrational Analysis of the 3130 Å $^1B_2$ - $^1A_1$ Absorption System. *Journal of Molecular Spectroscopy*, **51**, 1974.

Chapter 4

The Vibrationally Resolved Spectrum

4.1 Introduction

At the start of this research project only very short survey spectra of SeO_2 were recorded, starting with the 1_0^3 band, as this was the one studied at higher resolution by King and McLean [1]. A couple of other bands in the symmetric stretching progression (ν_1) were recorded at the same time (1_0^4 and 1_0^2). However the main aim of this work was always to record the 1_0^3 band and other bands in the progression of the symmetric stretching vibration at rotational resolution, and to carry out a full rotational analysis of these bands. Such an analysis would enable us to determine the O−Se−O bond angle and the Se−O bond length. When analysing these rotationally resolved bands, perturbations were seen in a number of the bands, and as a result of this it was deemed necessary to carry out a much more extensive survey study to investigate possible causes of these perturbations. The results of this broader survey spectrum are presented here.

The absorption spectrum reported by King and McLean [2] is relatively simple, and all the bands they report have been assigned to one electronic transition. They observed progressions with intervals of 650 cm^{-1}, which corresponds to the symmetric stretching frequency in the excited state. The corresponding members of the different progressions were displaced by about 250 cm^{-1}, which is assigned to the excited state bending frequency.

The progressions can therefore be labelled $1_0^n 2_0^m$. These progressions are very long in ν_1, with a maximum intensity around $n = 5$. At higher n values the bands become very weak and diffuse, which suggests an onset of predissociation. In contrast, we find the spectrum recorded using the technique of Laser Induced Fluorescence to be much more complicated. The spectrum recorded contains almost 5 times as many bands as were observed by King and McLean in the same region. It is not possible to account for all of these bands by considering transitions to only one excited electronic state as King and McLean did, and it is safe to say that the spectrum must consist of transitions to at least two different electronic states.

4.2 Survey Spectrum

The survey spectrum of SeO_2, between 292 and 327 nm is shown in Figure 4.1. The assignments made by King and McLean are labelled on the spectrum [2]. The different sections are not all on the same intensity scale, but instead have been scaled so that the greatest number of peaks can be seen with a reasonable size. The positions of the bands and their relative intensities are given in Table 4.4, at the end of this chapter.

4.2.1 Measurement and Calibration

The spectrum was initially recorded in sections of about 4 nm of the fundamental wavelength which corresponds 2 nm of frequency doubled light, with the laser step size set to 0.005 nm for the fundamental frequency, which is equivalent to a step size of ~ 0.141 cm^{-1} in the region of interest. Consecutive scans always contained at least one peak in common, which could be used to scale the scans relative to each other, and hence obtain information about the relative intensities of the peaks. This was done firstly by normalising the baseline of the scan to be horizontal, and then by scaling adjacent scans so that the overlapping peaks were of the same height.

Each individual peak was then re-recorded using a smaller step size of 0.001 nm or 0.029 cm^{-1} of the fundamental frequency, and scanning no more than 1 nm of the fundamental frequency or 0.5 nm of the frequency doubled light at one time. These scans are done

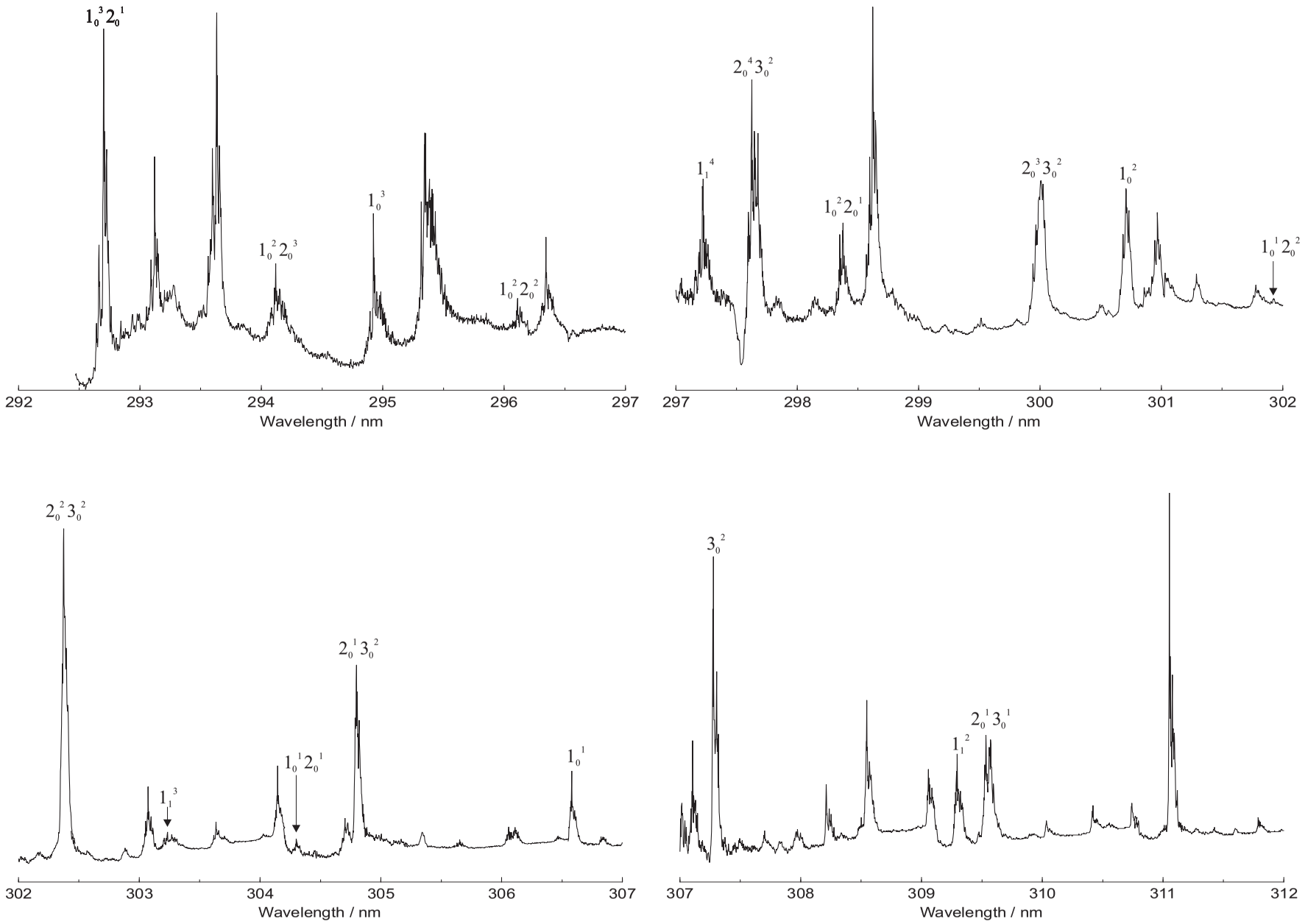

Figure 4.1: The vibrationally resolved survey spectrum of SeO_2 between 292 and 327 nm. The assignments made by King and McLean [2] are labelled on the spectrum.

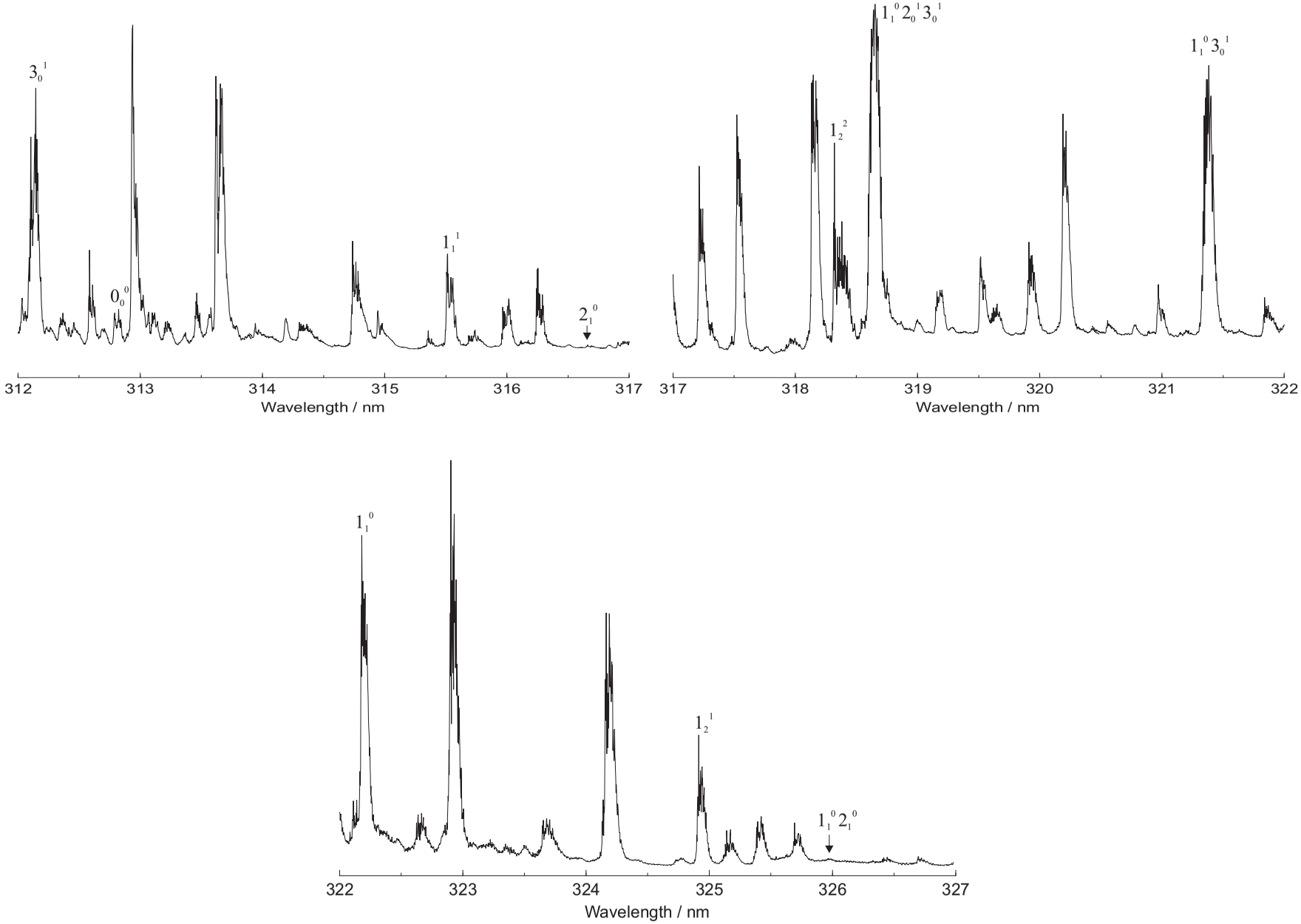

Figure 4.1 cont'd

with a smaller step size to provide a more fruitful recording and to enable a more accurate measurement of the position of maximum intensity in each band. These scans do show some of the rotational structure, but it is not fully resolved. The laser linewidth is 0.2 cm^{-1} for the fundamental frequency and approximately 0.28 cm^{-1} for the frequency doubled light. To resolve as much structure as possible it is necessary to have about 3 or 4 steps within the width of the laser line. The step size of 0.001 nm or 0.029 cm^{-1} of the fundamental frequency corresponds to a step size of 0.0005 nm or 0.059 cm^{-1} of the frequency doubled light, and hence between 4 and 5 steps within the 0.28 cm^{-1} linewidth. Therefore the resolution is limited by the laser linewidth, and as much structure as is possible is resolved in these scans. Use of a smaller step size would not improve the resolution.

The positions of the bands are measured from the feature of greatest intensity, and as a result are slightly different from those obtained by King and McLean, as they measured the positions of the band heads in the coarse $\Delta K = 0$ structure with a sample at 220 °C. The 1_0^1 band is shown in Figure 4.2 as an example of one of these scans done with a step size of 0.001 nm, to illustrate both the partially resolved rotational structure and the point of greatest intensity from which the position of the band is measured.

There is a small error in the wavelength reading given by the Lambda Physik FL3002 pulsed dye laser, and it was therefore necessary to calibrate the scans and peak positions using some other method. The procedure adopted for calibrating the spectrum, based on the assumption that the laser scans in a linear manner as far as wavelength is concerned, is as follows. The air wavelength of the fundamental frequency of the maximum of each peak was determined from the wavelength reading displayed by the laser. This value was then converted to vacuum wavenumbers, and then doubled, to convert from the fundamental frequency to the doubled frequency, and to get the position of the maximum intensity of the band in vacuum wavenumbers. The band origins of the 1_0^1, 1_0^2 and 1_0^3 bands and the rotational constants of these bands have been accurately determined from the analysis of the rotationally resolved spectra of these individual bands (Chapter 5). A simulated spectrum was produced for each of the bands, using the same linewidth as the laser. From these simulations it was possible to determine an accurate value for the position of maximum intensity in each band. Comparison of the positions of maximum intensity from

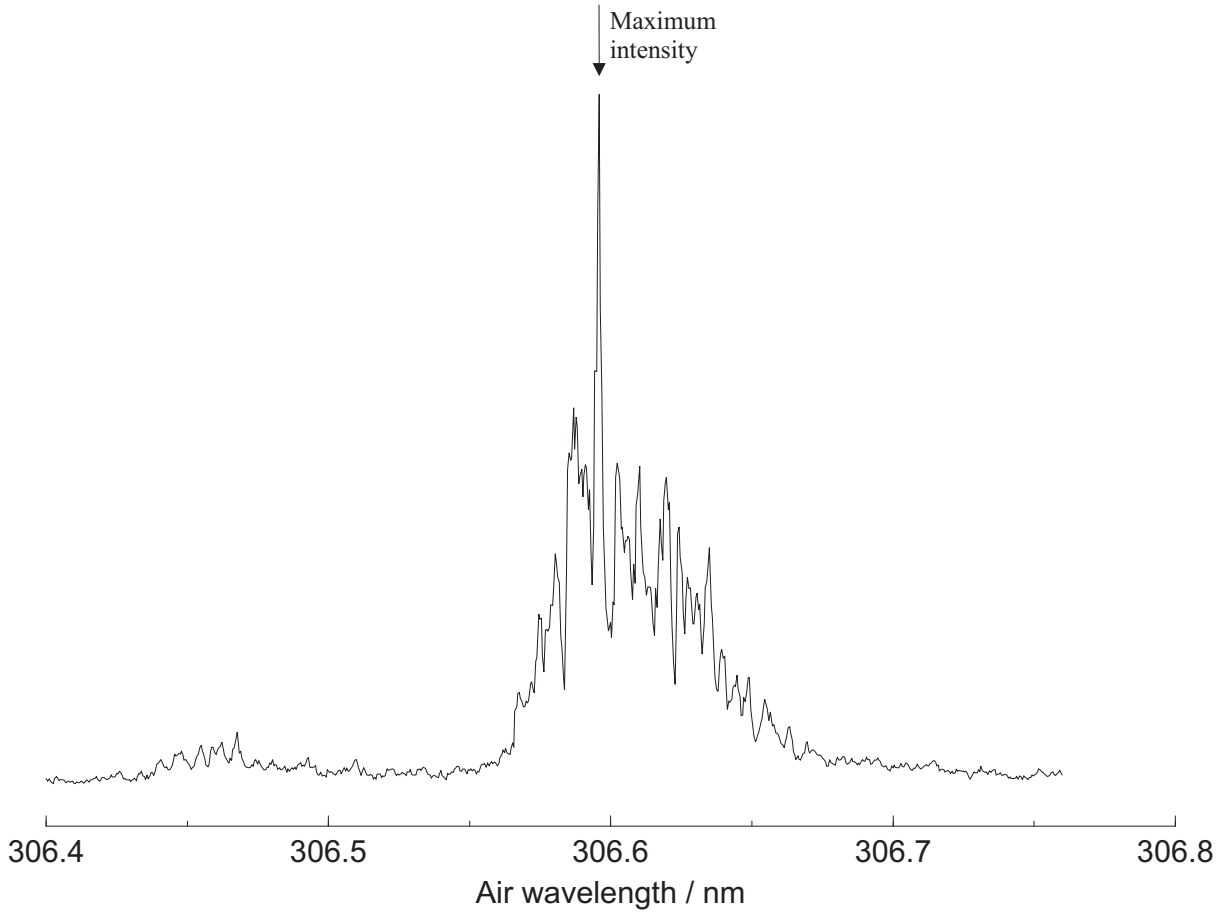

Figure 4.2: The 1_0^1 band recorded with a step size of 0.001 nm or 0.029 cm^{-1}. The rotational structure is visible, but not fully resolved. The point of maximum intensity, where the position of the band was measured from, is marked with an arrow.

the laser readings and the simulations showed there to be a linear relationship between the two, and it was possible to plot a 'correction curve'. From this linear relationship the corrected wavenumbers for all the other bands could be calculated from their laser reading. It is estimated that the positions of the features measured are accurate to 0.5 cm^{-1}.

The relative intensities of the transitions were measured by comparing the height of each peak with that of the most intense peak in the recorded spectrum. The intensity of a transition in a Laser Induced Fluorescence (LIF) spectrum is the convolution of the absorption intensity and the fluorescence intensity. The absorption intensity is a function of the Einstein coefficient of stimulated absorption, B, whereas the fluorescence intensity

is a function of the Einstein coefficient of spontaneous emission, A. King and McLean recorded the straight absorption spectrum so we would not expect the relative intensities observed here to be the same as the intensities they observed.

4.2.2 Assignments

4.2.2.1 Bands in the Symmetric Stretching Progression

Some of the bands assigned by King and McLean [2] have been reassigned in the present work, as can be seen in Table 4.4. By far the most significant of these is the reassignment of the 0_0^0 band. After recording and analysing the 1_0^1, 1_0^2 and 1_0^3 bands at rotational resolution (Chapter 5) it was possible to make predictions of the band origin and the rotational constants of the 0_0^0 band. The vibrational energy levels of a C_{2v}, AB_2 molecule are given by [3]:

$$\begin{aligned} G(v_1, v_2, v_3) &= \omega_1\left(v_1+\frac{1}{2}\right)+\omega_2\left(v_2+\frac{1}{2}\right)+\omega_3\left(v_3+\frac{1}{2}\right) \\ &+x_{11}\left(v_1+\frac{1}{2}\right)^2+x_{22}\left(v_2+\frac{1}{2}\right)^2+x_{33}\left(v_3+\frac{1}{2}\right)^2 \\ &+x_{12}\left(v_1+\frac{1}{2}\right)\left(v_2+\frac{1}{2}\right)+x_{23}\left(v_2+\frac{1}{2}\right)\left(v_3+\frac{1}{2}\right) \\ &+x_{13}\left(v_1+\frac{1}{2}\right)\left(v_3+\frac{1}{2}\right)+\ldots \end{aligned} \tag{4.1}$$

When considering only vibrations in the symmetric stretching progression, ν_1, this equation can be rewritten as

$$G(v_1) = \omega_1\left(v_1+\frac{1}{2}\right)+x_{11}\left(v_1+\frac{1}{2}\right)^2+\text{constant.} \tag{4.2}$$

For transitions from only the 0_0^0 vibrational level of the ground state, G'' is a constant, and hence

$$\nu = \nu_e + G' - G'' \tag{4.3}$$

$$= \omega_1' \left(v_1' + \frac{1}{2}\right) + x_{11} \left(v_1' + \frac{1}{2}\right)^2 + \text{constant} \quad (4.4)$$

where $\nu_e = T_e' - T_e''$.

The band origins of the 1_0^1, 1_0^2 and 1_0^3 bands of $^{80}SeO_2$ can be fitted to a to a simple quadratic equation of the form $Av_1^2 + Bv_1 + C$, from which we can obtain a good estimation for the band origin of the 0_0^0 band. Using this method the origin of the 0_0^0 band is estimated to be at 31983.00 cm^{-1}. Similarly, the A', B' and C' rotational constants of the 1_0^1, 1_0^2 and 1_0^3 bands can be fitted to linear equations to predict their values in the 0_0^0 band. The following values were obtained for the excited state rotational constants of the 0_0^0 transitions of $^{80}SeO_2$ from these fits:

$$\begin{aligned} A' &= 0.644469 \text{ cm}^{-1} \\ B' &= 0.290343 \text{ cm}^{-1} \\ C' &= 0.200275 \text{ cm}^{-1}. \end{aligned}$$

King and McLean assigned the 0_0^0 transition to a band at 31961.48 cm^{-1}, which from this point will be referred to as Band X. It is immediately obvious that the value predicted for the band origin of the 0_0^0 band based on the origins of the 1_0^1, 1_0^2 and 1_0^3 bands is considerably different from the position of Band X assigned to the 0_0^0 transition by King and McLean.

A simulation of the 0_0^0 band was performed, combining $^{80}SeO_2$ and $^{78}SeO_2$ as the two major isotopomers. The constants above were used for $^{80}SeO_2$. Isotopic shifts of the 1_0^1, 1_0^2 and 1_0^3 bands predict the band origin of $^{78}SeO_2$ to be about 0.4 cm^{-1} below the origin of the $^{80}SeO_2$ band (Section 5.9), so a value of 31982.60 cm^{-1} was used in the simulation for the origin of the $^{78}SeO_2$. The line width was taken as 0.3 cm^{-1}, and hence it was not deemed necessary to calculate different rotational constants for the $^{78}SeO_2$ isotopomer as the differences from the $^{80}SeO_2$ isotopomer are too small to be resolved. The results of this simulation are shown in Figure 4.3. The first thing to notice from this figure is that the band at 31983.24 cm^{-1} agrees much better with the position of the simulated band than the band at 31961.48 cm^{-1} (Band X) does. Perhaps more importantly, the resolved structure of the band also agrees remarkably well with the simulation. The structure of Band X does not agree as well with the simulation. This new assignment of the 0_0^0 band

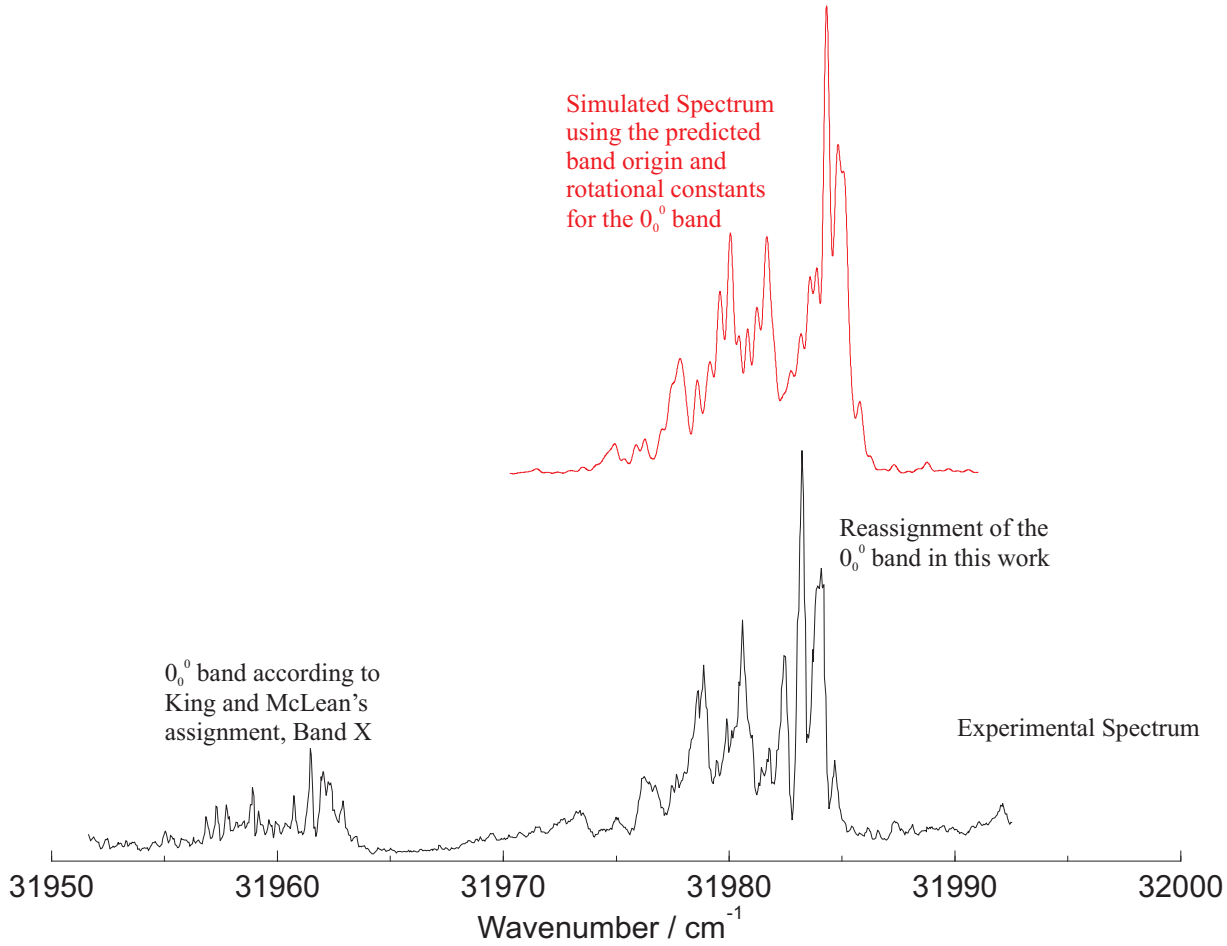

Figure 4.3: A simulation of the 0_0^0 band, along with the experimental spectrum to show King and McLean's assignment and the reassignment of the band in this work.

to 31983.24 cm^{-1} also gives a more convincing vibrational progression in ν_1'. Combining these observations we can say with some confidence that this new assignment is much more credible that than of King and McLean.

By comparing the simulation of the 0_0^0 band with the experimentally observed band we can make a better estimation of the origin of this band. The simulated band, which used 31983.00 cm^{-1} as the origin, has its maximum at 31984.3104 cm. The difference between the maximum and origin in the experimental band will be the same as that in the simulated band. Therefore, from the experimental maximum of 31983.24 cm^{-1}, the new estimate of the band origin is 31981.93 cm^{-1}.

A similar process can be used to predict the position of the origin of the 1_0^4 band. Although the survey scan was not fully extended as far as this at the short wavelength end, the 1_0^4 band had been previously recorded. The band origin was predicted to be at 34554.38 cm^{-1} using the same quadratic equation used to predict the origin of the 0_0^0 band. Similarly, the same linear equations as those used for the 0_0^0 band can be used to predict the rotational constants and the isotopic splitting. The following values were obtained for the rotational constants of $^{80}SeO_2$ in the $v_1 = 4$ excited state:

$$\begin{aligned} A' &= 0.640968 \text{ cm}^{-1} \\ B' &= 0.285180 \text{ cm}^{-1} \\ C' &= 0.198984 \text{ cm}^{-1} \end{aligned}$$

and the $^{78}SeO_2$ isotopomer was predicted to have its band origin about 5.55 cm^{-1} higher in energy than that of $^{80}SeO_2$. The maximum in the simulation was 1.22 cm^{-1} above the band origin. Experimentally, the 1_0^4 band was observed with its maximum at 34555.45 cm^{-1}, and therefore we can estimate the experimental value for the band origin of the 1_0^4 band to be 34554.23 cm^{-1}.

4.2.2.2 Bands Involving the Bending Vibration

Transitions involving only quanta of the bending vibration (ν_2) excited in the upper electronic state were not observed by King and McLean [2]. However we would expect to see such transitions, and the 2_0^1 band should be seen about 258 cm^{-1} above the 0_0^0 band. There is a band observed at 32245.78 cm^{-1}, which very close to where we would expect this band to be, and so is provisionally assigned to the 2_0^1 transition. It is possible to perform an approximate simulation of this band using the rotational constants of the 0_0^0 band. These rotational constants are obviously not going to be exactly the right values for the 2_0^1 band; however as is seen Chapter 5, the excited state constants do not vary very much between the different vibrational bands, so the values estimated for the 0_0^0 band can also be used as a first estimate for the rotational constants of the 2_0^1 band. We also need to estimate a value for the isotopic splitting between the $^{78}SeO_2$ and $^{80}SeO_2$ isotopes. From the rotational analysis of the 1_0^1 band (Section 5.6), the band origin of $^{78}SeO_2$ was determined to be 1.1042 cm^{-1} higher in energy than that of $^{80}SeO_2$. In King and McLean's work they found

the $^{78}SeO_2$ isotopomer of the $1_0^1 2_0^1$ band to be 2.0 cm^{-1} higher in energy than the same band for $^{80}SeO_2$. From this, we can estimate that in the 2_0^1 band the origin of $^{78}SeO_2$ should be shifted 0.9 cm^{-1} to higher wavenumber than the origin of $^{80}SeO_2$. Comparisons between the 1_0^2 and $1_0^2 2_0^1$ bands and the 1_0^3 and $1_0^3 2_0^1$ bands should yield similar results, enabling us to make a good estimate of the isotopic splitting in the 2_0^1 band. However it is found that the 1_0^2 and $1_0^2 2_0^1$ bands suggest $^{78}SeO_2$ to be shifted to only 0.3 cm^{-1} higher wavenumber than $^{80}SeO_2$, whereas the 1_0^3 and $1_0^3 2_0^1$ bands suggest this shift to be 1.3 cm^{-1}. From these different values we cannot obtain an reliable estimate of the splitting, but can say that it is likely to be between 0.5 and 1.0 cm^{-1}. The results of simulations using isotopic shifts of 0.5 and 1.0 cm^{-1}, and the rotational constants of the 0_0^0 band are illustrated in Figure 4.4. These simulations agree reasonable well with the experimental band, especially given

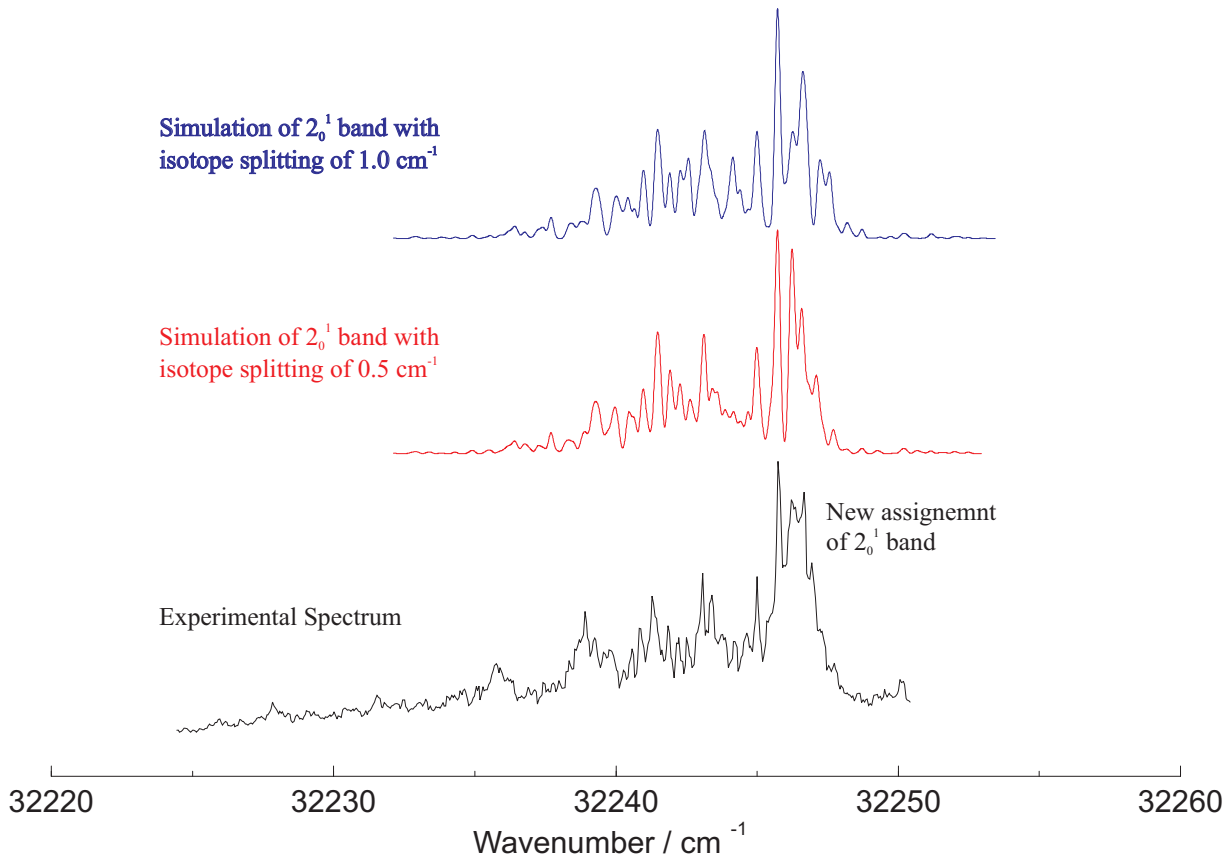

Figure 4.4: The band assigned to the 2_0^1 transition, along with simulations of this band using the estimated rotational constants of the 0_0^0 band as a first estimate, with isotope splittings of 0.5 cm^{-1} and 1.0 cm^{-1}.

the fact that the rotational constants and values used for the isotope splitting are only first estimates of the true values. By looking at the structure on the right hand side of the three spectra it seems likely that the value of 0.5 cm^{-1} for the isotopic splitting is closer to the true value than 1.0 cm^{-1} is, although it not exactly right.

This new assignment of the 2_0^1 band is 262.54 cm^{-1} above the 0_0^0 band, and so we would expect the 2_0^2 to be approximately another 263 cm^{-1} higher in energy. A band is observed at 32512.78 cm^{-1}, which is 267 cm^{-1}above the 2_0^1 band. Allowing for anharmoncities, this is a perfectly acceptable assignment for the 2_0^2 band.

The $1_0^1 2_0^1$ and $1_0^1 2_0^2$ bands have also been reassigned. According to King and McLean's assignments, the difference between the positions of the 1_0^1 and $1_0^1 2_0^1$ bands is 245.69 cm^{-1}, and that between the $1_0^1 2_0^1$ and $1_0^1 2_0^2$ bands is 261.79 cm^{-1}. The difference between these two differences gives us the anharmonic term of the vibrational frequency, which is 16.1 cm^{-1} using these values. This is much too large a value when compared with the anharmonic terms in the other progressions observed. The new assignments given in Table 4.4 result in a much smaller anharmonic term, and also enable the progression to be extended to the $1_0^1 2_0^3$ and $1_0^1 2_0^4$ bands. These reassignments also agree well with the new assignments of the 2_0^1 and 2_0^2 bands. As for the 2_0^1 band, we can perform a simulation of the $1_0^1 2_0^1$ band using the rotational constants determined for the 1_0^1 band (Section 5.6) as a first estimate for those of the $1_0^1 2_0^1$ band, to help confirm this reassignment. The isotopic splitting between $^{78}SeO_2$ and $^{80}SeO_2$ is taken to be 2.0 cm^{-1}, as determined by King and McLean. The results of this simulation are shown in Figure 4.5. The simulation shows a broader band with more resolved structure than the experimental band, however as is the case with the simulations for the 2_0^1 band, the rotational constants used have not been accurately determined for this band and so are not necessarily correct, but are taken to be the same as those of the 1_0^1 band as a first estimate. Given this fact, the simulation reproduces the main features of the experimental spectrum fairly well. In addition, the peaks assigned to these transitions by King and McLean were quite small in the LIF spectrum, especially that for the $1_0^1 2_0^1$ band, as can be seen in Figure 4.5. The new assignments are more intense and compare more favourably with the intensities of other progressions observed.

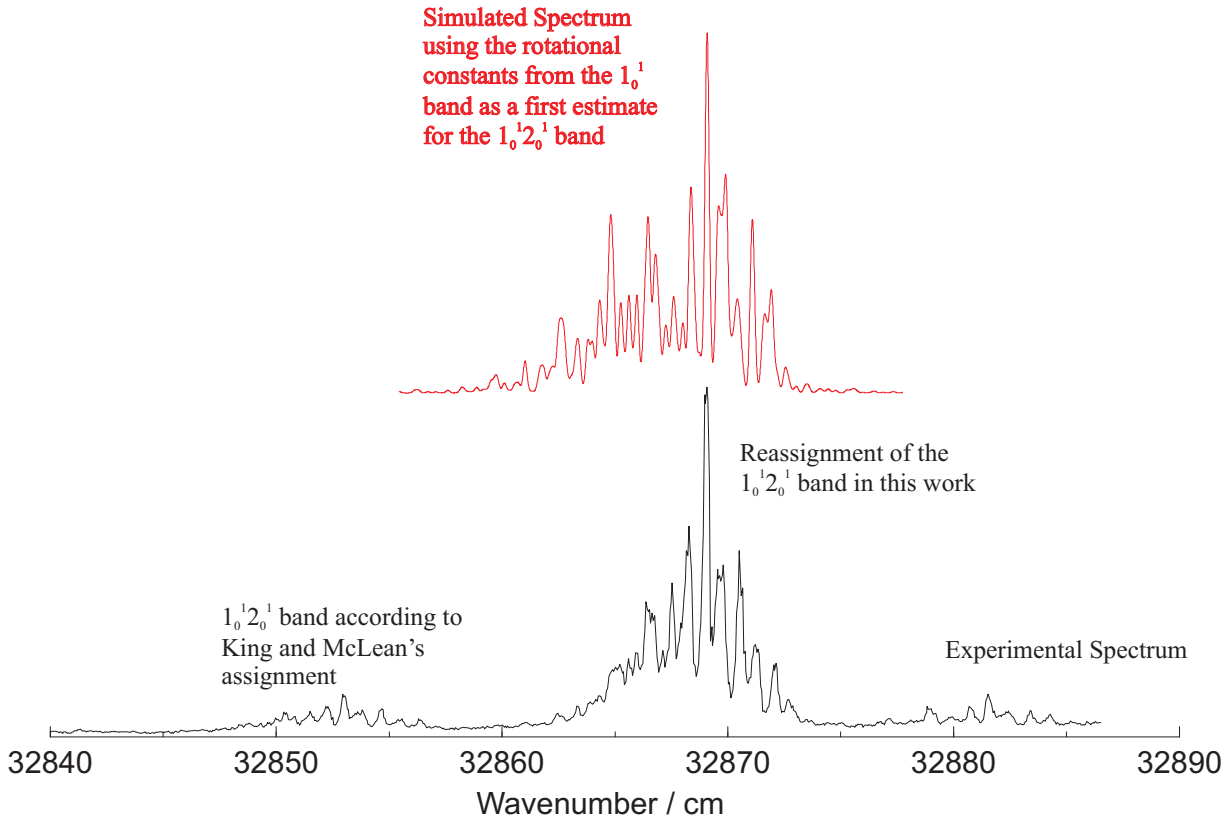

Figure 4.5: The band assigned to the $1_0^1 2_0^1$ transition, along with a simulation of this band using the rotational constants determined for the 1_0^1 band as a first estimate.

4.2.2.3 Determination of Excited State Vibrational Wavenumbers

After making these new assignments it was possible to fit the band origins of all these bands together with those of the 1_0^1, 1_0^2 and 1_0^3 bands determined from their rotational analysis (Chapter 5). This was done using a simple Fortran program called VIBFIT which can fit various combinations of the excited and lower state vibration constants. All the transitions assigned here originate from the (000) vibrational level of the ground state, and have quanta of ν_1 or ν_2 or a combination of the two excited in the upper electronic state. By considering Equations 4.1 and 4.3, we can see that these transitions can be fitted to the equation

$$\begin{aligned}\nu &= \nu_e + \omega_1'\left(v_1' + \frac{1}{2}\right) + \omega_2'\left(v_2' + \frac{1}{2}\right) + x_{11}'\left(v_1' + \frac{1}{2}\right)^2 \\ &\quad + x_{12}'\left(v_1' + \frac{1}{2}\right)\left(v_2' + \frac{1}{2}\right) + x_2'\left(v_2' + \frac{1}{2}\right)^2.\end{aligned} \tag{4.5}$$

However it is often more convenient to refer the energies to the lowest vibrational level in each state, in which case Equation 4.5 becomes [3]

$$\nu = \nu_{(000)} + \omega_1^0 v_1' + \omega_2^0 v_2' + x_{11}^0 v_1'^2 + x_{12}^0 v_1' v_2' + x_{22}^0 v_1'^2. \tag{4.6}$$

The origins of the 1_0^1, 1_0^2 and 1_0^3 bands were accurately determined in their rotational analysis and so the origins of these bands were given an uncertainty of 0.005 cm^{-1} in the fit. The origins of all the other bands had to be estimated from their points of maximum intensity, and so were given an uncertainty of 0.5 cm^{-1}. The origins of the 0_0^0 and 1_0^4 bands were estimated from the difference between the point of maximum intensity and the origin in the simulations of these bands, as previously discussed. The origins of the other bands were estimated by assuming that the difference between the point of maximum intensity and the origin would be approximately the same for the same total number of vibrational quanta excited in the upper state. For example, the origin of the 1_0^3 band is 1.2237 cm^{-1} below the maximum, so the difference between the origin and the maximum of the $1_0^1 2_0^2$ band was taken to be the same as this, as both transitions involve exciting a total of three quanta of the normal vibrations in the upper electronic state. The $1_0^1 2_0^4$ has a total of five quanta excited in the upper electronic state. Although it would be possible to estimate the difference between the maximum and the origin in the 1_0^5 band in the same way as for the 0_0^0 and 1_0^4 bands, the rotational constants have not been confirmed for either of these two bands so an estimate of the rotational constants in the 1_0^5 band would be less reliable. Therefore the origin of the $1_0^1 2_0^4$ band was taken to be 1.2191 cm^{-1} below the maximum, which is the value obtained for the 1_0^4 band. This is as good an estimate as any of the origins estimated in this way, especially given the fact that these transitions have an uncertainty of 0.5 cm^{-1} in the fit, and the observed differences between maxima and

band origins vary by less than 0.1 cm^{-1}.

The vibrational constants determined from this fit are given in Table 4.1, and the results of the fit are given in Table 4.2. From these results, the positions of the maxima of the various bands recorded in this study can be considered to be accurate to ± 0.5 cm^{-1}.

Table 4.1: Vibrational constants determined from for the $^1B_2$ state of SeO_2 from the fit of the $1_0^n 2_0^m$ bands. The numbers in brackets represent 1 standard deviation in the units of the last digit given.

Vibrational constant	Value / cm^{-1}
$\nu_{(000)}$	31982.99(11)
ω_1^0	619.32(13)
ω_2^0	266.7(15)
x_{11}^0	5.880(31)
x_{12}^0	-3.7(15)
x_{22}^0	-1.66(55)

Table 4.2: Results of the fit of the $1_0^n 2_0^m$ bands for the $\tilde{C}^1B_2 \leftarrow \tilde{X}^1A_1$ transitions of SeO_2.

Transition	Wavenumber / cm^{-1}	o-c / cm^{-1}	Uncertainty / cm^{-1}
0_0^0	31981.9289	-1.0692	0.5
1_0^1	32608.19988	0.00092	0.005
1_0^2	33245.16241	-0.00089	0.005
1_0^3	33893.88811	0.00033	0.005
1_0^4	34554.2292	-0.1432	0.5
2_0^1	32244.5050	-3.5279	0.5
2_0^2	32511.5154	1.7640	0.5
$1_0^1 2_0^1$	32867.8409	-1.6694	0.5
$1_0^1 2_0^2$	33127.3293	0.1728	0.5
$1_0^1 2_0^3$	33385.2500	3.0758	0.5
$1_0^1 2_0^4$	33631.7237	-1.8031	0.5

The standard deviations of some of the constants in this fit are relatively large, particularly those of ω_2^0 and x_{12}^0, which is also reflected in a large o-c value for some of the transitions assigned. This could be simply due to the method used to estimate the band origins, and a full rotational analysis of each individual bands would be required to obtain accurate values for these origins. The vibrational constants determined here, ω_1^0 and ω_2^0,

are not exactly the same as ν_1 and ν_2 determined by King and McLean [2]. However the two can be related to each other by the equation [3]

$$\nu_i = \omega_i^0 + x_{ii} \tag{4.7}$$

$$= \omega_i + 2x_{ii} + \frac{1}{2}\sum_{k\neq i} x_{ik} + \ldots \tag{4.8}$$

where $x_{ik} = x_{ik}^0$ if higher order terms are neglected. From this equation we can calculate ν_1' to be equal to 625.20 cm^{-1} and ν_2' to be equal to 265.04 cm^{-1}. Unfortunately King and McLean just quote single values for the vibrational constants they determined ($\nu_1' = 648.8$ cm^{-1}, $\nu_2' = 258$ cm^{-1} and $\nu_3' = 77.9$ cm^{-1} for $^{80}SeO_2$), and do not give any indication of their accuracy. Neither do they determine anharmonicities. Therefore when comparing these two sets of results it is only possible to say that the value for ν_1' calculated in this work is significantly smaller than that determined by King and McLean, whereas the value of ν_2' is larger than that of King and McLean. Although we cannot compare the accuracy of the two sets of results directly, the higher resolution of the present work and colder rotational temperature of the sample mean that we can place much more confidence in our values than in those determined by King and McLean.

4.2.2.4 Hot Bands and Other Progressions

The 1_1^0 and 2_1^0 hot bands have also been assigned as a result of the reassignment of the 0_0^0 band in this work. As seen in Table 4.4, these transitions are assigned to features with their maxima at 31062.43 cm^{-1} and 31613.39 cm^{-1} respectively. By comparing simulated spectra of these bands with the experimentally observed structure it is possible to estimate values for the origins of both these bands, in the same way as was done for the 0_0^0 band. The origin of the 1_1^0 band is estimated to be 31061.11 cm^{-1}, which implies that ν_1 is about 920.82 cm^{-1}. Similarly, the origin of the 2_1^0 band is estimated to be at 31612.62 cm^{-1}, which leads to ν_2 being 369.31 cm^{-1}.

A number of other progressions were observed in the spectrum, which cannot be attributed to the same electronic transition, $\tilde{C}^1B_2 \leftarrow \tilde{X}^1A_1$. These progressions are listed

in Table 4.4. The bands in Progression 1 have an initial spacing of 264.44 cm^{-1}, which decreases regularly through the progression, so it is very likely that this progression is in the bending vibration in the excited state. This is very close to the value of 266.7 cm^{-1} determined above for ω_2^0, although we would not necessarily expect the value to be exactly the same in a different electronic state. Similarly bands in Progression 2 have a spacing of around 260 cm^{-1} and so are also very likely to belong to a progression in the bending vibration of the excited state. The spacing between the bands in Progression 3 is around 626 cm^{-1}. This value is slightly larger than the value of 619.32 cm^{-1} determined above for ω_1^0, but it is reasonable to assume that this progression is one in the symmetric stretching vibration of the excited state. The band at 32512.78 cm^{-1} in this progression is at about 10 cm^{-1} higher energy than expected, but the spacing between the bands at 31876.81 and 33128.55 cm^{-1} is exactly twice what we would expect. Therefore we propose that the band at 32509.82 cm^{-1} is perturbed for some reason. It is not possible at this stage to say which electronic transitions these progressions involve, nor if these progressions all arise from the same electronic transition. Further work is required to determine the exact nature of these transitions. However we can say that there are bands from at least one other electronic transition overlapping with the bands from the $\tilde{C}^1B_2 \leftarrow \tilde{X}^1A_1$ transition.

4.3 Lifetime Measurements

In order to determine the fluorescence lifetime of a molecule it is necessary to look at the intensity of the fluorescence at a given time, as a function of the initial intensity and the time:

$$I = I_0 e^{-kt} \tag{4.9}$$

which can be rearranged to

$$\ln\left|\frac{I_0}{I}\right| = kt \tag{4.10}$$

where k is related to the lifetime, τ by

$$\tau = \frac{1}{k}. \tag{4.11}$$

Therefore a plot of $\ln\left|\frac{I_0}{I}\right|$ versus t will be linear, and have a gradient of $\frac{1}{\tau}$.

The lifetimes of the 1_0^1, 1_0^2, 1_0^3 and 1_0^4 bands were measured, along with the band originally thought to be the 0_0^0 transition, Band X, by setting the laser to the point of maximum intensity of these bands, and recording the fluorescence decay curve seen on the oscilloscope at a given instance in time. An example of one of these decay curves is shown in Figure 4.6 for the 1_0^1 band. From this and the equivalent curves for the other bands, the lifetime was calculated to be of the order of 50 ns for the 1_0^1 band, and was found to decrease as v_1' increases. The precise values for the different vibrational states are given

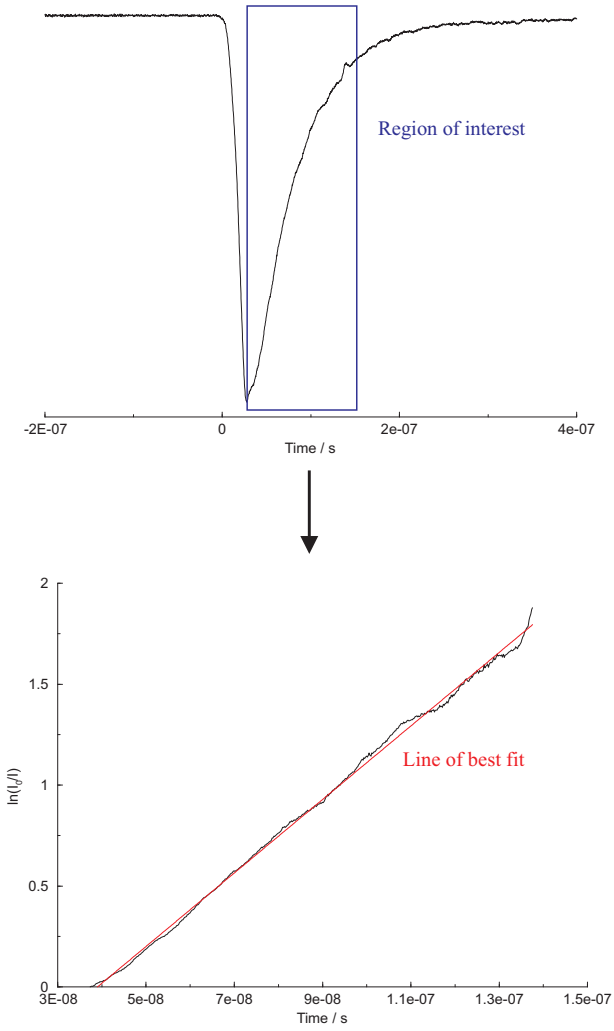

Figure 4.6: The fluorescence decay curve for the 1_0^1 band, along with a plot of $\ln\left|\frac{I_0}{I}\right|$ against the time.

Table 4.3: Fluorescence lifetimes for different vibrational levels of the $^1B_2$ electronic state, and Band X, of SeO_2.

Vibrational level of excited state	Lifetime / ns
Band X	52.8 ± 0.2
(100)	54.9 ± 0.1
(200)	28.3 ± 0.2
(300)	21.8 ± 0.1
(400)	10.9 ± 0.1

in Table 4.3. These values for the lifetimes are very much what we would expect for the fluorescence lifetime of such a molecule connected to the ground state by a fully allowed transition. The fact that the lifetime decreases as v_1' increases may be an indication of the onset of predissociation.

An interesting feature is seen in the fluorescence decay curve of the 1_0^4 band. Figure 4.7 shows this decay curve, in which is is possible to see that the decay curve is not a smooth exponential decay as we would expect to see. This is further illustrated in the plot of $\ln\left|\frac{I_0}{I}\right|$, which does not form one continuous straight line, but rather has a 'step' about two thirds of the way along. This indicates that there is more than one fluorescence process occuring here, with different lifetimes. The value for the lifetime of the 1_0^4 band given in Table 4.3 is that of the dominant process.

As previously mentioned, the lifetime of SeO_2 in the $^1B_2$ state was measured by Miziolek in 1980 [4]. He measured the lifetime of the 1_0^4 band to be 31.1 ± 2.5 μs. Obviously, this value is considerably different from that calculated here. There are a number of aspects of the previous work which suggest that the recent measurements give a far more reliable lifetime. Miziolek's work was carried out using the natural vapour pressure of a sample of SeO_2 at room temperature, which is only 9.1×10^{-8} Torr, and so it is entirely possible that the species he was looking at was not actually SeO_2. His experiment was done by just setting the laser to a wavelength taken from King and McLean's paper; he did not scan either side of this wavenumber to find the position of maximum fluorescence intensity so he may not have actually been detecting fluorescence from SeO_2. In contrast, in this

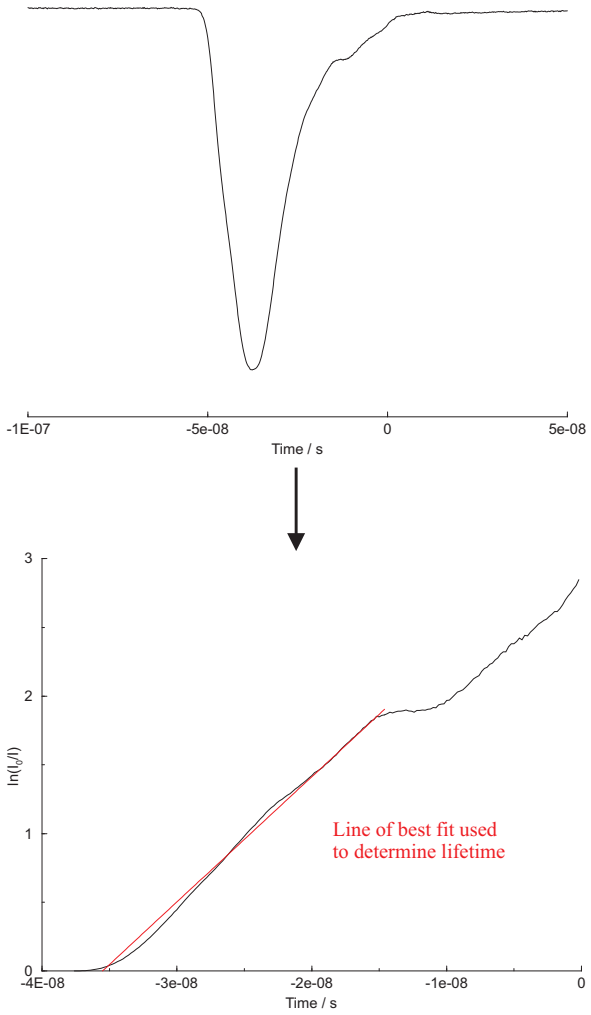

Figure 4.7: The fluorescence decay curve for the 1_0^4 band, along with a plot of $\ln\left|\frac{I_0}{I}\right|$ against the time, to show that the curve is not smooth.

work we know that we are observing maximum fluorescence for each band, and that this fluorescence is from the SeO_2 molecule. Finally a lifetime of 31 μs is unacceptably long for what is supposed to be an allowed transition. Indeed if it were correct, the present detection of SeO_2 by LIF would have been impossible.

4.4 Discussion of Results

The survey spectrum recorded in this study is much more complicated than that observed by King and McLean [2]. In the region studied almost 100 new bands have been observed in addition to the 28 bands previously reported. Some of these bands may possibly be hot bands, but it is not possible to account for all of them by only considering transitions from the ground state to a single excited electronic state; there must be bands involving at least one other electronic state overlapping with those attributed to the $\tilde{\mathrm{C}}^1B_2 \leftarrow \tilde{\mathrm{X}}^1A_1$ transition.

King and McLean recorded a straight absorption spectrum, whereas this spectrum was recorded using the technique of Laser Induced Fluorescence, a technique which depends on both absorption and fluorescence. It is possible that the new bands fluoresce very strongly, yet only absorb weakly, which would explain why these bands were not apparently observed by King and McLean. Another possible explanation is the difference in temperature used between this work and the work carried out by King and McLean. King and McLean performed their experiments at around 200 °C, whereas this work was done at a rotational temperature of about 10 K. At 10 K only the lower energy J levels are populated, and a typical band only extends over about 15 cm^{-1}. In contrast, at 200 °C many more rotational levels will be populated and the bands observed by King and McLean are seen to extend up to about 80 cm^{-1}, more than five times the maximum width of the bands observed in this study. Therefore it is quite possible that many of the weaker bands observed in this work could have been swamped by the extended rotational structure of the stronger bands in King and McLean's observations.

As discussed above, the survey spectrum of SeO_2 was recorded to try to explain the perturbations seen in the rotational analysis of the 1_0^3 band, and it was never the intention to carry out a full vibrational analysis of this spectrum. However, it has been possible to reassign a few peaks, and make a number of new assignments. A few new progressions in the symmetric stretching vibration and the bending vibration have been picked out, which are likely to involve a different upper electronic state, but further work, possibly including a full rotational analysis, is required to determine the nature of these transitions.

4.4.1 The Asymmetric Stretching Vibration

King and McLean observed strongly irregular spacings in transitions they assigned to the asymmetric stretching vibration [2]. They attributed this to a double-minimum potential in this vibrational coordinate, which would result in the two Se−O bonds being unequal in length at equilibrium. Information about ν_3' is contained in the isotopic shift of the 0_0^0 band (Section 5.9), and in the light of this, King and McLean's assignment begins to look suspect. Using information about the isotopic shift of the 0_0^0 band in combination with data about the frequencies and isotopic shifts of the other vibrational modes it is possible to make an estimate of ν_3'. Extending Equation 5.13 to take account of all the normal vibrations gives us the following expression for the isotopic shift:

$$\Delta\nu_{(000)} = \nu(^{78}SeO_2) - \nu(^{80}SeO_2) \tag{4.12}$$

$$= \frac{1}{2}\left[\nu_1'(\rho_1' - 1) + \nu_2'(\rho_2' - 1) + \nu_3'(\rho_3' - 1)\right] \tag{4.13}$$

$$-\frac{1}{2}\left[\nu_1''(\rho_1'' - 1) + \nu_2''(\rho_2'' - 1) + \nu_3''(\rho_3'' - 1)\right]$$

from which it is possible to make an estimation of ν_3' if all the other quantities are known or can be estimated. It is important to realise that the reliability of the estimate of ν_3' will depend entirely on the reliability of the other values used, and small changes in these numbers can result in significant changes in ν_3'.

We now consider the various terms in Equation 4.13 in turn, beginning with the ground state values. ν_1'' is taken to be 922.6 cm^{-1}, which is the value obtained for $^{80}SeO_2$ by King and McLean [2]. It is also possible to obtain a value for ρ_1'' from King and McLean's work. However a value obtained from an infrared matrix isolation study would be more accurate because of the fact that in the matrix there is no rotational motion and a sharp vibrational peak is observed. Hastie *et al.* [5] observed the spectrum of SeO_2 in a neon matrix, from which they calculated ν_1'' to be 923.4 cm^{-1} for $^{80}SeO_2$ and 924.4 cm^{-1} for $^{78}SeO_2$, implying a value of 1.0011 for ρ_1''. The values used for ν_2'' and ν_3'' are 364 cm^{-1} and 968 cm^{-1} respectively, from Konings' gas phase infrared study [6]. Unfortunately this

work did not resolve the different isotopes, and so ρ_2'' has to be calculated from King and McLean's assignment, which gives a value of 1.0027. ρ_3'', on the other hand, can be calculated from the ratio of the reduced masses of each isotopomers:

$$\mu_3 = \frac{2m_{\mathrm{Se}}m_{\mathrm{O}}}{m_{\mathrm{Se}} + 2m_{\mathrm{O}}\sin^2\left(\frac{\theta}{2}\right)} \tag{4.14}$$

and hence

$$\rho_3 = \sqrt{\frac{\mu_3(^{80}\mathrm{SeO_2})}{\mu_3(^{78}\mathrm{SeO_2})}} \tag{4.15}$$

$$= \sqrt{\frac{m_{80}\left(m_{78} + 2m_{\mathrm{O}}\sin^2\left(\frac{\theta_{78}}{2}\right)\right)}{m_{78}\left(m_{80} + 2m_{\mathrm{O}}\sin^2\left(\frac{\theta_{80}}{2}\right)\right)}}. \tag{4.16}$$

The ground state rotational constants have been determined from microwave spectroscopy [7], and so we can calculate the bond angle and hence ρ_3'', which turns out to be 1.0028. This value is very close to that determined from the matrix isolation study (1.0027) [5].

In the excited state of SeO_2 ν_1' and ν_2' can be calculated from the values for ω_1^0 and ω_2^0 determined in the fit discussed above, using the equation [3]

$$\nu_i = \omega_i^0 + x_{ii} \tag{4.17}$$

which gives 625.20 cm^{-1} and 265.04 cm^{-1} for ν_1' and ν_2' respectively. In Section 5.9 we see that when only considering the symmetric stretching vibration the isotopic shift is given by

$$1.47882 = \nu_1'\left(\rho_1' - 1\right) \tag{4.18}$$

so using the value for ν_1' above we calculate ρ_1' to be 1.0024. Unfortunately there is no such information available for the bending vibration, and it is necessary to estimate a value of ν_2' for $^{78}SeO_2$ and from that estimate a value of ρ_2'. In the reassignment of the 2_0^1 band above the isotopic shift was observed to be between 0.5 and 1.0 cm^{-1}. If this is assumed to be 0.7 cm^{-1}, ν_2' for $^{78}SeO_2$ would be 1.1 cm^{-1} greater than that of $^{80}SeO_2$ when the

shift of approximately -0.4 cm^{-1} in the 0_0^0 band has also been taking into account. From these values, ρ_2' is estimated to be 1.0042. This is probably the least reliable term in the calculation as the isotopic shift in the 2_0^1 band is not known accurately, a fact which must be taken into consideration when assessing the final value obtained for ν_3'. ρ_3' is calculated to be 1.0024 using Equation 4.16, with the bond angles used being those estimated for the (000) vibrational level of the excited state in Section 5.8. Again, these angles are only estimates and so introduce another possible source of error into the calculation.

Now that all the terms in Equation 4.13 are known, we can calculate an estimate for ν_3', using the fact that $\Delta\nu_{(000)}$ was found to be -0.3670 cm^{-1} in Section 5.9. This gives us a value of 571 cm^{-1}, which is of a more reasonable magnitude that the value of 78 cm^{-1} proposed by King and McLean. Changing the isotopic shift of the 2_0^1 band, within reasonable limits, and repeating this calculation suggests that the value initially obtained of 571 cm^{-1} is accurate to $\pm$ 100 cm^{-1}. Although the results of these calculations cover a large range, we can still place more confidence in this result than in the value of 78 cm^{-1} for ν_3' observed by King and McLean.

4.5 Tables of Data

Table 4.4 contains the positions of the vibrational bands observed, their relative intensities, and assignments. Table 4.5 summarises the differences between the positions of the peaks assigned by King and McLean, and the positions at which those peaks are observed in this work.

Table 4.4: Positions, intensities and assignments of the bands observed in the survey spectrum of SeO_2.

Band position / cm^{-1}	Relative intensity	Assignment from King and McLean's work	Assignment from this work
30601.57	0.00120		
30625.28	0.000800		Progression 3
30670.55	0.000400	$1_1^0 2_1^0$	
30695.92	0.00560		Progression 1
30724.58	0.00680		
30748.34	0.00520		
30769.94	0.0172	1_2^1	
30783.39	0.000800		
30841.29	0.0324		
30887.33	0.00480		
30903.65	0.00160		Progression 2
30960.36	0.0352		Progression 1
30983.15	0.00360		
31029.89	0.0280	1_1^0	
31049.37	0.00280		
31062.43	0.0100		1_1^0
31109.41	0.0770	$1_1^0 3_0^1$	
31146.63	0.0150		
31164.60	0.00300		Progression 2
31187.18	0.00400		
31200.68	0.00200		
31223.19	0.0640		Progression 1
31250.53	0.0230		Progression 3
31277.16	0.00800		
31289.43	0.0190		
31324.36	0.0110		
31339.87	0.00300		
31364.37	0.00200		
31376.34	0.0820	$1_1^0 2_0^1 3_0^1$	
31406.20	0.0450	1_2^2	
31424.00	0.0610		Progression 2
31440.84	0.00300		
31461.48	0.00100		
31485.00	0.0520		Progression 1
31515.52	0.0410		
31541.04	0.0100		
31553.44	0.0100		
31571.81	0.0100		
31587.49	0.0100	2_1^0	
31613.39	0.170		2_1^0

Table 4.4 cont'd.

Band position / cm^{-1}	Relative intensity	Assignment from King and McLean's work	Assignment from this work
31620.59	0.0100		
31640.54	0.110		
31668.72	0.0400		
31687.05	0.210	1_1^1	Progression 2
31702.64	0.0400		
31743.46	0.100		Progression 1
31764.18	0.250		
31808.08	0.0400		
31819.85	0.0600		
31844.64	0.0400		
31855.39	0.0400		
31876.81	0.620		Progression 3
31881.28	0.0700		
31892.97	0.120		
31933.47	0.0500		
31947.16	0.750		Progression 2
31961.48	0.0800	0_0^0	Band X
31983.24	0.230		0_0^0
32008.03	0.0600		
32032.36	0.600	3_0^1	
32040.17	0.0900		
32064.09	0.500		
32084.60	0.200		
32102.35	0.200		
32119.66	0.200		
32140.63	11.3		
32171.93	1.50		
32191.91	0.100		
32205.93	0.900		
32245.78	0.500		2_0^1
32264.33	0.100		
32298.83	3.50	$2_0^1 3_0^1$	
32323.30	3.00	1_1^2	
32347.33	3.20		
32401.57	4.50		
32423.26	0.200		
32436.67	2.00		
32463.20	0.700		
32477.31	0.700		
32491.10	0.700		
32512.78	0.500		2_0^2, Progression 3

Table 4.4 cont'd.

Band position / cm^{-1}	Relative intensity	Assignment from King and McLean's work	Assignment from this work
32535.01	10.0	3_0^2	
32553.14	3.60		
32562.79	1.60		
32580.42	2.00		
32609.47	20.0	1_0^1	
32623.12	1.00		
32666.39	5.00		
32710.19	1.00		
32743.62	3.00		
32768.13	1.00		
32799.98	46.0	$2_0^1 3_0^2$	
32810.24	10.0		
32837.06	2.00		
32852.97	4.00	$1_0^1 2_0^1$	
32869.10	22.0		$1_0^1 2_0^1$
32881.58	3.00		
32924.37	7.00		
32970.95	4.00	1_1^3	
32985.60	18.0		
33006.40	3.00		
33065.48	85.0	$2_0^2 3_0^2$	
33086.38	3.00		
33114.69	3.00	$1_0^1 2_0^2$	
33128.55	13.5		$1_0^1 2_0^2$, Progression 3
33181.36	18.0		
33217.57	54.0		
33246.43	70.5	1_0^2	
33267.49	9.00		
33324.26	82.5	$2_0^3 3_0^2$	
33346.07	4.50		
33386.47	7.50		$1_0^1 2_0^3$
33476.34	184		
33503.83	52.5	$1_0^2 2_0^1$	
33588.71	135	$2_0^4 3_0^2$	
33632.94	70.5	1_1^4	$1_0^1 2_0^4$
33680.42	40.0		
33733.34	300		
33757.63	100	$1_0^2 2_0^2$	
33846.55	650		
33895.11	460	1_0^3	
33988.54	250	$1_0^2 2_0^3$	

Table 4.4 cont'd.

Band position / cm^{-1}	Relative intensity	Assignment from King and McLean's work	Assignment from this work
34043.91	970		
34103.32	550		
34152.46	1000	$1_0^3 2_0^1$	
34555.45		1_0^4	

Table 4.5: Summary of the bands observed by King and McLean, and the differences between their line positions and those observed in this work.

King and McLean's assignment	Band position from King and McLean's work / cm^{-1}	Band position from this work / cm^{-1}	Difference / cm^{-1}
1_0^4	34561.0	34555.45	5.55
$1_0^3 2_0^1$	34153.2	34152.46	0.74
$1_0^2 2_0^3$	34024.6	34043.91	-19.31
1_0^3	33895.5	33895.11	0.39
$1_0^2 2_0^2$	33763.7	33757.63	6.07
1_1^4	33634.5	33632.94	1.56
$2_0^4 3_0^2$	33591.9	33588.71	3.19
$1_0^2 2_0^1$	33505.0	33503.83	1.17
$2_0^3 3_0^2$	33326.1	33324.26	1.84
1_0^2	33247.6	33246.43	1.17
$1_0^1 2_0^2$	33113.0	33114.69	-1.69
$2_0^2 3_0^2$	33064.4	33065.48	-1.08
1_1^3	32974.9	32970.95	3.95
$1_0^1 2_0^1$	32845.0	32852.97	-7.97
$2_0^1 3_0^2$	32801.5	32799.98	1.52
1_0^1	32610.5	32609.47	1.03
3_0^2	32533.6	32534.78	-1.18
1_1^2	32324.5	32323.30	1.20
$2_0^1 3_0^1$	32302.1	32298.83	3.27
3_0^1	32035.3	32032.36	2.94
0_0^0	31957.4	31961.48	-4.08
1_1^1	31687.4	31687.05	0.35
2_1^0	31585.0	31587.49	-2.49
1_2^2	31406.9	31406.20	0.70
$1_1^0 2_0^1 3_0^1$	31379.9	31376.34	3.56
$1_1^0 3_0^1$	31112.4	31109.41	2.99
1_1^0	31034.8	31029.89	4.91
1_2^1	30769.0	30769.94	-0.94
$1_1^0 2_1^0$	30673.0	30670.55	2.45

Bibliography

[1] G.W. King and P.R. McLean. Selenium Dioxide: Rotational Analysis and Franck-Condon Calculations for the 3130 Å $^1B_2$ - $^1A_1$ Absorption System. *Journal of Molecular Spectroscopy*, **52**, 1974.

[2] G.W. King and P.R. McLean. Selenium Dioxide: Vibrational Analysis of the 3130 Å $^1B_2$ - $^1A_1$ Absorption System. *Journal of Molecular Spectroscopy*, **51**, 1974.

[3] G. Herzberg. *Electronic Spectra and Electronic Structure of Polyatomic Molecules*, Volume 3 of *Molecular Spectra and Molecular Structure*. Krieger Publishing Company, 1991.

[4] A.W. Miziolek. Radiative Lifetime and Quenching Rates of SeO_2 Vapor. *Chemical Physics Letters*, **74**(1), 1980.

[5] J.W. Hastie, R. Hauge, and J.L. Margrave. Infrared Spectra and Geomotry of SO_2 and SeO_2 in Rare Gas Matricies. *Journal of Inorganic and Nuclear Chemistry*, **31**, 1969.

[6] R.J.M. Konings, A.S. Booij, and A. Kovács. The Infrared Spectra of SeO_2 and TeO_2 in the Gas Phase. *Chemical Physics Letters*, **292**, 1998.

[7] E.A. Alekseev, O.I. Baskakov, and S.F. Dyubko. Microwave Spectrum of Selenium Dioxide. *Proceedings of SPIE - International Society of Optical Engineers*, **3090** (High Resolution Molecular Spectroscopy), 1997.

Chapter 5

The Rotationally Resolved Spectrum

5.1 Introduction

A number of individual bands of what is believed to the the $\tilde{C}^1B_2 \leftarrow \tilde{X}^1A_1$ system of SeO_2 have been recorded at rotational resolution. The 1_0^1 band was recorded between 32601 and 32618 cm^{-1}, the 1_0^2 band between 33236 and 33254 cm^{-1}, and the 1_0^3 band between 33882 and 33904 cm^{-1}. For all of these bands it is possible to identify the isotope structure due to the $^{78}SeO_2$ and $^{80}SeO_2$ isotopomers, and in some cases the structure due to the less abundant $^{76}SeO_2$ and $^{82}SeO_2$ isotopomers has also been identified. An additional band was recorded in the region between 31952 and 31964 cm^{-1}, which, on the basis of King and McLean's assignment, was initially believed to be due to the 0_0^0 transition [1] (Band X). However, as was discussed in Chapter 4, the 0_0^0 band has been reassigned as the result of a survey spectrum recorded subsequently, and the nature of Band X is not currently known.

As previously discussed, the rotational temperature of the molecules in the free-jet expansion is between 10 and 15 K, which is considerably colder that the temperatures used by King and McLean [1, 2] when they attempted to analyse the rotational contour of the 1_0^3 band. Consequently the number of rotational transitions observed here is considerably less than in the spectrum recorded by King and McLean, so that the spectrum is less congested and hence easier to analyse. The great increase in resolution of this experiment compared with that of King and McLean also means that we can resolve individual rotational lines

whereas they only resolved K sub-bands. Therefore the present analysis will allow us to determine much more accurate values for the excited state rotational parameters of the 1_0^3 band, along with new excited state rotational constants for the other bands recorded.

This chapter describes the methods used to analyse the rotational structure of the spectra, and examines the features of the individual bands.

5.2 Procedure for Analysing the Rotational Structure

Once all the bands had been recorded at rotational resolution, the individual scans had to be calibrated from the absorption spectrum of iodine and the étalon fringes, and the positions of the individual lines measured. It was then necessary to stitch together all the scans of each band to form a continuous spectrum. This was done by simply ensuring that adjacent scans always had at least one peak in common, and then fixing the height of one scan and scaling the height of the adjacent scan to make the overlapping peaks the same size. This does not necessarily always give us reliable peak intensities, as it is always possible for the laser power to fluctuate during a scan, or for mistakes to be made in the scaling process; however it does give an acceptable indication of the relative intensities.

The rotational lines in the individual vibrational bands of the electronic spectrum of SeO_2 were assigned using the method of lower state combination differences. The principle behind this method is the fact that the difference in energy between transitions to a common upper state depends only on the properties of the lower state. This method can be used when the properties of the lower state of a molecule are accurately known, but it is not necessary to know the properties of the upper state. This is suitable for SeO_2 because, as was previously discussed (Section 1.2.1), the rotational parameters for the ground electronic state are accurately known [3], whereas the rotational constants for the excited state are only very approximately known.

Let us now consider an example by way of explanation of the method of lower state combination differences. P, Q and R transitions from $J'' = 3$, 2 and 1 levels of the ground

state respectively all involve the same rotational level of the excited state, $J' = 2$. These are fully labelled P_{QP} for the transition $2_{12} \leftarrow 3_{13}$, Q_{QR} for the transition $2_{12} \leftarrow 2_{11}$ and R_{QR} for the transition $2_{12} \leftarrow 1_{11}$, in the notation $J_{K_aK_c}$. Using data given in Table 1.6 we can determine the energies of these rotational levels in the ground state. For $^{80}SeO_2$ the energy of the 2_{11} level is calculated to be 1.1577 cm^{-1} higher than that of the 1_{11} level. The 3_{13} level, in turn, is 1.2271 cm^{-1} higher in energy than the 2_{11} level, and hence 2.3848 cm^{-1} higher in energy than the 1_{11} level. This is illustrated in Figure 5.1 as a theoretical example, and in Figure 5.2 using the real assignments in the 1_0^3 band. So if we find a set of three lines in the spectrum separated by these values (within the limits of the experimental error), they can be considered as possible candidates to be assigned as these transitions. This leads to a number of candidates for the transitions, but it is possible to reduce this

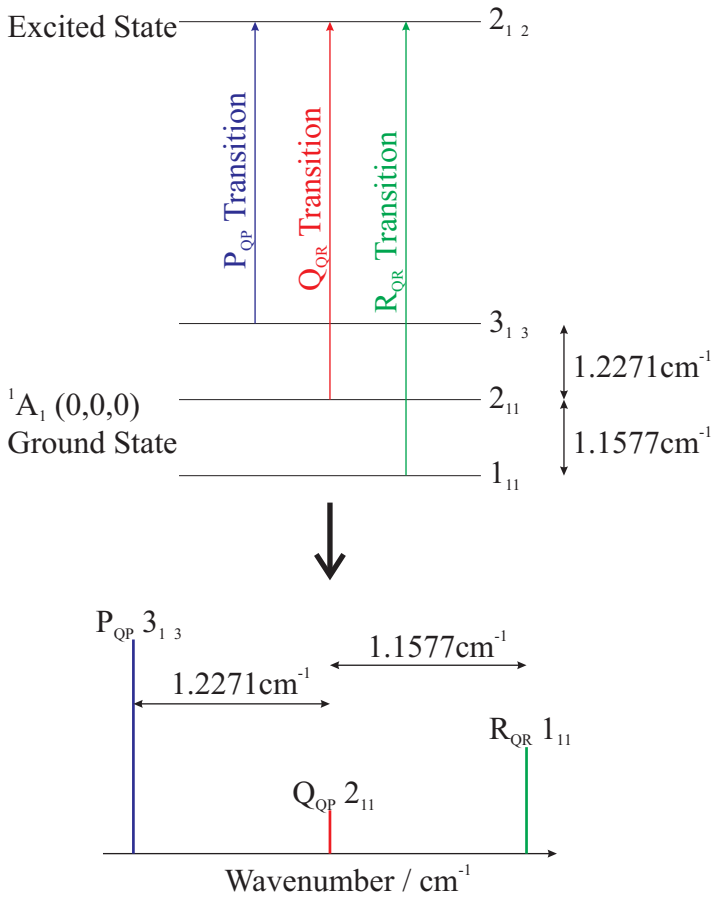

Figure 5.1: An illustration of the lower state combination differences method used in assigning the rotational structure of the spectra.

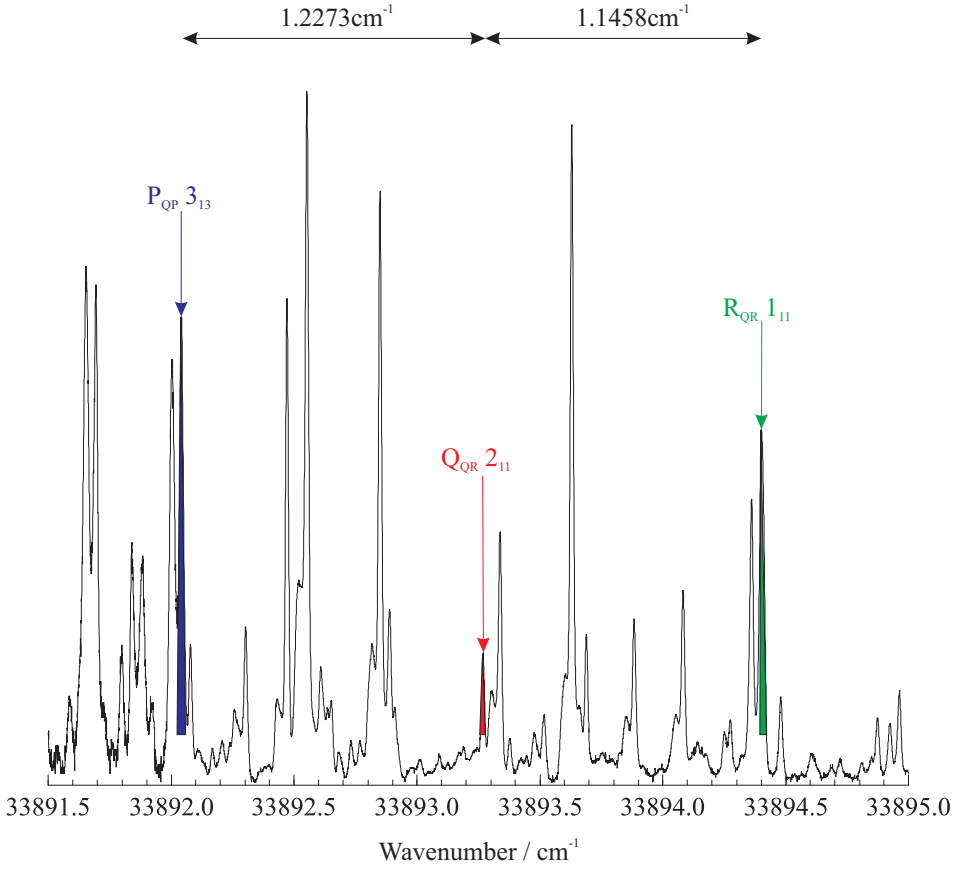

Figure 5.2: A section of the 1_0^3 band, to illustrate the real combination differences for $^{80}SeO_2$.

number by accepting only the sets in which the lines have the correct intensities relative to each other. This number is reduced even further by looking for the lines of a few different sets of transitions and considering their positions relative to each other.

The procedure used was to look firstly for transitions for which $\Delta K_a = 0$, from $K_a = 0$ levels in the ground state. Note that due to the nuclear spin statistics only levels with even J are present in the $K_a = 0$ sub-band in the ground state and hence no Q transitions are seen here. Once a few sets of pairs of lines were found which fitted the combination differences, a computer program called ASYROT (Section 5.3) was used to fit the transitions to the model of a rigid, asymmetric rotor, and calculate values for the band origin and the rotational parameter $\bar{B}$. These new constants were then used to predict the positions of further transitions in the $K_a = 0$ sub-band. Once this sub-band

had been extended as far as possible, we then moved on to the $K_a = 1$ sub-band (in which Q transitions are seen) and repeated the same procedure. This time it was possible to calculate the band origin, and A, B and C with the ASYROT program. Again, once this sub-band had been extended as far as possible, the $K_a = 2$ and then the $K_a = 3$ sub-bands were considered. By this stage it was possible to make reliable predictions for the positions of these sub-bands using the ASYROT program. A simulation of the whole spectrum, produced using the computer program TWO2, also showed a good comparison with the shape and structure of the experimental spectrum. A small number of $\Delta K_a = 2$ transitions were also assigned in the same way.

For each band the $^{80}SeO_2$ transitions were assigned first, since this is the most abundant isotopomer and hence its transitions should be the strongest. Once this had been done, assigning the transitions of the other isotopomers became a much simpler task as the rotational constants in the excited state were quite similar for the different isotopomers, and hence the positions of the transitions could be predicted fairly reliably. The $^{78}SeO_2$ transitions were assigned next as this is the next most abundant isotopomer, followed by transitions due to $^{76}SeO_2$ and $^{82}SeO_2$ where possible.

5.3 Computer Programs

Two Fortran programs were used to assist in assigning the rotational lines of the SeO_2 spectra, and to calculate the rotational constants of the excited states. These programs were ASYROT and TWO2.

5.3.1 TWO2

TWO2 is a simulation program, which can be used to simulate a complete rotational band for a rigid rotor from a given set of parameters. The input parameters required are the rotational constants for the ground and excited states and the band origin, along with the rotational temperature, FWHM, type of transition (A-, B- or C-type) and the nuclear spin statistics. This program generates a list of allowed transitions, their frequencies and relative intensities under the given conditions, and a plot of the simulated spectrum.

5.3.2 ASYROT

This is a much more complex program than TWO2, which can be used to fit transitions to various parameters or to predict the positions of specific lines from a given set of parameters. In total this program has around 100 different parameters which can be used to model transitions. In practice, most of these are not required for a closed shell molecule such as SeO_2 in the absence of any external electric or magnetic fields, and it is only necessary to consider the rotational constants and distortion constants of the ground and excited states, along with the band origin.

Least-Squares Fitting Mode

This mode of the program is used to fit the wavenumbers of the transitions and to determine better values for various parameters from approximate starting values. The input file for this program must include the relevant rotational parameters, indicating which are to be fitted or 'floated', and a list of observed transition wavenumbers and their assignments. The values of the floated parameters are optimised by refining them to fit the transition wavenumbers, according to the criterion of a least squares fit. During each cycle of the fit, small changes are made to the initial values of the floated parameters, in an attempt to minimise the sum of the squared deviations of the observed and calculated transition frequencies. This procedure is repeated for the requested number of cycles or until the standard deviation converges. When the program has run successfully it creates an output file, which lists the fitted values for the floated parameters along with their standard deviations, the overall standard deviation for each cycle, the calculated frequency for the transitions included in the fit, and the difference between these calculated values and the experimental values put in at the start (observed - calculated value, or o-c). Small standard deviations and o-c values signify a good fit.

There are two slightly different versions of this program, one which uses the rotational constants A, B and C, and one which fits A, $\bar{B} = \frac{1}{2}(B + C)$ and $\frac{1}{4}(B - C)$. For a near

prolate asymmetric top the transitions can be fitted to the equation [4]

$$F(J,K) = \bar{B}J(J+1) + (A-\bar{B})K_a^2 \pm \frac{1}{2}(B-C)J(J+1)\delta_{K_a=1} \tag{5.1}$$

where $\delta_{K_a=1}$ indicates that $\pm\frac{1}{2}(B-C)J(J+1)$ is splitting of the $K_a = 1$ levels, where the K_a doubling is the largest. Although in reality SeO_2 cannot be approximated to a symmetric top, this equation illustrates the fact that when starting to assign a band and trying to fit just the $K_a = 0$ sub-band it is not possible to fit both B and C, but only $\bar{B}$. Adding $K_a = 1$ transitions for odd J values enables A to also be fitted. It is only once even J transitions for the $K_a = 1$ sub-band have been added, and we can then see the K-type doubling caused by the deviations from the symmetric top model, that $\frac{1}{4}(B-C)$ can also be fitted. At this point it is also possible to fit B and C separately which are the parameters that we actually wish to calculate, instead of fitting $\bar{B}$ and $\frac{1}{4}(B-C)$, in order to be able to ultimately determine the bond angle and bond length.

Prediction Mode

Another mode of the program enables us to predict the transition wavenumbers of specific transitions, along with their relative intensities. The input file is very similar to that used for the least-squares fitting mode, requiring the rotational parameters and the quantum number of the transitions. However this time the frequencies of the transitions are not included, but are determined from the quantum numbers and the rotational parameters. The frequencies of the transitions are written to an output file.

On the surface it may appear that this mode of ASYROT is essentially the same as TWO2, and therefore it might seem unnecessary to use two different programs. However where ASYROT will only predict the frequencies of specified transitions, TWO2 will predict the frequencies of all allowed transitions (above a certain chosen intensity) which is very helpful when predicting a large number of transitions or simulating a complete band. ASYROT gives more accurate predictions than TWO2 because it includes the distortion constants in its calculations, whereas TWO2 just uses the A, B and C rotational constants. Consequently, the two programs each have their individual merits.

5.4 The 1_0^3 Band

The rotational structure of the 1_0^3 band is shown in Figure 5.3.

This band is seen to be very congested due to the isotopic structure. Whereas it may initially seem a better idea to begin the analysis of the rotationally resolved bands with the origin band, where the isotope structure might not be resolved, this band was chosen as the starting point because it was the one previously studied by King and McLean [2]. It was hoped that the values they determined for the rotational constants in the excited state would provide a simulated spectrum close to that seen experimentally and hence could be used as a starting point for analysing this band. However as can be seen in Figure 5.4 the simulation and the experimental spectrum are very different, and hence King and McLean's previous work was not as helpful in analysing this band as we had hoped.

Since it was not possible to predict the positions of any transitions using the excited state rotational constants determined by King and McLean, it was necessary to use the method of lower state combination differences to assign the lines in the spectrum from scratch, as described above. The vast majority of the lines in the spectrum were assigned to A-type transitions using this method, with transitions being observed for both $^{76}SeO_2$ and $^{82}SeO_2$, as well as the two most abundant isotopomers, $^{78}SeO_2$ and $^{80}SeO_2$. A small section of the spectrum is shown in Figure 5.5 to illustrate an example of some of the transitions assigned to $^{80}SeO_2$ and $^{78}SeO_2$. As expected, the transitions due to $^{78}SeO_2$ are about half as intense as the corresponding transitions due to $^{80}SeO_2$. The transitions of the lesser isotopomers also have relative intensities consistent with their natural abundances. The detailed assignments are listed in Tables A.1 to A.4 in Appendix A. The band origin and rotational constants determined from the fit of the assigned lines are given in Table 5.1. The values of the band origin and A rotational constant of $^{80}SeO_2$ can be quoted to greater precision that those for the other isotopomers simply because more transitions were assigned and fitted for this isotopomer, due to its greater abundance. Unfortunately there were not enough high J or K data available to determine the values of the distortion constants in the excited state. However these are expected to be fairly similar to those in the ground state (Table 1.6) and so were fixed to the same values in the fit. A new simula-

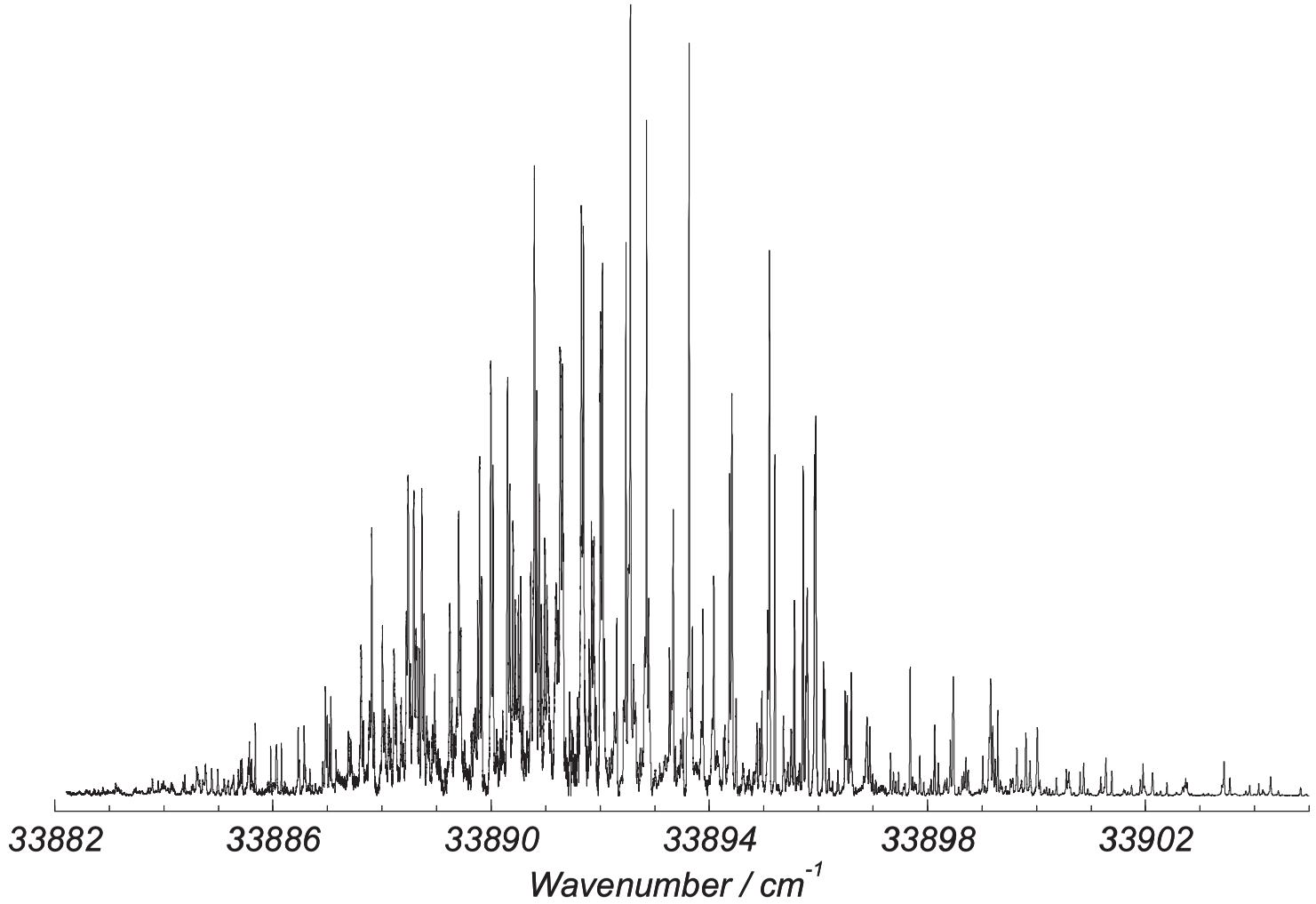

Figure 5.3: The rotationally resolved spectrum of the 1_0^3 band of the assumed $\tilde{\mathrm{C}}^1B_2 \leftarrow \tilde{\mathrm{X}}^1A_1$ transition of SeO_2.

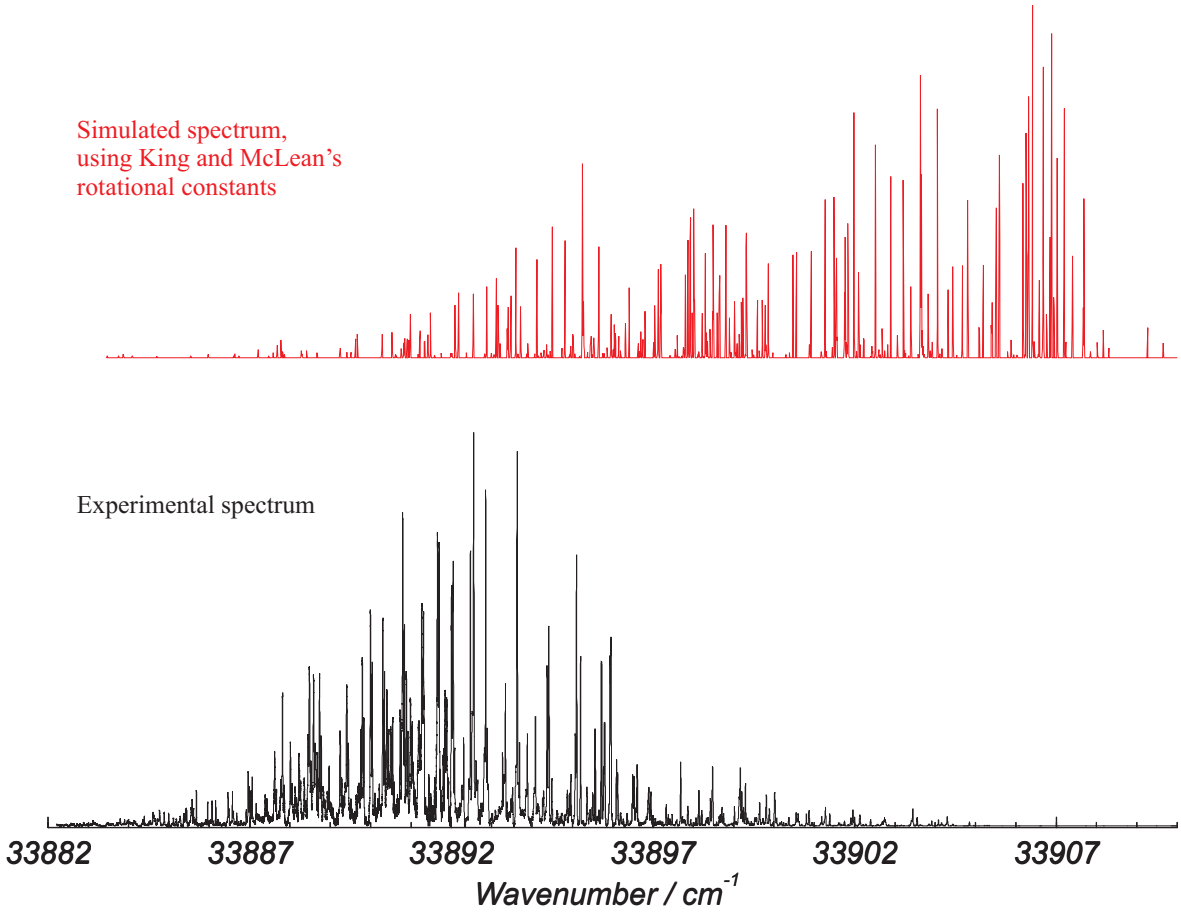

Figure 5.4: A simulation of the 1_0^3 transition of $^{78}SeO_2$ and $^{80}SeO_2$ using the excited state rotational constants determined by King and McLean [2], compared with the experimental spectrum.

tion, using these rotational constants and including all the isotopomers assigned multiplied by their relative abundances shows much better agreement with the experimental experiment than that of King and McLean, as can be seen in Figure 5.6. This simulation can be considered to reproduce the overall structure of the experimental spectrum very well. Some of the intensities are not exactly right, but this could be due to a number of reasons, most significantly the method used to stitch together individual scans to form the overall spectrum, and the fact that the laser power is not necessarily exactly the same in all the individual scans.

As can be seen from the band origins, the isotopic shift is to higher wavenumber as the

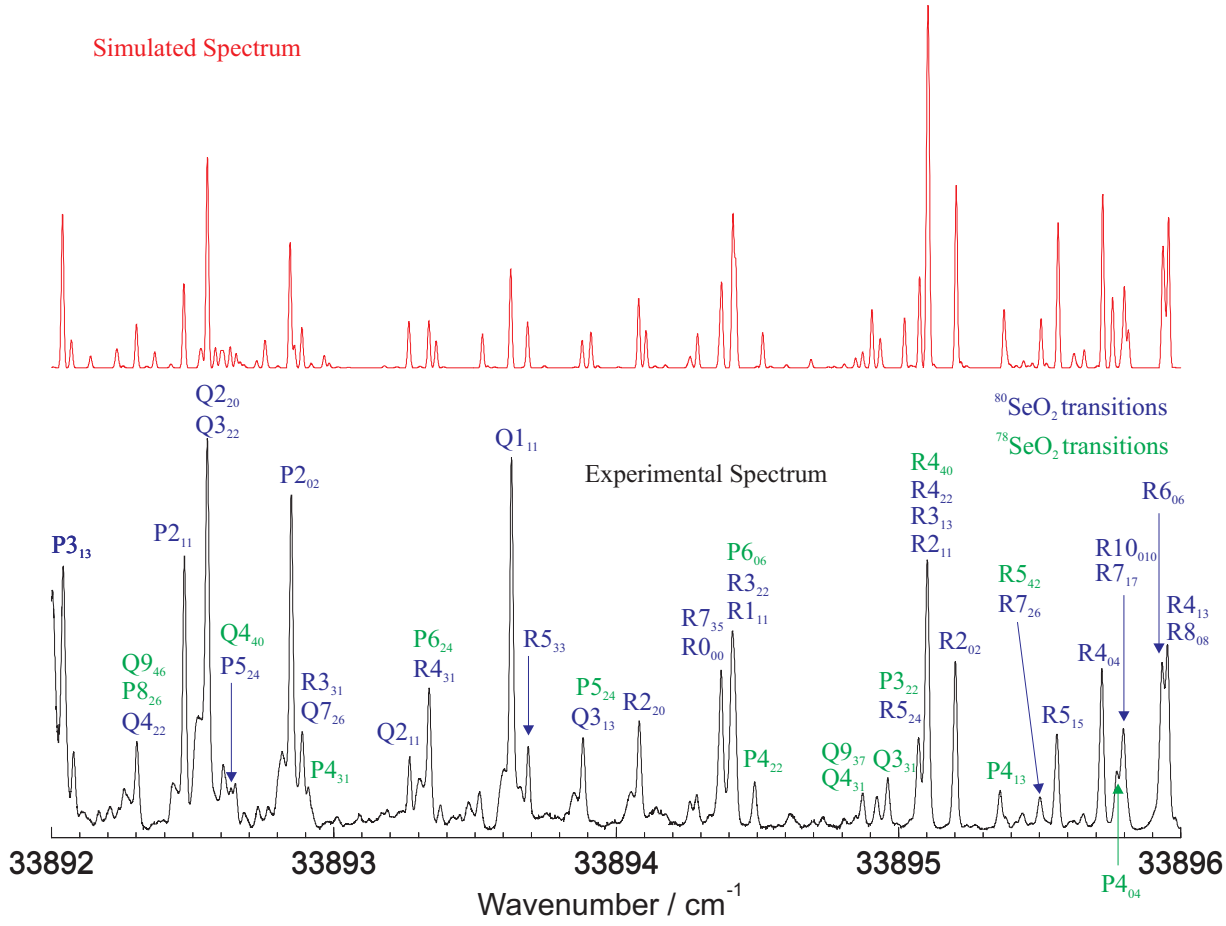

Figure 5.5: A section of the 1_0^3 spectrum, with the major transition of $^{78}SeO_2$ and $^{80}SeO_2$ occuring in this region labelled. The simulation was produced using the rotational constants in Table 5.1.

mass of the Se atom decreases. This shift is around 4 cm^{-1} between the isotopomers, and more specifically, 4.0620 cm^{-1} to higher wavenumber for the band origin of $^{78}SeO_2$ relative to that of $^{80}SeO_2$. This value is smaller than the shift of 5.4 cm^{-1} to higher wavenumber for $^{78}SeO_2$ reported by King and McLean, but is more reliable given the nature of the spectrum and the method of anaylsis used. The significance of these isotopic splittings will be discussed in more detail later (Section 5.9).

There are a number of peaks in the spectrum assigned to more than one transition. This can occur if the energies of two or more transitions are separated by less than the FWHM of the lines. Such transitions may or may not be for the same isotopomer of SeO_2.

Table 5.1: The band origin and rotational constants for the (300) vibrational level of the $^1B_2$ excited state of SeO_2. The numbers in brackets represent 1 standard deviation in the units of the last digit given.

Parameter	$^{76}SeO_2$ / cm^{-1}	$^{78}SeO_2$ / cm^{-1}	$^{80}SeO_2$ / cm^{-1}	$^{82}SeO_2$ / cm^{-1}
ν_0	33902.2201(13)	33897.9501(12)	33893.88811(62)	33890.00650(94)
A	0.64491(34)	0.63953(18)	0.635198(60)	0.63062(20)
B	0.287863(75)	0.286784(41)	0.286585(18)	0.286778(40)
C	0.199979(50)	0.199751(23)	0.199288(17)	0.199045(32)

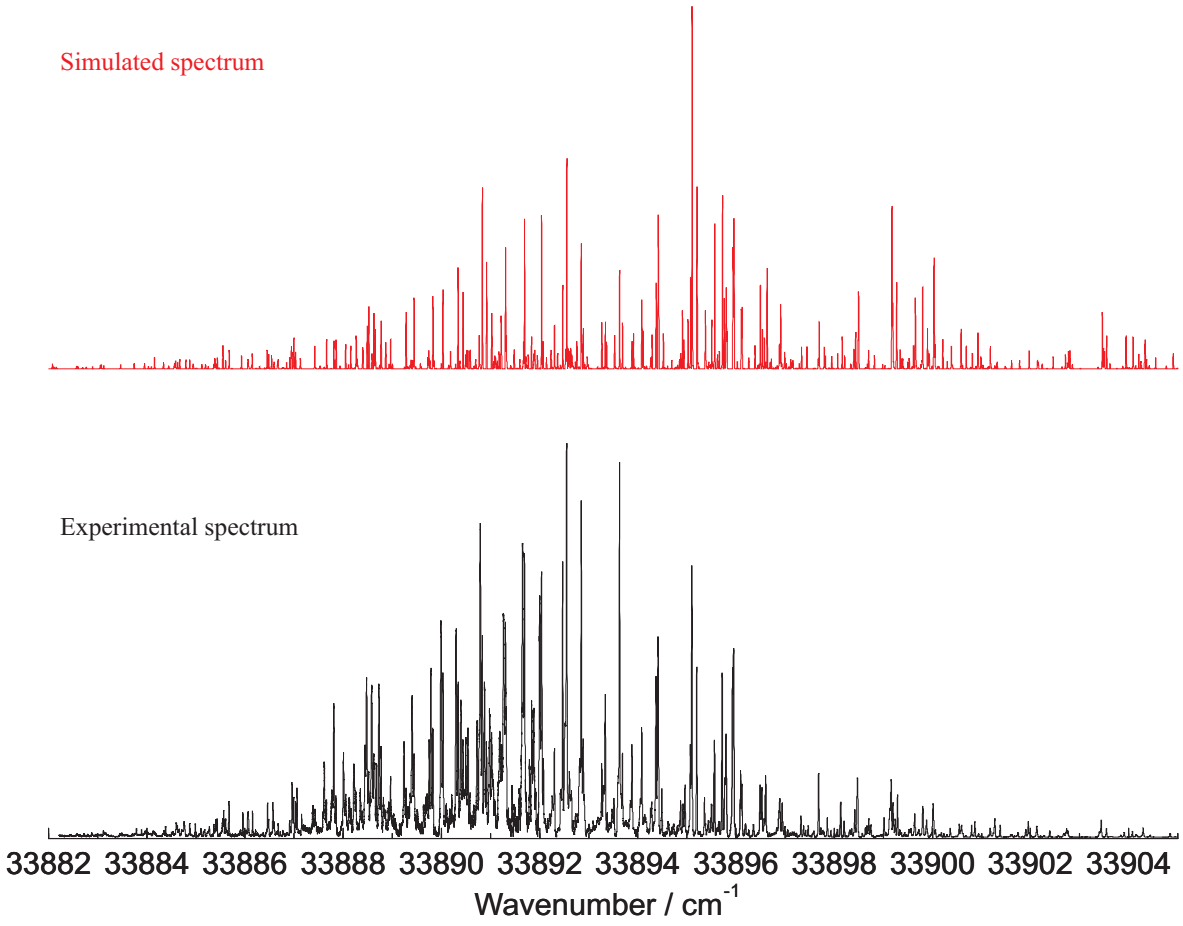

Figure 5.6: A simulation of the 1_0^3 transition using the excited state constants determined for the four isotopes considered.

When considering the assignments of these peaks it was necessary to look at the predicted intensities of the individual transitions as a fraction of the total intensity. As a general rule, for this band and the others considered, if a transition intensity accounted for less than 25 % of the total intensity of the line, that transition was given a weight of zero in the fit as it is more difficult to be absolutely certain of the assignment. Transitions for which the intensity accounted for 25 % or more of the total line intensity of an overlapped peak were treated as normal, fully resolved transitions.

5.4.1 Perturbations

Some of the transitions to $K'_a = 0$ levels of $^{78}SeO_2$ in the excited state are perturbed by up to ~ 0.02 cm^{-1}. This is shown by the large o-c values for the $\Delta K_a = 0$ transitions to these levels in Table A.2. Figure 5.7 also illustrates these perturbations for the R branch transitions, showing how the o-c value varies with the rotational quantum number of the excited state, J', for these $K'_a = 0$ transitions. This figure shows that the transitions are most greatly perturbed for lower J' values, 1, 3 and 5. Therefore these transitions were given a weight of zero in the least squares fit. It is notable that the perturbation only affects the $K_a = 0$ levels of $^{78}SeO_2$, not any other K_a levels nor any other isotopomer. The exact cause of the perturbation is unknown, but it is reasonable to speculate that it is due to mixing with another vibrational level observed in this region, quite possibly belonging to a different electronic state.

An interesting feature of this band is that there are a number of intense lines at the low frequency end of the spectrum which cannot be assigned. Some of these lines are illustrated in Figure 5.8, and the positions of all the intense unassigned lines are given in Table 5.2 The simulation for $^{80}SeO_2$ is shown above the experimental spectrum, to illustrate the fact that these unassigned lines are not present in the simulation. There are no significantly intense $^{78}SeO_2$ transitions in the region. Initially it appears that these lines are one half of a doublet, partnering some of the intense lines which have been assigned to $^{80}SeO_2$ transitions. However this is not true for all the unassigned lines, and so must be considered to be purely accidental in the cases where it does happen. None of these lines appear in the final simulation of the band, so we can conclude that they are not part of

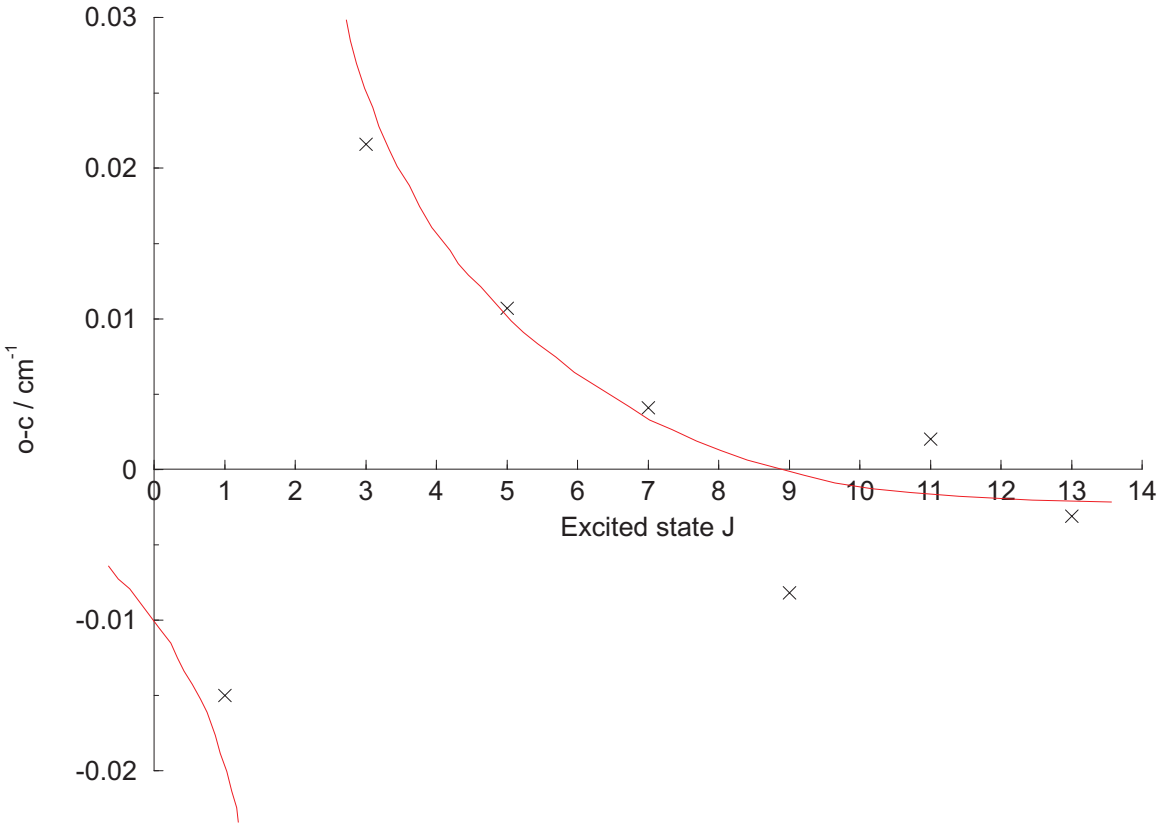

Figure 5.7: A plot to show how the o-c values vary for $\Delta K_a = 0$ transitions in the R branch of the $K_a = 0$ sub-band.

the 1_0^3 band. Further evidence for this comes from the fact that there are no corresponding unassigned lines in the similar part of the $^{78}SeO_2$ isotope structure. These lines are much too intense to be due to transitions of one of the lesser isotopomers of SeO_2. Attempts to find the same combination differences for transitions from the (000) vibrational level of the ground state were unsuccessful, suggesting that these transitions might belong to a hot band or a different electronic state.

Table 5.2: Intense unassigned lines in the 1_0^3 band of SeO_2.

33892.0069	33890.8789	33889.9912	33888.4460
33891.8400	33890.7918	33889.7862	33888.2208
33891.6534	33890.7270	33889.7513	33888.0066
33891.2682	33890.5414	33889.4036	33887.8102
33891.2264	33890.4982	33889.2386	33887.6158
33891.1926	33890.3972	33888.7284	
33890.9844	33890.2990	33888.5809	

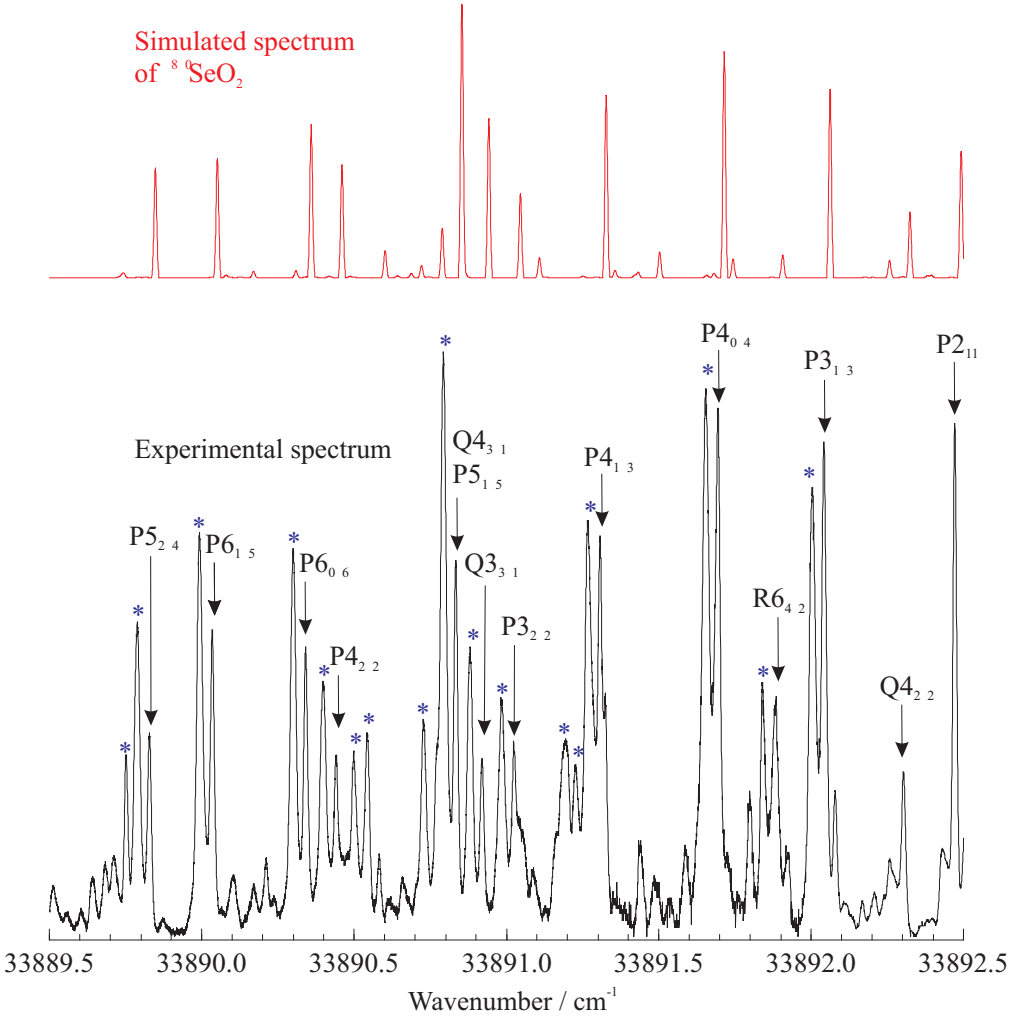

Figure 5.8: A section of the experimental spectrum showing a number of the intense unassigned lines, which are marked with a blue star. The transitions labelled are for $^{80}SeO_2$, as is the simulation.

5.5 The 1_0^2 Band

The rotational structure of the 1_0^2 band is shown in Figure 5.9.

As was the case with the 1_0^3 band, this band is very congested due to the presence of four isotopomers of SeO_2. However its overall structure is very similar to that of the 1_0^3 band. As a result of this, the rotational constants determined for the 1_0^3 band could be used as a first approximation for those of the 1_0^2 band. The ground state combination differences required were exactly the same as those searched for in the analysis of the 1_0^3 band as the two bands originate from the same vibrational level of the $^1A_1$ ground state. The positions of the transitions relative to each other were expected to be fairly similar to those in the 1_0^3 band. Hence the assignment of the lines in this band as A-type transitions was much more straight forward than it was for the 1_0^3 band. Again the vast majority of the lines were assigned to the four major isotopomers of SeO_2, and their assignments are given in Tables A.1 to A.4. The band origins and rotational constants for these isotopomers, determined from fitting the transitions, are given in Table 5.3. Once the transitions had

Table 5.3: The band origin and rotational constants for the (200) vibrational level of the $^1B_2$ excited state of SeO_2. The numbers in brackets represent 1 standard deviation in the units of the last digit given.

Parameter	$^{76}SeO_2$ / cm^{-1}	$^{78}SeO_2$ / cm^{-1}	$^{80}SeO_2$ / cm^{-1}	$^{82}SeO_2$ / cm^{-1}
ν_0	33250.4943(11)	33247.76801(70)	33245.16241(53)	33242.6779(14)
A	0.65266(36)	0.64745(10)	0.642719(65)	0.63803(36)
B	0.287450(77)	0.287022(28)	0.287532(16)	0.28752(19)
C	0.200394(30)	0.200048(15)	0.199667(12)	0.199275(51)

been assigned and the band origin and rotational constants had been determined, it was possible to simulate the rotational structure of the 1_0^2 band. This simulation is illustrated in Figure 5.10. As was the case with the 1_0^3 band, the simulation reproduces the structure of the experimental spectrum very well.

We can see from Table 5.3 that in this band the band origin of the $^{78}SeO_2$ isotopomer is 2.60560 cm^{-1} above that of the $^{80}SeO_2$ isotopomer. For the other isotopomers the shift is also between 2.7 and 2.5 cm^{-1} to higher wavenumber for the lighter molecule. This value

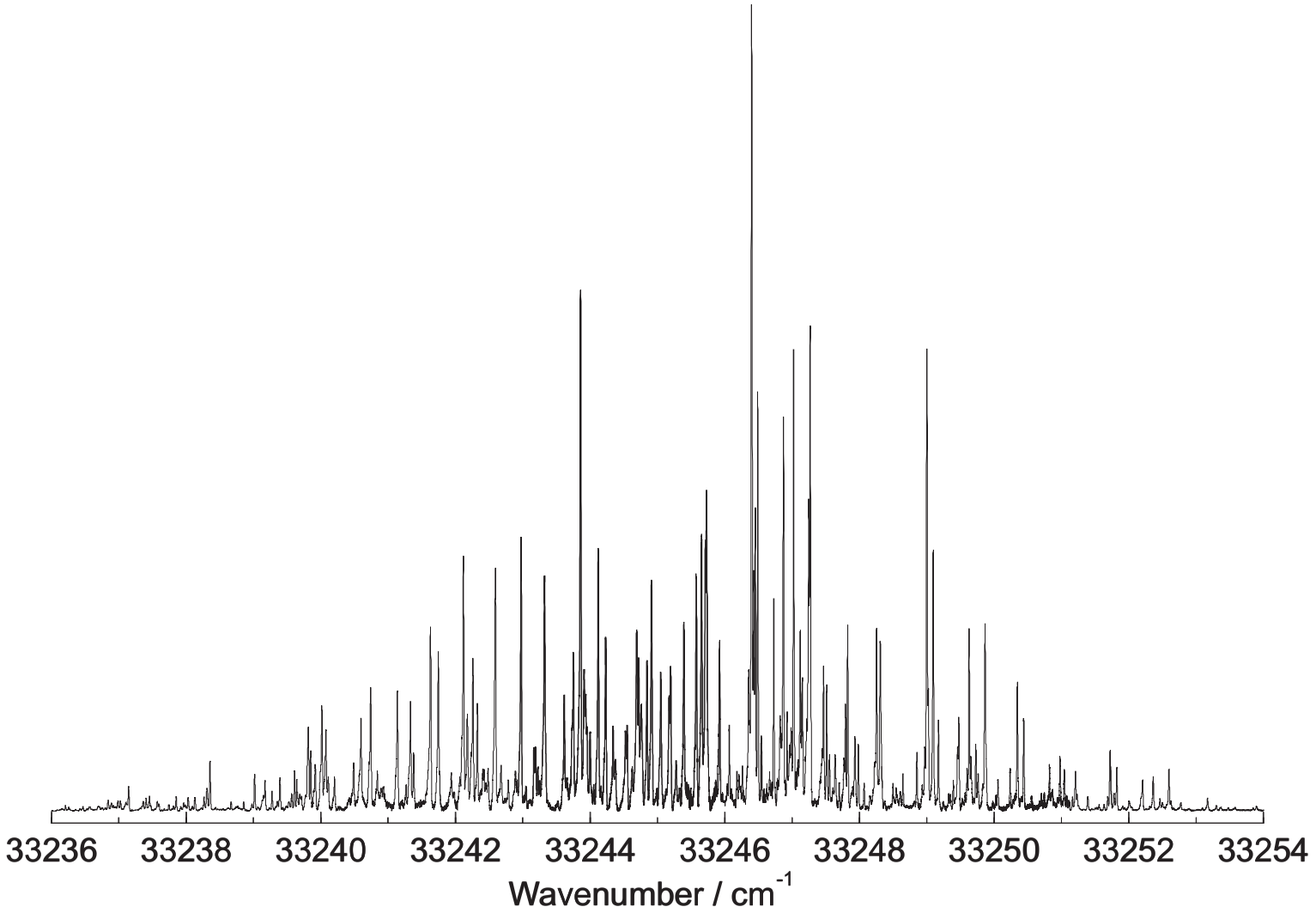

Figure 5.9: The rotationally resolved spectrum of the 1_0^2 band of the assumed $\tilde{\mathrm{C}}^1B_2 \leftarrow \tilde{\mathrm{X}}^1A_1$ transition of SeO_2.

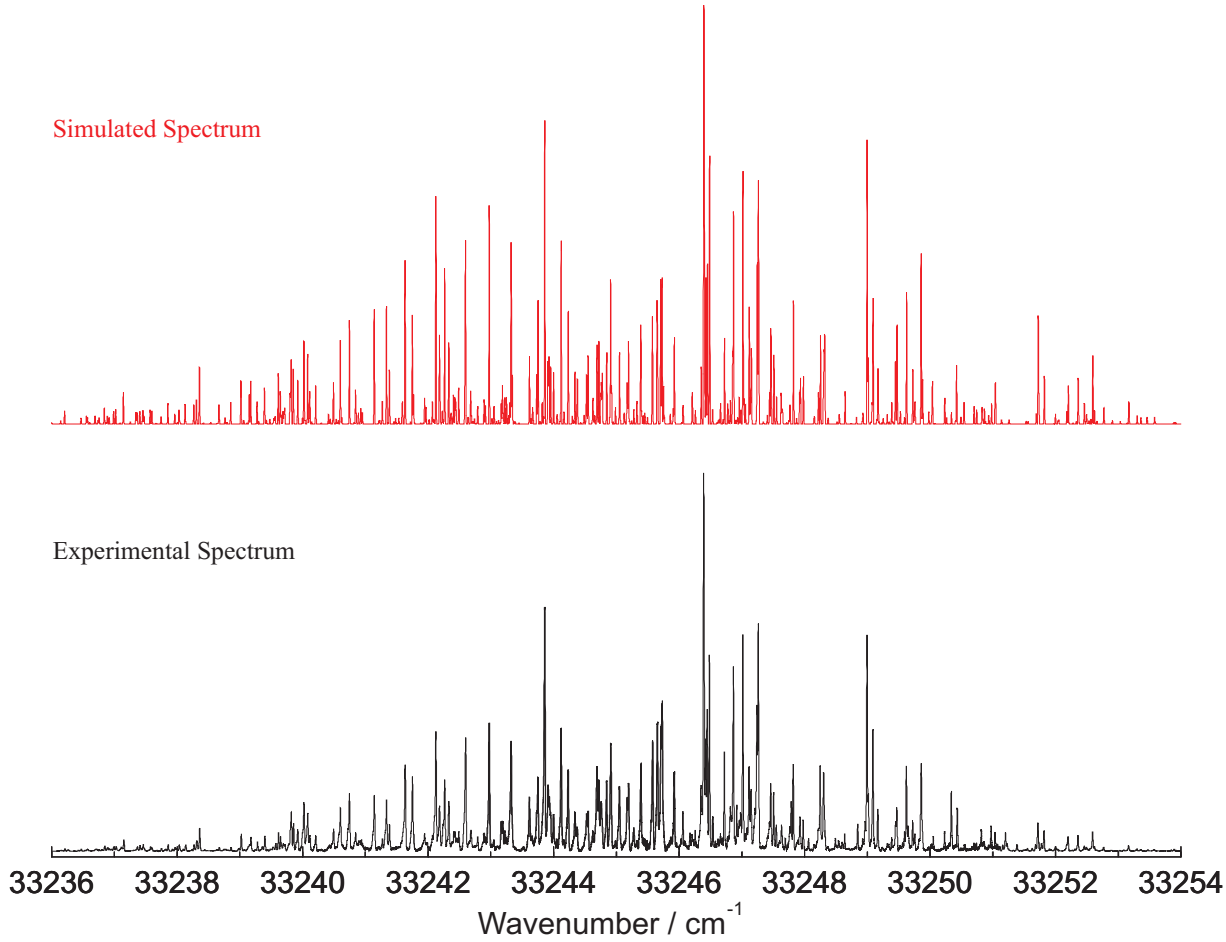

Figure 5.10: A simulation of the 1_0^2 transition using the excited state constants determined for the four isotopes considered.

is smaller than that seen in the 1_0^3 band, the significance of which will be discussed later (Section 5.9). In contrast to the 1_0^3 band, the isotopic shift observed here is larger than that reported by King and McLean. They observed $^{78}SeO_2$ to be only 1.8 cm^{-1} above $^{80}SeO_2$ in the 1_0^2 band; however as already mentioned, the value determined in this work is more reliable that that of King and McLean.

No perturbations of the type seen for $^{78}SeO_2$ in the 1_0^3 band were observed in this band. Nor were there any 'extra' intense lines that could not be assigned to transitions of the 1_0^2 band, as was the case in the 1_0^3 band. As a result, this band could be considered to be a good example of a 'well behaved' band in the $\tilde{C}^1B_2 \leftarrow \tilde{X}^1A_1$ transition which is free

from overlap of other bands, and hence is unperturbed. Consequently, it provides a good example of the structure and features of the type of band one would expect to see.

5.6 The 1_0^1 Band

The 1_0^1 band is shown in Figure 5.11.

Yet again, this band is very congested due to the isotope structure, and a large number of lines are observed in a relatively small region. Based on the isotope shifts determined above for the 1_0^3 and 1_0^2 bands, it seems reasonable to expect the shifts to be even smaller in this band, which would certainly explain why this band is noticeably narrower than the 3_0^1 band.

As was the case with the 1_0^2 band, assignment of the transitions in this band as A-type transitions was much more straight forward than that of those in the 1_0^3 band. This time the rotational constants determined above for the 1_0^2 band could be used as a first approximation to those of the 1_0^1 band. The vast majority of the lines, including all the intense lines were assigned to transitions of $^{76}SeO_2$, $^{78}SeO_2$ and $^{80}SeO_2$. The detailed assignments are given in Tables A.1 to A.3. The band origins and rotational constants determined from fitting these transitions are given in Table 5.4 and a simulation of the band using these constants is given in Figure 5.12. Again, the agreement between the experimental

Table 5.4: The band origin and rotational constants for the (100) vibrational level of the $^1B_2$ excited state of SeO_2. The numbers in brackets represent 1 standard deviation in the units of the last digit given.

Parameter	$^{76}SeO_2$ / cm^{-1}	$^{78}SeO_2$ / cm^{-1}	$^{80}SeO_2$ / cm^{-1}
ν_0	32610.4618(32)	32609.30424(68)	32608.19988(70)
A	0.6553(12)	0.648332(79)	0.643594(77)
B	0.28894(14)	0.289251(20)	0.289167(22)
C	0.20061(17)	0.200255(15)	0.199933(15)

spectrum and the spectrum simulated using the calculated rotational constants is very good. The intensities of some lines are not exactly as expected from the simulation, which is most likely to be due to the method used to overlap individual scans or fluctuating laser

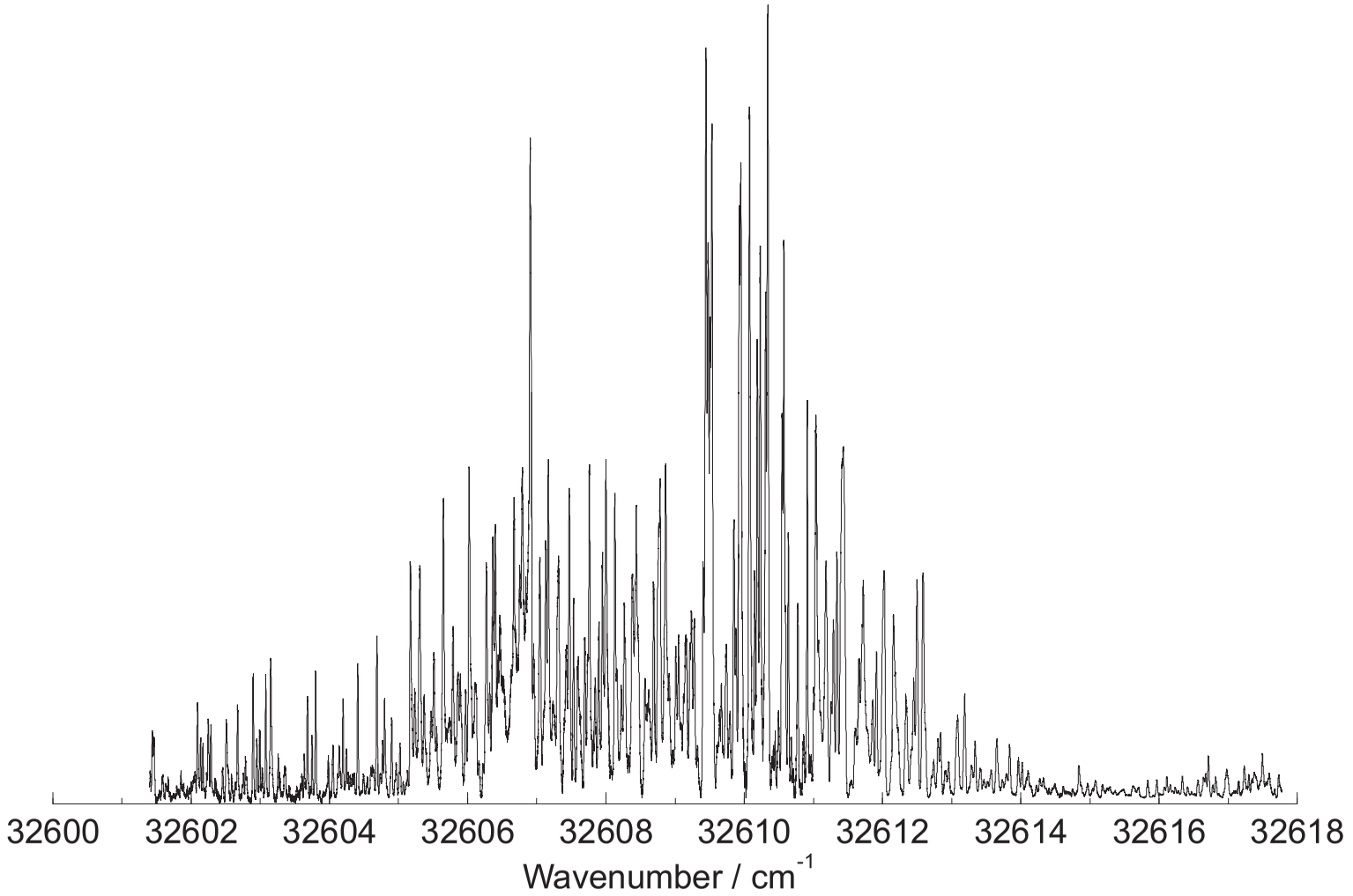

Figure 5.11: The rotationally resolved spectrum of the 1_0^1 band of the assumed $\tilde{\mathrm{C}}^1B_2 \leftarrow \tilde{\mathrm{X}}^1A_1$ transition of SeO_2.

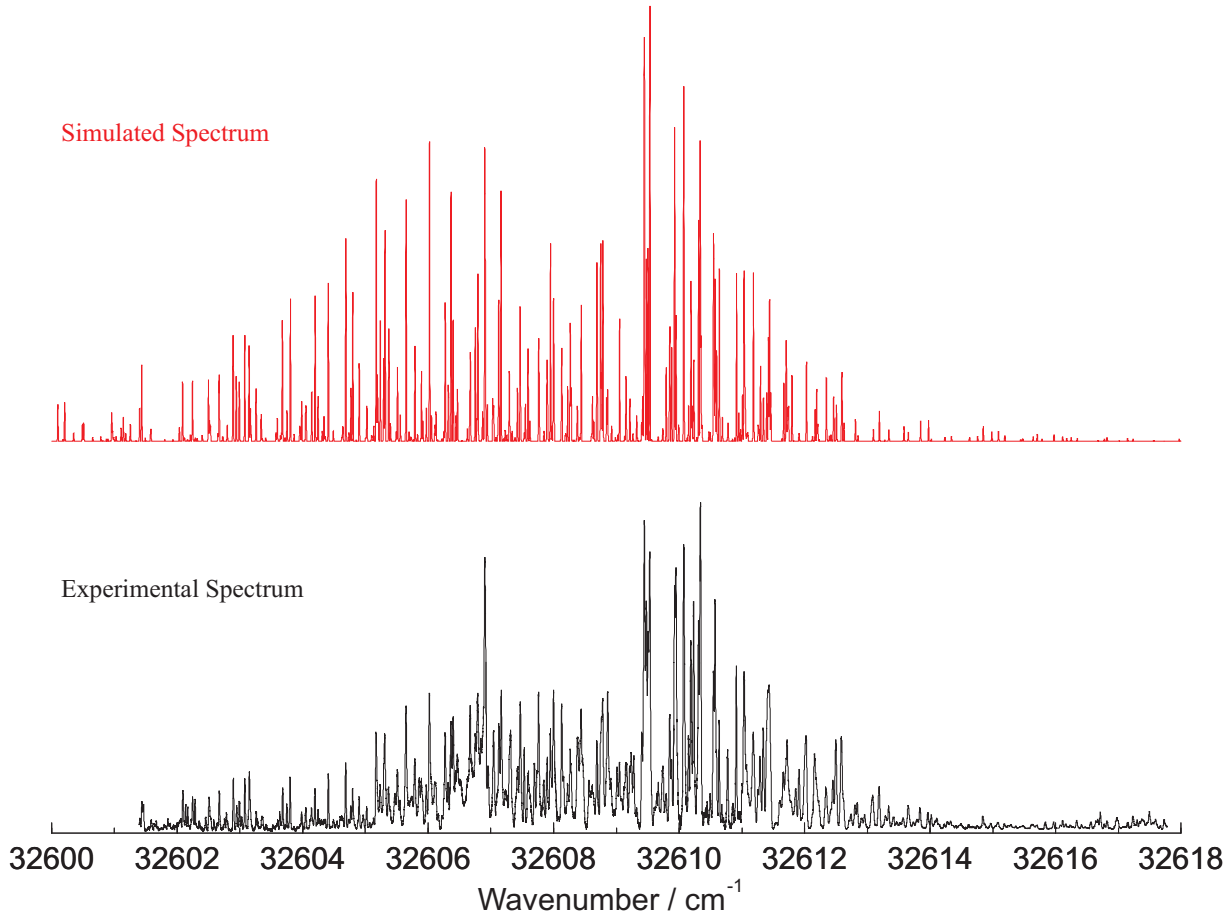

Figure 5.12: A simulation of the 1_0^1 transition using the excited state constants determined for the three isotopes considered.

power, as already discussed.

As was expected, the isotopic shifts are smaller than those seen in the 1_0^3 and 1_0^2 bands. The band origin of the $^{78}SeO_2$ isotopomer is only 1.10436 cm^{-1} above that of the $^{80}SeO_2$, and the $^{76}SeO_2$ isotopomer is only 1.1576 cm^{-1} above the $^{78}SeO_2$ isotopomer. In contrast, King and McLean reported $^{78}SeO_2$ to lie 3.6 cm^{-1} below $^{80}SeO_2$ in the 1_0^1 band.

Although no transitions were assigned to the $^{82}SeO_2$ isotopomer in this band, this does not mean that these transitions do not exist. From the isotopic shifts of the $^{76}SeO_2$ and $^{78}SeO_2$ band origins relative to that of the $^{80}SeO_2$ isotope, we would expect the origin of the $^{82}SeO_2$ isotopomer to be about 1 cm^{-1} below that of $^{80}SeO_2$. Given the fact that ^{82}Se accounts for only 9.2 % of the natural abundance of Se, compared with 49.7 % for

^{80}Se, we would expect to see weak lines due to $^{82}SeO_2$ interspersed with, and possibly overlapped with, the much stronger transitions of $^{80}SeO_2$, and hence it would be very difficult to distinguish and isolate the transitions due to $^{82}SeO_2$ from those of $^{80}SeO_2$. In contrast, it was possible to distinguish transitions due to $^{76}SeO_2$, even though this has a similar abundance to $^{82}SeO_2$. The reason for this is the fact that this isotopomer is shifted to higher wavenumber than the $^{80}SeO_2$ and $^{78}SeO_2$ isotopomers and as a result is found in a region of the spectrum which is considerably less congested, where it is possible to isolate the transitions due to $^{76}SeO_2$ from those of $^{78}SeO_2$ and $^{80}SeO_2$. Fewer transitions of $^{76}SeO_2$ were assigned than of $^{78}SeO_2$ and $^{80}SeO_2$, a fact which is reflected in the band origin and rotational constants being less precisely determined by the fitting program.

Similarly to the 1_0^2 band, no intense lines remained unassigned in this band. In addition, no perturbations of the type seen for $^{78}SeO_2$ in the 1_0^3 band were observed here.

5.7 The 0_0^0 Band

It would seem logical to present the results of the rotational analysis of the 0_0^0 transition at this point. As has already been mentioned, a band was recorded in the region between 31952 and 31964 cm^{-1}, which was believed to be the 0_0^0 transitions on the basis of King and McLean's assignment [1]. However the subsequent work on the vibrationally resolved spectrum of SeO_2 (Chapter 4) has led to a reassignment of the 0_0^0 band, and the band initially recorded at rotational resolution is not actually the 0_0^0 transition. This band has been named Band X, and will be discussed in detail later in this chapter. Unfortunately time constraints have meant that it has not been possible to record the true 0_0^0 transition at rotational resolution since its reassignment. It is possible to make some predictions about the nature this band, as will be seen in Sections 5.8 and 5.9 but it is still necessary to record and analyse the band in the future to obtain more accurate parameters than afforded by such predictions.

5.8 Bond Angles and Bond Lengths

It is now possible to use the rotational constants determined above to calculate the O−Se−O bond angle and the Se−O bond length of SeO_2. All three rotational constants have been determined, however only two of the three constants are required to calculate the geometry of SeO_2. A and B are chosen for two reasons. Firstly, for a rigid planar bent molecule such as SeO_2 only the moments of inertia about the a- and b-axes, I_a and I_b, are independent, and the moment of inertia about the c-axis is the sum of the these two, $I_c = I_a + I_b$. More importantly, the constant C is perturbed by the Coriolis interaction. The major contribution to the inertial defect of a molecule is the vibrational component, which arises when the Coriolis coupling constant is non-zero, i.e. when the direct product of the symmetry species of a pair of vibrational co-ordinates contain one of the species of rotation. The three vibrational modes of SeO_2 are of symmetry A_1, A_1 and B_2 respectively, which lead to two possible direct products, A_1 and B_2. In the C_{2v} symmetry group the three rotations R_a, R_b and R_c belong to the species B_1, A_2 and B_2 respectively. Therefore it follows that the only possible non-zero Coriolis coupling constants are ζ^c_{13}, ζ^c_{31}, ζ^c_{23} and ζ^c_{32}. No such interactions arise from rotations about the a- and b-axes.

Using the A and B rotational constants the O−Se−O bond angle of SeO_2 is given by the equation [5]

$$\tan\left(\frac{\theta}{2}\right) = \sqrt{\left(\frac{m_{\mathrm{Se}} I_b}{M I_a}\right)} \tag{5.2}$$

and the Se−O bond length is given by

$$r = \sqrt{\frac{1}{2m_{\mathrm{O}}}\left(\frac{M I_a}{m_{\mathrm{Se}}} + I_b\right)} \tag{5.3}$$

where M is the total mass of the molecule, m_{Se} and m_{O} are the masses of the Se and O atoms respectively, and I_a and I_b are the moments of inertia about the a- and b-axes:

$$I_a = \frac{h}{8\pi^2 c A}, \quad I_b = \frac{h}{8\pi^2 c B}. \tag{5.4}$$

From the rotational constants determined for each isotopomer in the individual ro-

tationally resolved bands it is possible to calculate the O−Se−O bond angle and Se−O bond length for each individual case using the equations above. However, in practice, it is more useful and convenient to calculate the equilibrium geometry, which will not vary with isotopic substitution. Unfortunately we do not have enough information at this point to calculate values for the equilibrium geometry. Therefore it is best to calculate the zero-point geometry instead, that is the geometry determined from the rotational constants in the (000) vibrational level. This will be isotopically dependent, but the change on substitution should not be very large, and should be smaller than would be observed in the vibrationally excited levels.

Although we do not have a set of accurately determined rotational constants for the (000) vibrational level of the excited state, we can make a reasonable estimate of these constants as was done in Section 4.2.2.1 for the low resolution simulation of the 0_0^0 transition. This time it is necessary to estimate the rotational constants of the different isotopomers; in the low resolution simulation the same constants were used for $^{78}SeO_2$ as for $^{80}SeO_2$ because the line width of the laser was such that the differences between the proper rotational constants would not be resolved. However for the high resolution data these differences are significant and it is necessary to use the accurate rotational constants for each isotopomer of SeO_2. If we look at the rotational constants for the (100), (200) and (300) vibrational levels of the excited state, as illustrated in Figure 5.13, for the four major isotopomers of SeO_2 we see that in fact there is not actually a linear trend between the three vibrational levels. Although a linear relationship of all three bands was used to predict the values of B' and C' for the low resolution spectrum, only the (100) and (200) values were considered when predicting a value for A'. The reason for this was that the analysis of the 1_0^3 band has shown that the (300) vibrational level of the excited state is perturbed, and hence the rotational constants determined may be anomalous. Obviously fitting just two data points to a linear equation is far from ideal, but it is thought that using only the rotational constants from the (100) and (200) vibrational levels to predict those of the (000) level will actually give a better estimate of the correct value than would be obtained by including the (300) values. The estimated rotational constants for the (000) vibrational level using a linear extrapolation from the values for the (100) and (200) vibrational levels are given

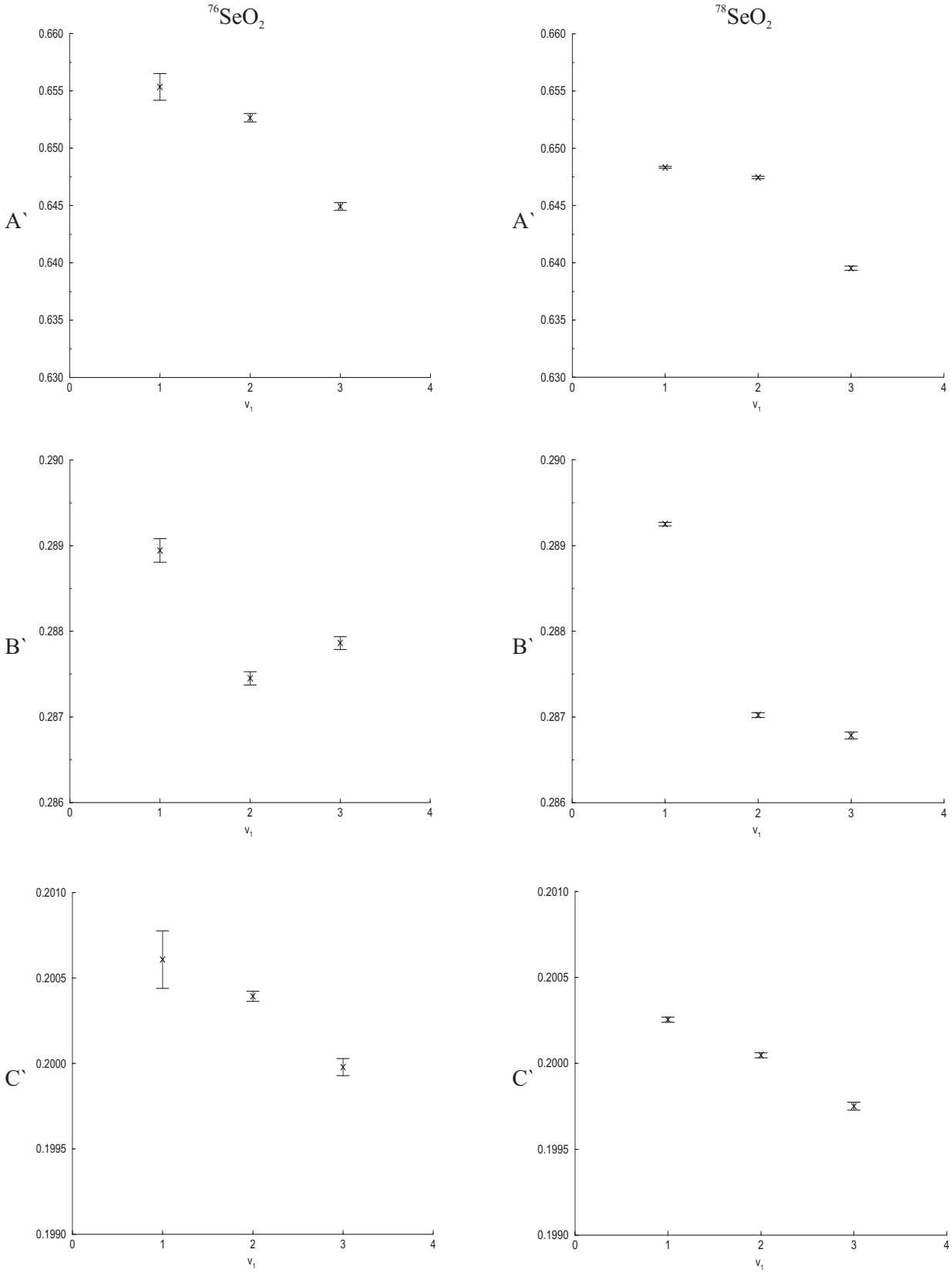

Figure 5.13: Plots of the A, B and C rotational constants (in cm^{-1}) vs v_1' for the four major isotopes of SeO_2, from the least-squares fit. The error bars represent plus and minus one standard deviation.

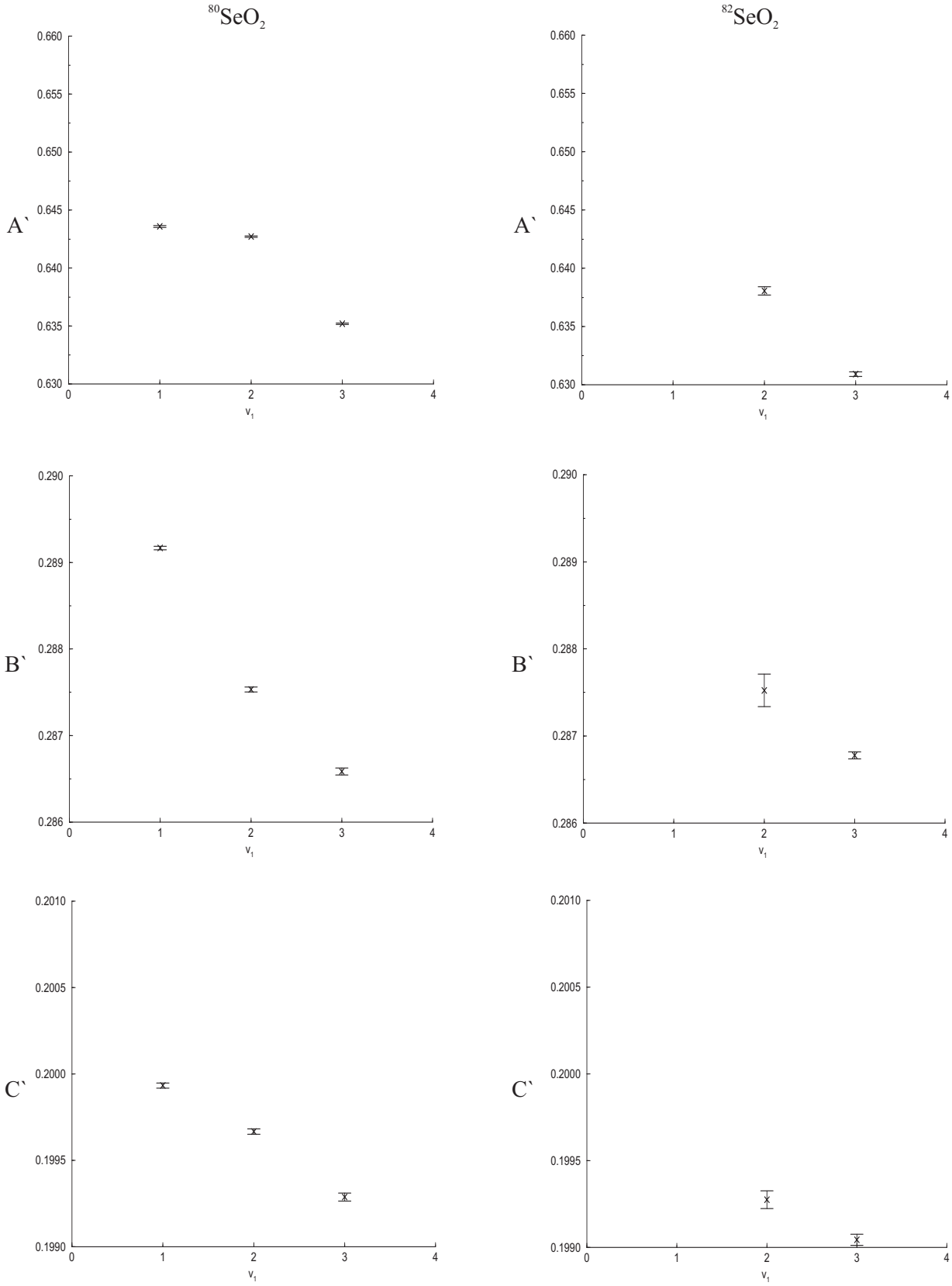

Figure 5.13 cont'd.

Table 5.5: The estimated rotational constants for the (000) vibrational levels of the $^1B_2$ excited state of SeO_2. The numbers in brackets represent 1 standard deviation in the units of the last digit given.

Parameter	$^{76}SeO_2$ / cm^{-1}	$^{78}SeO_2$ / cm^{-1}	$^{80}SeO_2$ / cm^{-1}
A	0.6580(12)	0.64921(13)	0.64447(10)
B	0.29044(16)	0.291480(35)	0.290802(27)
C	0.20082(17)	0.200462(21)	0.200199(19)

in Table 5.5. It is worth noting that the only reason that $^{82}SeO_2$ values are not estimated here is because of the fact that transitions were not assigned to this isotopomer in the 1_0^1 band, and it is not possible to predict the rotational constants of the (000) vibrational level using only those of the (200) level. We would expect the values for $^{80}SeO_2$ to be the most reliable, simply because ^{80}Se is the most abundant isotope and hence has the strongest lines in the various spectra recorded, and therefore the rotational analysis of these lines will be the most reliable.

It is now possible to estimate the Se−O bond length and the O−Se−O bond angle for each isotopomer. However it is best to consider just the values for $^{80}SeO_2$ (as being the most reliable), and an averaged value over the three isotopes. These are given in Table 5.6. As would be expected, the averaged values are not as accurate as the values obtained

Table 5.6: Bond angles and bond lengths of SeO_2 in the (000) vibrational level of the $^1B_2$ excited state, calculated from the estimated rotational parameters. The numbers in brackets represent 1 standard deviation in the units of the last digit given.

Isotope	r Se−0 / pm	θ O−Se−O / ^{o}
$^{80}SeO_2$	171.963(10)	103.0384(70)
$^{76}SeO_2$, $^{78}SeO_2$ and $^{80}SeO_2$ average	171.878(84)	103.08(15)

for $^{80}SeO_2$ alone, due to the fact that there is still some isotopic dependence seen in the bond angles and bond lengths of the (000) vibrational level, and the averaged value has to encompass this.

The Se−O bond length reported by King and McLean [2] from their analysis of the

1_0^3 transition was 174 pm for both $^{78}SeO_2$ and $^{80}SeO_2$, and the O−Se−O bond angle was 101.1 ° in the (300) vibrational level of the $^1B_2$ state. Since they only determined one rotational parameter, $(A - \bar{B})$, in their fit and not the individual A, B and C rotational constants, King and McLean fixed the bond length to 174 pm, and varied the angle in the region around 100 ° to find a value which gave the best agreement between the experimental spectrum and a simulation of the rotational contour. They found A to be very sensitive to changes in the angle but not sensitive to changes in the bond length, whereas B and C were insensitive to changes in the bond angle. The value adopted for the bond length by King and McLean differs by over 2 pm from the values calculated for the (000) vibrational level in this work. The bond angle differs from the values here by about 2 °. For another means of comparison, the bond lengths and bond angles for the (300) vibrational state determined in this work are 173.2191(66) pm and 103.0416(44) ° respectively for $^{80}SeO_2$, and 173.199(17) pm and 103.008(12) ° for $^{78}SeO_2$. These values are closer to those determined by King and McLean, as might be expected, for the simple reason that they are for the same vibrational state, but still differ by almost 1 pm and 2 °. The differences we see arise from the way in which the spectra were recorded and analysed. As has been seen in the analysis of the 1_0^3 band, these differences are enough to make a significant difference to the structure of the spectrum.

It is also possible to calculate the bond angle and bond length in the (000) vibrational level of the ground state using the rotational constants determined by Alekseev [3], and given in Table 1.6. The bond angles and bond lengths are given in Table 5.7. As would be expected, there is a slight isotopical dependence seen in these values, but the difference is

Table 5.7: Bond angles and bond lengths of SeO_2 in the (000) vibrational level of the $^1A_1$ ground state, calculated from Alekseev's ground state rotational parameters [3]. The numbers in brackets represent 1 standard deviation in the units of the last digit given.

Isotope	r Se−0 / pm	θ O−Se−O / °
$^{76}SeO_2$	160.8788279(62)	114.0157865(41)
$^{78}SeO_2$	160.8783934(71)	114.0155707(47)
$^{80}SeO_2$	160.8779978(40)	114.0153684(27)
$^{82}SeO_2$	160.8776251(81)	114.0151792(55)

very small. The change in geometry on going from the ground state to the excited state is very significant. The bond length increases by around 11 pm on excitation, and the bond angle decreases by about 11 °. This is consistent with the long progressions observed in the symmetric stretching and bending vibrations. More significantly, this change is consistent with the change in geometry expected for a $\tilde{C}^1B_2 \leftarrow \tilde{X}^1A_1$ transition (Section 3.2). A weakly antibonding electron on the oxygen atom, in the (a_2'') orbital, is promoted to the ($\bar{b}_1''$) orbital, which has a bonding component between the two oxygen atom and an antibonding component between the selenium atom and each oxygen atom. Combining this with the fact that all the bands discussed above have been assigned as A-type transitions, enables us to confirm the tentative assignment of the symmetry of the excited state made by King and McLean. It is now possible to assign definitively the excited state as $^1B_2$, and hence the electronic transition is $\tilde{C}^1B_2 \leftarrow \tilde{X}^1A_1$.

5.9 Isotope Structure

As mentioned for the individual rotationally resolved bands studied, we see evidence of the effects of the different isotopes of selenium in all the bands studied. Transitions due to the two most abundant isotopomers, $^{78}SeO_2$ and $^{80}SeO_2$ are identified in all three of the bands, along with transitions due to $^{76}SeO_2$. Transitions of $^{82}SeO_2$ are also assigned in the 1_0^3 and 1_0^2 bands. The isotopic shifts for the different rotational bands are summarised in Table 5.8, where all the values are the position of the band origins relative to that of $^{80}SeO_2$, the most abundant isotopomer.

The isotopic splitting can be estimated by a simple model. To a first approximation

Table 5.8: Isotopic shifts for $^{76}SeO_2$, $^{78}SeO_2$ and $^{82}SeO_2$ relative to the position of the band origin of $^{80}SeO_2$, in the 1_0^1, 1_0^2 and 1_0^3 bands.

Band	$^{76}SeO_2$ shift / cm^{-1}	$^{78}SeO_2$ shift / cm^{-1}	$^{82}SeO_2$ shift / cm^{-1}
1_0^1	2.2619	1.10436	
1_0^2	5.3319	2.60560	-2.4845
1_0^3	8.3320	4.0620	-3.88746

the energy of the n^{th} normal vibration is given by

$$G(v_n) = \omega_n \left(v_n + \frac{1}{2} \right) \tag{5.5}$$

where ω_n, in cm^{-1}, is related to the force constant or bond strength and reduced mass of the molecule by

$$\omega_n = \frac{1}{2\pi c} \sqrt{\frac{k_n}{\mu_n}}. \tag{5.6}$$

If we consider just the $^{78}SeO_2$ and $^{80}SeO_2$ isotopomers for the vibration v_n, the vibrational constants, ω_n of the two isotopomers can be related by the simple relationship:

$$\omega_n(^{78}\mathrm{SeO_2}) = \omega_n(^{80}\mathrm{SeO_2})\rho_n \tag{5.7}$$

where

$$\rho_n = \sqrt{\frac{\mu(^{80}\mathrm{SeO_2})}{\mu(^{78}\mathrm{SeO_2})}} > 1. \tag{5.8}$$

Therefore the transition wavenumbers for vibrational transitions involving only quanta of the symmetric stretching vibration excited, in the two isotopomers are given by

$$\nu(^{80}\mathrm{SeO_2}) = \omega_1' \left(v_1' + \frac{1}{2} \right) - \omega_1'' \left(v_1'' + \frac{1}{2} \right) \tag{5.9}$$

$$\nu(^{78}\mathrm{SeO_2}) = \omega_1'\rho_1' \left(v_1' + \frac{1}{2} \right) - \omega_1''\rho_1'' \left(v_1'' + \frac{1}{2} \right) \tag{5.10}$$

and hence the isotope shift is given by

$$\Delta\nu_1 = \nu(^{78}\mathrm{SeO_2}) - \nu(^{80}\mathrm{SeO_2}) \tag{5.11}$$

$$= \left(v_1' + \frac{1}{2} \right) (\rho_1' - 1)\omega_1' - \left(v_1'' + \frac{1}{2} \right) (\rho_1'' - 1)\omega_1''. \tag{5.12}$$

Since the transitions considered here are all from the (000) vibrational level of the ground state this equation can be simplified further to

$$\Delta\nu_1 = \left(v_1' + \frac{1}{2} \right) (\rho_1' - 1)\omega_1' - \frac{1}{2}(\rho_1'' - 1)\omega_1''. \tag{5.13}$$

From Equation 5.13, we would expect the shift of the origin of $^{78}SeO_2$ relative to that of $^{80}SeO_2$ to be a function of the number of quanta of the symmetric stretching vibration excited in the upper electronic state, v_1', and for this relationship to be linear in v_1'. A plot of the shift versus v_1', shown in Figure 5.14, illustrates this. From this graph, we can

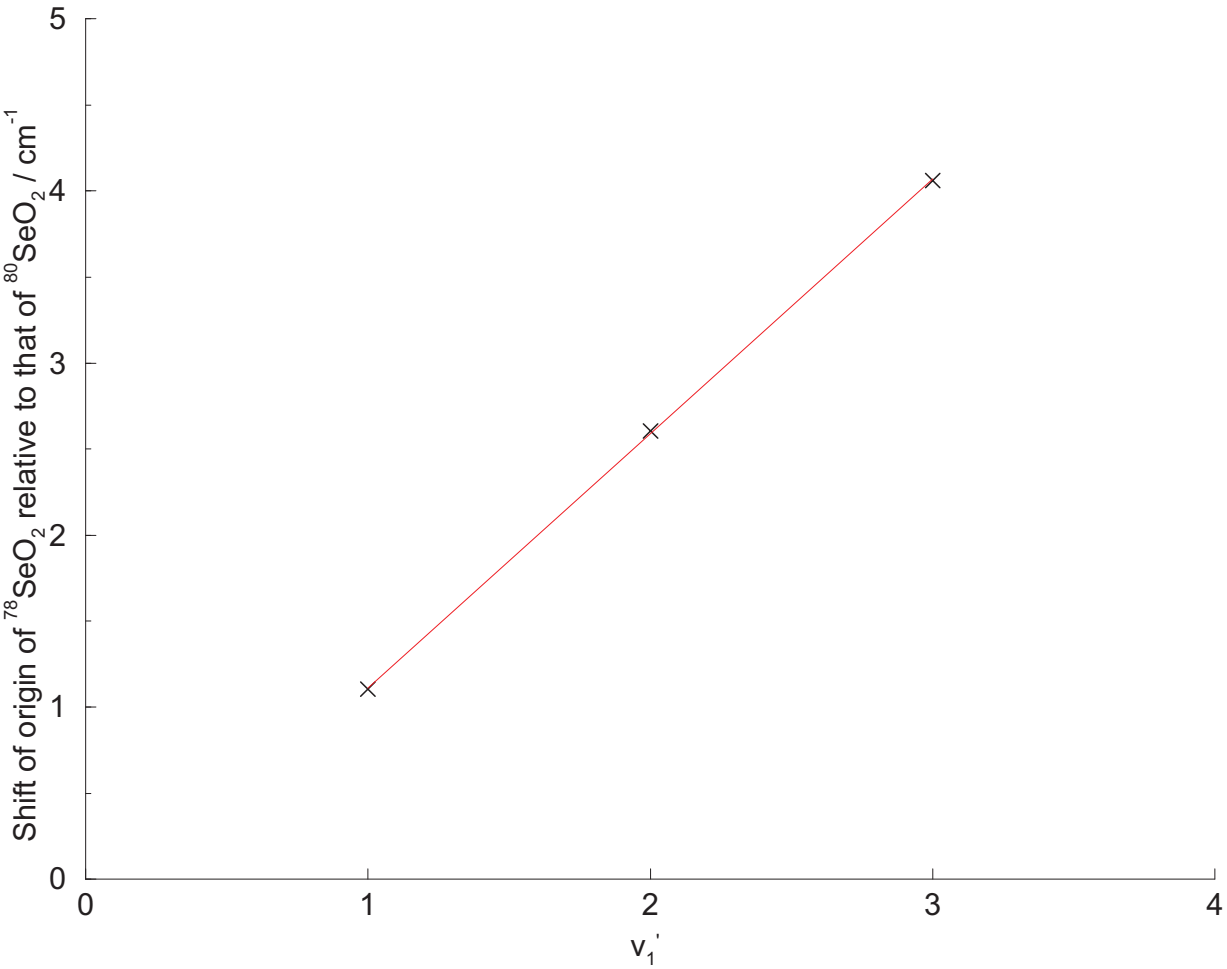

Figure 5.14: A plot of the shift of the origin of $^{78}SeO_2$ relative to that of $^{80}SeO_2$ versus v_1'.

calculate the gradient to be 1.4788 cm^{-1}, which is equal to $\omega_1' (\rho_1' - 1)$, and the intercept with the x-axis, which is equal to the remaining terms in the equation to be equal to -0.3670 cm^{-1}. Unfortunately there is not enough information here to determine ω_1', ω_1'', ρ_1' and ρ_1'' individually, however Equation 5.13 can be summarised as

$$\Delta\nu_1/\text{cm}^{-1} = 1.4789 v_1' - 0.3670. \tag{5.14}$$

From this, we can estimate that in the 0_0^0 band the origin of the $^{78}SeO_2$ band should be 0.3670 cm^{-1} below that of $^{80}SeO_2$, i.e at 31981.56 cm^{-1}, which is in the opposite sense to that observed in the other bands. Although one might expect the isotope structure to collapse down in the 0_0^0 transition, and not be resolvable, this result implies that this is not the case here. It is also possible to estimate the shift in other 1_0^n bands from this equation. We would expect the $^{78}SeO_2$ band origin about 5.5486 cm^{-1} above that of the $^{80}SeO_2$ in the 1_0^4 band, as was used earlier in the low resolution simulation of this band (Section 4.2.2.1).

5.10 Band X

As has already been discussed, King and McLean assigned the 0_0^0 transition to a band they observed with its band head at 31957.4 cm^{-1} [1]. This band was recorded at rotational resolution between 31952 and 31963 cm^{-1}, and is illustrated in Figure 5.15. However the subsequent work on the survey spectrum in Chapter 4 suggests that this is not actually the 0_0^0 band, and the band with a maximum at 31983.24 cm^{-1} and origin at 31981.93 cm^{-1} is a much better candidate for this transition.

The first thing to notice about this band is that the signal to noise ratio is not as good as in the other bands recorded at rotational resolution, especially towards the lower energy end of the band. The intensity of this band was much weaker than that of the other bands studied. The doubling crystal in the Coherent 899-21 ring dye laser is optimised for maximum uv intensity at the start of a scan, and then its position remains fixed throughout the scan. This means that at the end of the scan the crystal is not optimised for ultraviolet intensity, although the short length of the scans mean that it is not far off the maximum intensity. In the bands previously studied the signal was so strong that this effect was barely noticeable, but in this weaker band it was quite a marked effect. In each individual scan the base line was seen to drop off as the laser was scanned to higher frequency. As a result, it was necessary to try to normalise the baseline of each scan before stitching all the scans together. An example of one such scan is shown in Figure 5.16, along with the attempt at normalising the baseline. Although the change in the base line may not seem

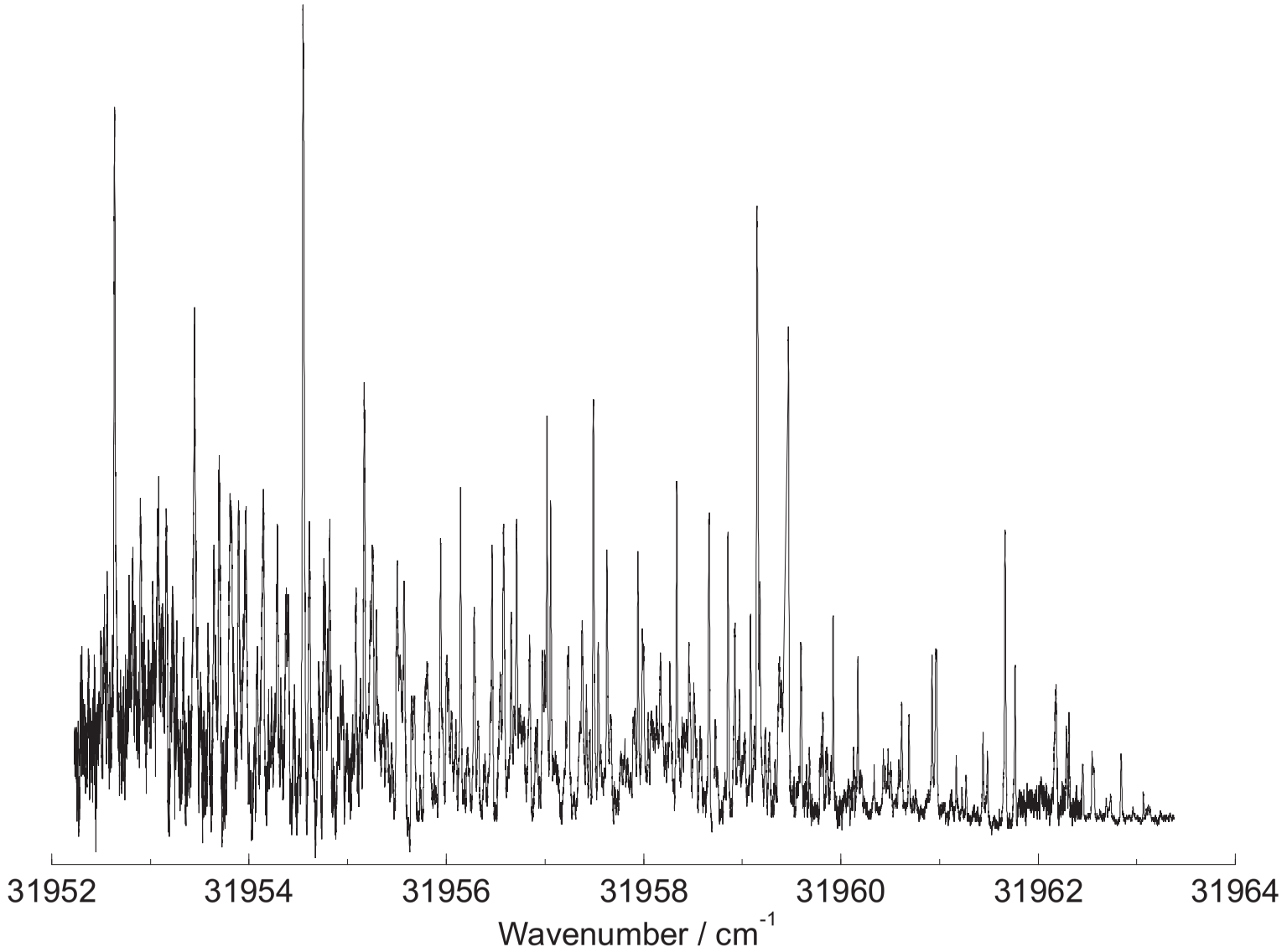

Figure 5.15: The rotationally resolved spectrum of the Band X.

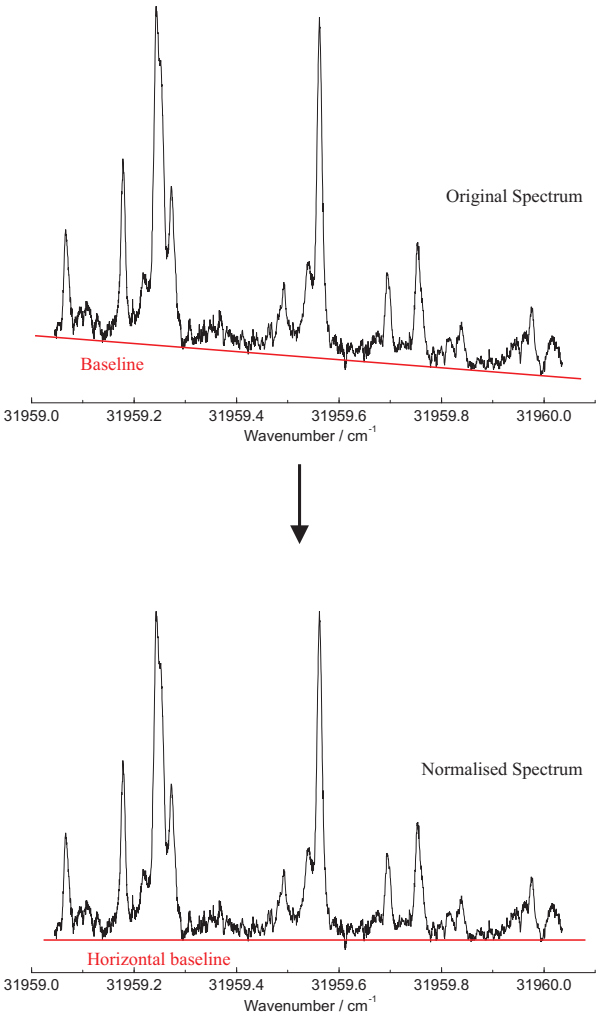

Figure 5.16: An example of one of the scans of Band X to show how the baseline dropped off with the laser power, and the result of normalising the scan to have a horizonal baseline.

too great in one individual scan, it does become significant when stitching together a large number of scans, and could result in the relative intensities being distorted. This method of normalising the base line becomes more difficult as the intensity of the signal decreases, and the low wavenumber side of the spectrum probably still gives a distorted impression of the intensities in that region relative to the rest of the band.

Attempts were made to assign some of the lines seen in this band as A-type transitions originating from the (000) vibrational level of the $^1A_1$ ground state, based on the initial assignment to the 0_0^0 transition proposed by King and McLean. This was done using the

same ground state combination differences used in the other bands, but did not prove very successful. Attempts were first made to assign transitions of the $^{80}SeO_2$ isotopomer, as was the procedure for assigning the lines in all the other bands. A number of possible P and R transitions were observed for the $\Delta K_a = 0$ transitions of the $K_a = 0$ sub-band, which were self-consistent. The analysis was then extended to the $K_a = 1$ sub-band, and again, a number of possible self-consistent P, Q and R transitions were identified within this sub-band. However problems began to arise when attempts were made to fit these two sub-bands together, and hence obtain a value for the A rotational constant. Unfortunately the values for $\bar{B}$ determined for the two sub-bands were not consistent with each other and so the two sets of assignments could not be combined in a single fit. The same was true of the $K_a = 2$ sub-band - a number of possible P, Q and R transitions could be found which fitted together well with each other, but they could not be combined with either of the other two sub-bands. Figure 5.17 shows a small section of the spectrum, indicating which lines are provisionally assigned to R transitions of $^{80}SeO_2$. The simulation above the experimental spectrum was produced using the expected rotational constants for the 0_0^0 band, and show the relative spacings of the transitions if this band was similar in structure to the 0_0^0 band. We recall that the rotational constants did not change very much between the 1_0^1, 1_0^2 and 1_0^3 bands, so even though this is not the 0_0^0 band we would still expect the rotational constants, and hence the structure of the spectrum, to be similar if this was an unperturbed cold band in the $\tilde{C}^1B_2 \leftarrow \tilde{X}^1A_1$ transition. However it is obvious from Figure 5.17 that the experimental and simulated spectra do not match up at all well.

Searches for transitions of $^{78}SeO_2$ and $^{82}SeO_2$ yielded similar results. Since this band was initially thought to be the 0_0^0 transition, transitions of $^{78}SeO_2$ were looked for to lower wavenumber than those of $^{80}SeO_2$, whereas transitions of $^{82}SeO_2$ were searched for at higher energy, as was predicted in Section 5.9. For both of these isotopomers it was possible to find possible assignments for the different K_a sub-bands, as for the $^{80}SeO_2$ isotopomer, however problems arose once again when trying to fit the different sub-bands together. Transitions of $^{76}SeO_2$ were not looked for in this spectrum, for the same reason as $^{82}SeO_2$ transitions were not assigned in the 1_0^1 band. Weak lines due to $^{76}SeO_2$ are expected to be interspersed with much stronger lines due to $^{78}SeO_2$, and it would be very difficult to isolate the

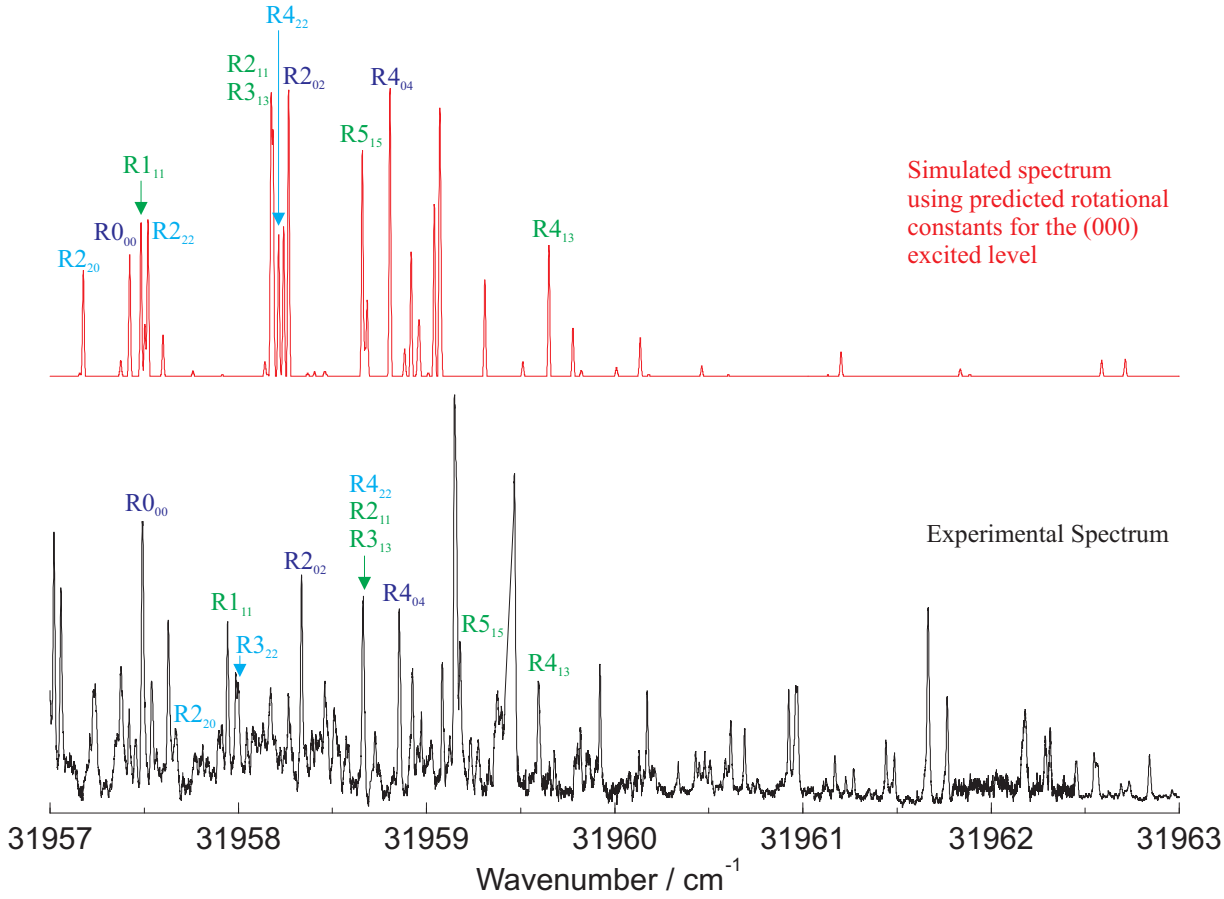

Figure 5.17: A section of Band X, illustrating the tentative assignments made for $^{80}SeO_2$. The simulation shows the expected structure of the spectrum if the rotational constants were to be similar to those predicted for the 0_0^0 band.

$^{76}SeO_2$ transitions from those of $^{78}SeO_2$.

As a result of the fact that the individual K_a sub-bands could not be fitted together for any of the Se isotopes, this band was initially thought to be very heavily perturbed. The need to find out the cause of this perturbation was one of the main factors which prompted the more extensive survey study than had originally been intended, as explained in Chapter 4. However, as discussed in Section 4.2.2.1, the results of the survey spectrum suggested that this in not actually the 0_0^0 band, and the transition was reassigned to a band with its origin at 31981.93 cm^{-1}. As a result of the reassignment of the 0_0^0 band to a band which is higher in energy that this band, it becomes clear that Band X may not actually

originate from the (000) vibrational level of the $^1A_1$ ground state. The energy of the 0_0^0 transition is the minimum required to excite the molecule from the (000) vibrational level of the ground state to the $^1B_2$ excited state. There are a couple of possible explanations for the transition which results in this band being observed in the spectrum. It could be a hot band of the $\tilde{\mathrm{C}}^1B_2 \leftarrow \tilde{\mathrm{X}}^1A_1$ transition, originating from a vibrational level of the ground state other than the (000) level. The other possible explanation is that Band X originates from a completely different electronic state. Neither of these possibilities would have the same ground state combination differences as transitions from the (000) vibrational level of the $^1A_1$ state which would explain why the possible assignments found based on these combination differences could not be fitted together to determine a value for the A rotational constant. Alternatively it could be due to a transition from the $^1A_1$ ground state to a different excited state with different rotational constants. The attempts made here to fit this band were based on the assumption that it was a A-type transitions, however if the symmetry of either of the electronic states was different then this would not necessarily be the case. Obviously further work is required here to confirm or reject any of these possibilities.

Bibliography

[1] G.W. King and P.R. McLean. Selenium Dioxide: Vibrational Analysis of the 3130 Å $^1B_2$ - $^1A_1$ Absorption System. *Journal of Molecular Spectroscopy*, **51**, 1974.

[2] G.W. King and P.R. McLean. Selenium Dioxide: Rotational Analysis and Franck-Condon Calculations for the 3130 Å $^1B_2$ - $^1A_1$ Absorption System. *Journal of Molecular Spectroscopy*, **52**, 1974.

[3] E.A. Alekseev, O.I. Baskakov, and S.F. Dyubko. Microwave Spectrum of Selenium Dioxide. *Proceedings of SPIE - International Society of Optical Engineers*, **3090** (High Resolution Molecular Spectroscopy), 1997.

[4] G. Herzberg. *Electronic Spectra and Electronic Structure of Polyatomic Molecules*, Volume 3 of *Molecular Spectra and Molecular Structure*. Krieger Publishing Company, 1991.

[5] W. Gordy and Cook R.L. *Microwave Molecular Spectra*, Volume 10, part 2 of *Techniques of Organic Chemistry*. Interscience Publishers, 1970.

Chapter 6

Discussion Of Results

6.1 Summary of Achievements

The spectrum of the $\tilde{\mathrm{C}}^1B_2 \leftarrow \tilde{\mathrm{X}}^1A_1$ transition of SeO_2 has been recorded at lower rotational temperatures and higher resolution than in any previous work.

In the initial phase of this project only short sections of the survey spectrum of SeO_2 were recorded. However it was later deemed necessary to extend this survey work to a much wider region in an attempt to explain perturbations observed in some of the bands recorded at rotational resolution. The more extensive survey spectrum revealed a large number (around 100) of new bands in the same region as the $\tilde{\mathrm{C}}^1B_2 \leftarrow \tilde{\mathrm{X}}^1A_1$ transition, which were not reported by King and McLean [1]. As a result the 0_0^0 band has been reassigned, which also resulted in the reassignment of a number of other transitions. Some of the progessions observed by King and McLean have been extended, which, in combination with the reassignments, leads to an improved calculation of some of the excited state vibrational constants, and an estimate of ν_3'. This estimated value of ν_3', which is around 571 cm^{-1}, is a far more acceptable value that the value of 78 cm^{-1} proposed by King and McLean [1]. While the reassignments and extensions of existing assignments accounted for some of the newly observed transitions, they only explain a small fraction of these transitions, and the remaining transitions are thought to be due to different electronic transitions which lie in the same region as the $\tilde{\mathrm{C}}^1B_2 \leftarrow \tilde{\mathrm{X}}^1A_1$ transition.

Selected bands were also recorded at rotational resolution, and successfully analysed.

The rotational analysis of these bands led to us being able to determine the excited state rotational constants, and hence calculate the molecular geometry of the $^1B_2$ excited state in the given vibrational levels. This in turn enabled the geometry of the (000) vibrational level of the excited state to be estimated. A large increase in the bond length was observed on excitation, from 160.878 pm in the ground state to 171.963 pm in the excited state, along with a large decrease in the bond angle from 114.0154 ° to 103.0384 °. This is consistent with the excitation of an electron from an (a_2'') orbital to a $(\bar{b}_1'')$ orbital. The $(\bar{b}_1'')$ orbital has a bonding component between the two oxygen atoms and an antibonding component between the selenium and each oxygen atom, whereas the (a_2'') orbital is localised on an oxygen atom, and is weakly antibonding. The change in geometry is also consistent with the long progressions observed for the symmetric stretching and bending vibrations in the excited state, ν_1' and ν_2'. Although King and McLean [2] proposed the excited state to be of $^1B_2$ symmetry, there were a number of questionable assumptions in their analysis. The present work confirms beyond all reasonable doubt that the excited state is $^1B_2$, and the transition studied is $\tilde{\mathrm{C}}^1B_2 \leftarrow \tilde{\mathrm{X}}^1A_1$. The $\tilde{\mathrm{C}}$ label of this $^1B_2$ state is consistent with the labelling of the electronic states of SO_2.

6.2 Comparison of SeO_2 with SO_2

Sulphur dioxide is an important molecule in the earth's atmosphere, primarily arising from the combustion of coal and other fossil fuels. It is also an important constituent of the atmosphere of Venus. As a result of this, and the fact that it is spectroscopically interesting as a typical bent triatomic molecule, SO_2 had been the subject of much spectroscopic investigation over recent years, and therefore provides an interesting and informative comparison with SeO_2.

The microwave spectrum of SO_2 has been studied in great detail. In 1985 Lovas [3] published a review of the microwave spectrum of SO_2, in which he gathered together all the available data from various laboratory measurements and fitted them to the Watson centrifugal distortion Hamiltonian. The rotational constants of the (000) vibrational level of the $^1A_1$ ground state of $^{32}SO_2$ are given in Table 6.1. We can see from this table that

Table 6.1: Rotational constants for the (000) vibrational level of the $^1A_1$ ground state of $^{32}SO_2$ [3]. The numbers in brackets represent 1 standard deviation in the units of the last digit given.

Rotational Parameter	Value / MHz	Value / cm^{-1}
A''	60778.5612(17)	2.027354577(56)
B''	10317.91538(23)	0.3441686108(77)
C''	8799.65360(25)	0.2935248491(83)

the ground state rotational constants of SO_2 are larger than those of SeO_2, particularly the A rotational constant. This is to be expected for a lighter molecule since, for a similar structure, it would have smaller moments of inertia.

The $^1B_2$ excited electronic state of SO_2 was studied by Brand *et al.* in 1976 [4], and they rotationally analysed eight bands of SO_2 in the 235 nm region as A-type transitions of a near-prolate asymmetric rotor. The most relevant of these bands for comparison with SeO_2 is the 0_0^0 transition, and the constants of the (000) vibrational level of the excited state are given in Table 6.2. As was the case for the ground state rotational constants, the rotational constants of the excited state of SO_2 are greater than those of SeO_2, in particular the A constant.

Table 6.2: The band origin and rotational constants for the (000) vibrational levels of the $^1B_2$ excited state of SO_2, as determined by Brand [4].

Constant	Value / cm^{-1}	Error / cm^{-1}
T_0	42573.450	$\pm$ 0.005
A	1.15053	$\pm$ 0.00014
B	0.34744	$\pm$ 0.00002
C	0.26543	$\pm$ 0.00002

Using the values given in Tables 6.1 and 6.2 it is possible to determine the geometry of SO_2 in the same way as for SeO_2. Equations 5.2 and 5.3 are used to calculate the O−S−O bond angle and the S−O bond length using only the A and B rotational constants for the same reasons as discussed in Section 5.8, the fact that the C rotational constant is affected by Coriolis coupling. The zero-point (i.e. those of the (000) vibrational level) geometries of

SO_2 are given in Table 6.3 for both the $^1A_1$ ground state and the $^1B_2$ excited electronic state, along with the corresponding values for $^{80}SeO_2$ from Section 5.8 for ease of comparison. As would be expected for the $\tilde{C}^1B_2 \leftarrow \tilde{X}^1A_1$ transition, and as was the case for $^{80}SeO_2$,

Table 6.3: Zero-point geometry for the $^1A_1$ ground state and $^1B_2$ excited states of SO_2 [3, 4] and $^{80}SeO_2$ [5]. The numbers in brackets represent 1 standard deviation in the units of the last digit given.

Molecule	State	r X−O / pm	θ O−X−O / ^{o}
SO_2	$^1A_1$	143.2179577(17)	119.5354299(13)
	$^1B_2$	155.9814(63)	104.2870(50)
$^{80}SeO_2$	$^1A_1$	160.8779978(40)	114.0153684(27)
	$^1B_2$	171.963(10)[a]	103.0384(70)[a]

[a] Estimated values as calculated in Section 5.8

the bond length of SO_2 increases on excitation but the bond angle decreases. The changes observed in the bond length and bond angles, as a percentage of the ground state value, are slightly larger for SO_2 than for SeO_2. The bond length of SO_2 increases by approximately 8.9 % of the ground state value on excitation, whereas that of $^{80}SeO_2$ increases by 6.9 %. Similarly, the bond angle of SO_2 decreases by almost 12.8 % of the ground state value on excitation but the bond angle of $^{80}SeO_2$ decreases by 9.6 %.

Another interesting point of comparison is provided by the fluorescence lifetimes of the two molecules. Ivanco *et al.* [6] measured the lifetimes of a number of vibrational levels of the $^1B_2$ state of SO_2 from the origin band at 234.8 nm down to 217 nm. These measurements were all well below the dissociation threshold. They quote the lifetime of a typical band in this region to be 33.3 ns. This value is in good agreement with the lifetimes of SeO_2 measured in this work, which covered the range between 52.8 and 10.9 ns. A summary of the lifetimes of the low lying vibrational levels shows that the lifetime of SO_2 does not have a very sensitive dependence on the excitation energy, and tends to increase only gradually as the energy of excitation increases. In other words, the lifetime of the (200) vibrational level is slightly larger than that of the (100) level, which is turn is slightly larger than that of the (000) vibrational level. Above 45400 cm^{-1}, which

corresponds to the energy of the 1_0^3 band, the lifetime of SO_2 drops sharply to below 10 ns [7], indicating that this is the threshold of predissociation :

$$SO_2\ (^1B_2) \rightarrow SO\ (X\ ^3\Sigma^-) + O\ (^3P).$$

The predominant mechanism for this predissociation is via a repulsive $^1A_1$ state, which undergoes an avoided electronic curve crossing with the $\tilde{C}^1B_2$ state [8]. Although the lifetime of the (000) vibrational level of SeO_2 was not recorded in this work, the opposite trend was observed in the lifetimes of SeO_2 compared with that seen in the low vibrational levels of SO_2, and the lifetime decreased as the number of quanta of the symmetric stretching vibration excited increased. This decrease might be indicative of the onset of predissociation in SeO_2, although further work would be required to determine the exact threshold.

Following the work of Brand *et al.*, Yamanouchi *et al.* [9] recorded further vibrational bands in the $\tilde{C}^1B_2 \leftarrow \tilde{X}^1A_1$ transition of SO_2 at rotational resolution. In these experiments they observed the Laser Induced Fluorescence (LIF) spectrum of SO_2 under jet-cooled conditions, the same technique as used in this study of SeO_2. The rotational constants they calculated for the (000), (100), (200) and (300) vibrational levels of the $^1B_2$ excited state show a non-linear dependence on v_1, as was the case with the constants for SeO_2. The prominent vibrational progressions in the SO_2 spectrum were in the bending vibration, ν_2', whereas the prominent progressions in the SeO_2 spectrum seem to involve the symmetric stretching vibration, ν_1'.

Yamanouchi *et al.* reported that the C rotational constant showed large fluctuations in the range 0.1397 cm^{-1} to 0.3673 cm^{-1} over the various vibrational bands, which is one of the characteristic features of the $^1B_2$ state vibronic levels. This is not due to a structural deformation to a molecule with unequal S−O bonds, but instead is due to strong c-axis Coriolis interaction. In certain places this interaction was too strong to allow the transitions to be fitted using only the A, B and C rotational constants. The extent of the Coriolis interaction is reflected in the inertial defects quoted by Yamanouchi *et al.*, which range from 56.80 u$Å^2$ to −16.93 u$Å^2$ in the vibrational bands reported. There is a tendency for the most strongly perturbed bands to have a non-zero value of v_3. In other words, excitation of the asymmetric stretching mode seems to significantly promote this

c-axis Coriolis interaction. Although it may not be explicitly evident in the C rotational constants of the bands studied in this work at rotational resolution, we would expect to see c-axis Coriolis interactions in SeO_2 also.

There has been much speculation about the geometry of SO_2 in this $^1B_2$ state, with some workers [4, 7, 10] accounting for the perturbations observed by means of an unsymmetrical equilibrium geometry in the excited state, in which the two S−O bonds are not of equal length, and a double-minimum potential along the normal co-ordinate of the asymmetric stretching vibration. Hoy and Brand [10] conclude that the anharmonicity in the asymmetric stretching vibration is due to a shallow double-minimum potential, however this does not account for the unexpectedly high intensity they observe in the 3_0^2 transition, which is attributed to a Fermi resonance. In this asymmetrical structure, the two S−O bond lengths are 163.9 nm and 149.1 nm. Ebata [7] observed a large anharmonicity for the (002), (004) and (006) vibrational levels of the $^1B_2$ state, but a double-minimum potential should result in an anharmonicity on the levels with an odd quanta of ν_3 excited, and these are not observed.

The most plausible explanation is to attribute these effects to interaction with another nearby electronic state. A $^1A_1$ state lies only about 2000 cm^{-1} above the $\tilde{C}^1B_2$ state of SO_2. Absorption from the ground state to this $^1A_1$ state is considerably weaker than to the $\tilde{C}^1B_2$ state. There is strong vibronic coupling involving the ν_3 vibrations of these two electronic states, which explains why vibrational levels with odd quanta of ν_3 excited are observed in the spectra of both the states. This coupling seems to be strong enough to push the $^1B_2$ state of SO_2 into a slightly asymmetric shape. Although King and McLean [1] reported a vibrational band 78 cm^{-1} above their assignment of the 0_0^0 band of SeO_2 and accounted for its presence by means of a double-minimum potential, no evidence to support this suggestion has been found in the present study, and all the bands analysed at rotational resolution could be accounted for by a symmetrical molecule. By analogy with SO_2, we would expect to find a $^1A_1$ state for SeO_2 a small distance above the $^1B_2$ state, although in contrast there was no evidence of such a state overlapping with the $^1B_2$ state in the vibrationally resolved spectrum of TeO_2 [11].

6.3 Future Work

There is a large amount of further work which should be done on SeO_2. The most obvious starting point would be to record the newly assigned 0_0^0 band at rotational resolution. A complete rotational analysis of this band will lead to an accurate calculation of the band origin and would provide the rotational constants of the (000) vibrational level of the $^1B_2$ state. In turn, this will lead to an accurate determination of the zero-point geometry of the molecule. In addition, rotational analysis of the 2_0^1 and 3_0^2 bands and determination of the excited state rotational constants of these levels would enable us to calculate the equilibrium geometry of the molecule in the excited state, which should be unchanged on isotopic substitution of Se. Recording these bands will also provide more accurate values for the vibrational intervals for the bending and asymmetric stretching vibrations.

The vibrationally resolved spectrum, which was initially only recorded to such an extent in an attempt to explain the perturbations observed in some of the rotational resolved bands, requires more work to understand it fully, and assign all the bands observed. Extending this survey to both higher and lower wavelength will allow us to determine the nature of the electronic states involved in the bands which cannot be assigned to the $\tilde{C}^1B_2 \leftarrow \tilde{X}^1A_1$ transition. It may also be necessary to record at least some, if not all, of these bands at rotational resolution to determine their exact nature.

6.4 Further Work on TeO_2

As has already been discussed, the initial motivation for this study was to assist with the analysis of rotationally resolved spectra of TeO_2. Although a number of vibrational bands of the assumed $\tilde{C}^1B_2 \leftarrow \tilde{X}^1A_1$ electronic transition of TeO_2 had been recorded previously at rotational resolution, attempts to analyse the rotational structure proved unsuccessful [11]. We are now in a position to make better estimates of the structure of TeO_2, and hence the rotational constants, which should make analysis of these spectra easier.

Initial attempts to assign the rotational structure of the 0_0^0 band of TeO_2 were based on the assumption that the isotope structure would not be resolved. However in the light

of the work discussed here it seems likely that this assumption was wrong, and a first attempt at simulating the structure of the band using an isotopic shift of approximately -0.5 cm^{-1} with increasing mass of the Te atom, for the three most abundant isotopomers ($^{126}TeO_2$, $^{128}TeO_2$ and $^{130}TeO_2$), produced a spectrum which agreed much better with the experimental spectrum, certainly in the density of lines even though the detail was not correct. Figure 6.1 shows the best simulation of the 0_0^0 band of TeO_2 to date. This

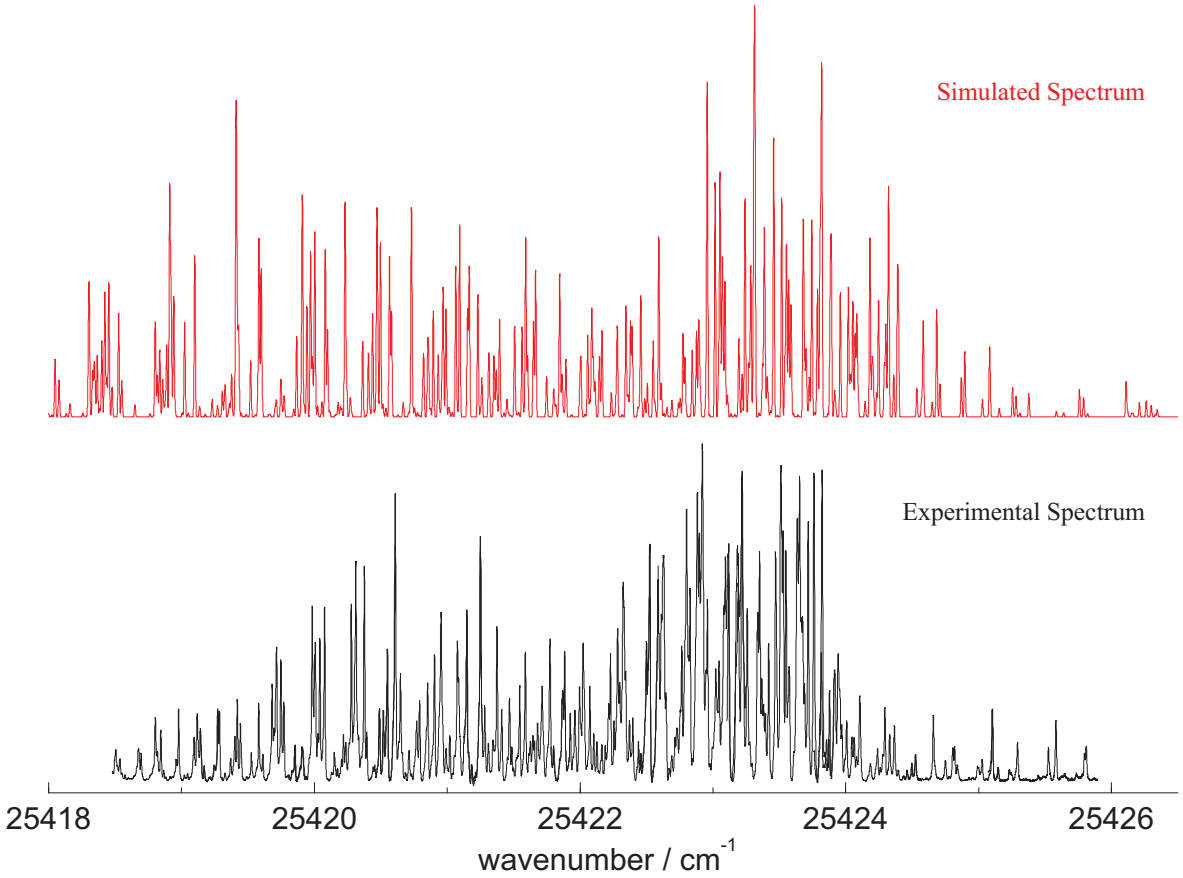

Figure 6.1: A simulation of the 0_0^0 transition of TeO_2, produced using the current best estimates of the molecular geometry and isotopic shifts.

simulation was produced using a O−Te−O bond angle of 111.7 ° and a Te−O bond length of 179.9 pm in the ground state, with a bond angle of 100 ° and bond length of 193.7 pm in the excited state. This geometry was obtained by comparing *ab initio* calculations of the geometry of SeO_2 [12] with the experimentally determined values from this work, and then making a 'best guess' of the geometry of TeO_2 from the same theoretical calculations.

For this geometry the bond length increases by 7.7 % on excitation, and the bond angle decreases by 10.5 %, changes which compare reasonably well with the changes seen in SO_2 and SeO_2. The rotational constants for these assumed geometries are given in Table 6.4. The band origin of $^{130}TeO_2$ was set at 25421.5 cm^{-1}, with the $^{128}TeO_2$ isotopomer

Table 6.4: Rotational constants of TeO_2 used in the simulation in Figure 6.1.

Isotopomer	A'' / cm^{-1}	B'' / cm^{-1}	C'' / cm^{-1}	A' / cm^{-1}	B' / cm^{-1}	C' / cm^{-1}
$^{126}TeO_2$	0.6477	0.2677	0.1738	0.4261	0.2393	0.1532
$^{128}TeO_2$	0.6457	0.2677	0.1737	0.4248	0.2393	0.1531
$^{130}TeO_2$	0.6437	0.2377	0.1736	0.4235	0.2393	0.1528

shifted 0.5 cm^{-1} to higher wavenumber, and the $^{126}TeO_2$ shifted another 0.5 cm^{-1} higher than $^{128}TeO_2$. This order of the isotopomers is consistent with that seen in the 0_0^0 band of SeO_2.

Although this simulation does not agree quantitatively with the experimental spectrum, the agreement is much better that any simulations produced prior to this work on SeO_2 [11]. We can see that many of the main features of the experimental spectrum are present in this simulation. The simulation spreads over a larger wavenumber range than the experimental spectrum, and so needs compressing to give better agreement with the experimental spectrum. Obviously further work is required here to obtain a simulation which does agree in detail with the experimental spectrum, and hence obtain values for the rotational constants and the geometry of TeO_2.

Once more work has been done on the analysis of the rotationally resolved bands of TeO_2, it will be possible to study the reactions between Te or TeO_2 and water or oxygen at high temperatures, which was the initial aim of this project.

Bibliography

[1] G.W. King and P.R. McLean. Selenium Dioxide: Vibrational Analysis of the 3130 Å $^1B_2$ - $^1A_1$ Absorption System. *Journal of Molecular Spectroscopy*, **51**, 1974.

[2] G.W. King and P.R. McLean. Selenium Dioxide: Rotational Analysis and Franck-Condon Calculations for the 3130 Å $^1B_2$ - $^1A_1$ Absorption System. *Journal of Molecular Spectroscopy*, **52**, 1974.

[3] F.J. Lovas. Microwave Spectra of Molecules of Astrophysical Interest XXII. Sulfur Dioxide (SO_2). *Journal of Physical and Chemical Reference Data*, **14**(2), 1985.

[4] J.C.D. Brand, P.H. Chiu, A.R. Hoy, and H.D. Bist. Sulfur Dioxide: Rotational Constants and Asymmetric Structure of the $\tilde{C}^1B_2$ State. *Journal of Molecular Spectroscopy*, **60**, 1976.

[5] E.A. Alekseev, O.I. Baskakov, and S.F. Dyubko. Microwave Spectrum of Selenium Dioxide. *Proceedings of SPIE - International Society of Optical Engineers*, **3090** (High Resolution Molecular Spectroscopy), 1997.

[6] M. Ivanco, J. Hager, W. Sharfin, and S.C. Wallace. Quantum interference phenomena in the radiative decay of the $\tilde{C}^1B_2$ state of SO_2. *Journal of Chemical Physics*, **78**(11), 1983.

[7] T. Ebata, O. Nakazawa, and M. Ito. Rovibrational Dependences of the Predissociation in the $\tilde{C}^1B_2$ state of SO_2. *Chemical Physics Letters*, **143**(1), 1988.

[8] P.C. Ray, M.F. Arendt, and L.J. Butler. Resonance emission spectroscopy of predissociation SO_2 $\tilde{C}^1B_2$: Coupling with a repulsive $^1A_1$ state near 200 nm. *Journal of Chemical Physics*, **109**(13), 1998.

[9] K Yamanouchi, M. Okunishi, Y. Endo, and S. Tsuchiya. Laser Induced Fluorescence Spectroscopy of the $\tilde{C}^1B_2$ - $^1A_1$ band of jet-cooled SO_2: Rotational and Vibrational Analyses in the 235 - 210 nm region. *Journal of Molecular Structure*, **352/353**(Com), 1995.

[10] A.R. Hoy and J.C.D. Brand. Asymmetric structure and force field of the $^1B_2(^1A')$ state of sulphur dioxide. *Molecular Physics*, **36**(5), 1978.

[11] D.F. Hullah. *The Electronic Spectra of FeH and TeO_2*. D.Phil thesis, University of Oxford, 1999.

[12] A.J. Bridgeman. Private communication. 2001.

Appendix A

Rotational Assignments

Tables A.1 to A.4 contain the rotational assignments made for the 1_0^1, 1_0^2 and 1_0^3 bands for the four most abundant isotopes of SeO_2. In addition, the attempts to assign Band X as the 0_0^0 transition are included, although subsequent work has proved this not to be the 0_0^0 transition.

Table A.1: Assigned lines in the $^1B_2(v_1,0,0) \leftarrow {}^1A_1(0,0,0)$ transitions of $^{76}SeO_2$

	Band X		(1,0,0)		(2,0,0)		(3,0,0)	
$J'_{KaKc} - J''_{KaKc}$	ν / cm^{-1}	o-c	ν	/ cm^{-1} o-c	ν	/ cm^{-1} o-c	ν / cm^{-1}	o-c
				$\Delta K = 0, K''_a = 0$				
$1_{0,1}$ - $2_{0,2}$					33249.4550	0.0044	33901.1802	0.0038
$3_{0,3}$ - $4_{0,4}$					33248.3044[a]	0.0023	33900.0173[a]	-0.0081
$5_{0,5}$ - $6_{0,6}$					33246.9626	0.0041	33898.6694	-0.0031
$7_{0,7}$ - $8_{0,8}$							33897.1032	-0.0007
$9_{0,9}$ - $10_{0,10}$							33895.3608[a]	0.0016
$1_{0,1}$ - $0_{0,0}$			32610.9484	-0.0029	33250.9766	-0.0055	33902.7158	0.0079
$3_{0,3}$ - $2_{0,2}$					33251.8194	-0.0036	33903.5459	-0.0004
$5_{0,5}$ - $4_{0,4}$			32612.3444	-0.0021	33252.3620	-0.0000	33904.0736	-0.0025
$7_{0,7}$ - $6_{0,6}$					33252.5956	-0.0002	33904.2940	-0.0021

[a] These transitions are overlapped, and make up less than 25 % of the total line intensity, and so were given a weight of zero in the fit.

Table A.1 cont'd.

	Band X		(1,0,0)		(2,0,0)		(3,0,0)	
$J'_{KaKc} - J''_{KaKc}$	ν / cm^{-1}	o-c	ν	/ cm^{-1} o-c	ν	/ cm^{-1} o-c	ν / cm^{-1}	o-c
				$\Delta K = 0, K''_a = 1$				
$1_{1,0}$ - $2_{1,1}$			32609.0514[a]	0.0017			33900.8012	0.0047
$2_{1,2}$ - $3_{1,3}$			32608.6282	0.0090	33248.6438	-0.0029	33900.3646	0.0011
$3_{1,2}$ - $4_{1,3}$					33247.9296	0.0093	33899.6412	0.0007
$4_{1,4}$ - $5_{1,5}$			32607.4268	0.0037	33247.4448	0.0009	33899.1606[a]	0.0039
$5_{1,4}$ - $6_{1,5}$					33246.6636	0.0028		
$6_{1,6}$ - $7_{1,7}$					33246.0636	0.0000	33897.7661	-0.0019
$7_{1,6}$ - $8_{1,7}$							33896.8924[a]	0.0042
$1_{1,0}$ - $1_{1,1}$					33250.2344	-0.0013	33901.9532	-0.0010
$2_{1,2}$ - $2_{1,1}$			32609.8498[a]	-0.0024			33901.5988	0.0023
$4_{1,4}$ - $4_{1,3}$							33900.8664[a]	0.0009
$5_{1,4}$ - $5_{1,5}$							33902.6108[a]	0.0054
$2_{1,2}$ - $1_{1,1}$			32611.0044	-0.0054	33251.0408	0.0035	33902.7618	0.0077
$3_{1,2}$ - $2_{1,1}$			32611.7078	-0.0008	33251.7214	-0.0041	33903.4390	-0.0066
$4_{1,4}$ - $3_{1,3}$			32611.7078	0.0036	33251.7214	-0.0036	33903.4390	0.0012
$5_{1,4}$ - $4_{1,3}$					33252.5956	0.0005		
$6_{1,6}$ - $5_{1,5}$			32612.1928	-0.0005	33252.2039	-0.0012	33903.9090	-0.0005
$7_{1,6}$ - $6_{1,5}$			32613.1870	-0.0046	33253.1688	-0.0012		
$8_{1,8}$ - $7_{1,7}$					33252.4606	0.0003	33904.1527	0.0008
$10_{1,10}$ - $9_{1,9}$					33252.4978	0.0001		

Table A.1 cont'd.

	Band X		(1,0,0)		(2,0,0)		(3,0,0)	
$J'_{KaKc} - J''_{KaKc}$	ν / cm^{-1}	o-c	ν / cm^{-1}	o-c	ν / cm^{-1}	o-c	ν / cm^{-1}	o-c
			$\Delta K = 0, K''_a = 2$					
$2_{2,1}$ - $3_{2,2}$							33899.3380	0.0028
$3_{2,1}$ - $4_{2,2}$			32607.0432	-0.0015	33247.0590	0.0010	33898.7496	-0.0057
$4_{2,3}$ - $5_{2,4}$					33246.4504[a]	0.0005		
$2_{2,1}$ - $2_{2,0}$			32609.1578	0.0059	33249.1716	-0.0004	33900.8664	-0.0004
$3_{2,1}$ - $3_{2,2}$			32609.1578	0.0004	33249.1716	0.0009	33900.8664	-0.0016
$4_{2,3}$ - $4_{2,2}$					33248.9304	-0.0014	33900.6186	-0.0076
$6_{2,5}$ - $6_{2,4}$							33900.0639	-0.0033
$3_{2,1}$ - $2_{2,0}$			32610.6816	-0.0074	33250.7006	-0.0017	33902.3955	-0.0041
$4_{2,3}$ - $3_{2,2}$			32611.0368[a]	0.0006			33902.7374	-0.0015
$5_{2,3}$ - $4_{2,2}$							33903.4390[a]	-0.0025
$6_{2,5}$ - $5_{2,4}$							33903.4222	0.0068
$7_{2,5}$ - $6_{2,4}$					33252.7697	-0.0019		
$9_{2,7}$ - $8_{2,6}$			32613.6540	0.0029			33905.2790	-0.0052
			$\Delta K = 0, K''_a = 3$					
$3_{3,0}$ - $4_{3,1}$							33897.1504	-0.0019
$4_{3,2}$ - $4_{3,1}$							33899.1328[a]	0.0058
$7_{3,4}$ - $7_{3,5}$							33899.0162	0.0014
$4_{3,2}$ - $3_{3,1}$							33901.1802[a]	-0.0053
$6_{3,4}$ - $5_{3,3}$					33250.3424	0.0009	33902.0012	0.0006
$7_{3,4}$ - $6_{3,3}$							33902.6108	0.0013
$10_{3,8}$ - $9_{3,7}$							33903.2210	0.0072

Table A.2: Assigned lines in the $^1B_2(v_1,0,0) \leftarrow {}^1A_1(0,0,0)$ transitions of $^{78}SeO_2$

	Band X		(1,0,0)		(2,0,0)		(3,0,0)	
$J'_{KaKc} - J''_{KaKc}$	ν / cm^{-1}	o-c	ν / cm^{-1}	o-c	ν / cm^{-1}	o-c	ν / cm^{-1}	o-c
			$\Delta K = 0, K''_a = 0$					
$1_{0,1}$ - $2_{0,2}$	31955.5274	-0.0001	32608.2648	0.0016	33246.7242	-0.0006	33896.8924[b]	-0.0139
$3_{0,3}$ - $4_{0,4}$	31954.3740	-0.0021	32607.1300	0.0067	33245.5784	0.0026	33895.7737[b]	0.0203
$5_{0,5}$ - $6_{0,6}$	31953.0236	0.0031	32605.7876	-0.0007	33244.2316	-0.0002	33894.4144[ab]	0.0143
$7_{0,7}$ - $8_{0,8}$			32604.2448	0.0010	33242.6798	0.0017		
$9_{0,9}$ - $10_{0,10}$							33891.0872	-0.0067
$1_{0,1}$ - $0_{0,0}$	31957.0574	-0.0004	32609.7942	0.0007	33248.2507	-0.0044	33898.4216[b]	-0.0150
$3_{0,3}$ - $2_{0,2}$	31957.8959	0.0029	32610.6390	-0.0012	33249.0930	0.0003	33899.2919[b]	0.0216
$5_{0,5}$ - $4_{0,4}$	31958.4122	-0.0034	32611.1826	-0.0007	33249.6268	0.0000	33899.8058[b]	0.0107
$7_{0,7}$ - $6_{0,6}$			32611.4278	0.0050	33249.8632	0.0061	33900.0173	0.0041
$9_{0,9}$ - $8_{0,8}$							33900.0173[a]	-0.0082
$11_{0,11}$ - $10_{0,10}$			32611.3420	0.0010			33899.8789[a]	0.0020
$13_{0,13}$ - $12_{0,12}$							33899.5634	-0.0031

[a] These transitions are overlapped, and make up less than 25 % of the total line intensity, and so were given a weight of zero in the fit.
[b] These transitions were perturbed by up to ~ 0.02 cm^{-1}, and so were given a weight of zero in the fit.

Table A.2 cont'd.

	Band X		(1,0,0)		(2,0,0)		(3,0,0)	
$J'_{KaKc} - J''_{KaKc}$	ν / cm^{-1}	o-c	ν / cm^{-1}	o-c	ν / cm^{-1}	o-c	ν / cm^{-1}	o-c
			$\Delta K = 0, K''_a = 1$					
$1_{1,0}$ - $2_{1,1}$	31955.5274	-0.0024	32607.8962	0.0032	33246.3538	-0.0001	33896.5263	-0.0016
$2_{1,2}$ - $3_{1,3}$	31955.1038	0.0047	32607.4668	0.0027	33245.9224	-0.0018	33896.0940	-0.0029
$3_{1,2}$ - $4_{1,3}$	31954.3953	0.0038	32606.7530	0.0035	33245.1950	0.0014	33895.3608	-0.0040
$4_{1,4}$ - $5_{1,5}$	31953.8932	-0.0094	32606.2729	0.0027	33244.7202	-0.0016		
$5_{1,4}$ - $6_{1,5}$	31953.1605	0.0021	32605.5114	0.0010	33243.9338	0.0046		
$6_{1,6}$ - $7_{1,7}$	31952.5296	0.0027	32604.9006	0.0000	33243.3406	-0.0010		
$7_{1,6}$ - $8_{1,7}$			32604.0504	0.0033				
$8_{1,8}$ - $9_{1,9}$					33241.7676	0.0008	33891.9210	0.0055
$10_{1,10}$ - $11_{1,11}$					33239.9956	-0.0022		
$1_{1,0}$ - $1_{1,1}$	31956.6892	0.0017	32609.0514	0.0007	33247.5108	-0.0008	33897.6836	-0.0019
$2_{1,2}$ - $2_{1,1}$			32608.6892[a]	-0.0048	33247.1500	-0.0041	33897.3238	-0.0031
$3_{1,2}$ - $3_{1,3}$	31956.9728	0.0077	32609.3240	0.0009	33247.7672	-0.0000	33897.9332	-0.0052
$5_{1,4}$ - $5_{1,5}$	31957.3772	-0.0101	32609.7423	0.0029	33248.1578	-0.0003		
$6_{1,6}$ - $6_{1,5}$	31954.4262	-0.0041						
$7_{1,6}$ - $7_{1,7}$	31957.7778	0.0039					33898.6694[a]	0.0012
$9_{1,8}$ - $9_{1,9}$			32610.2898	0.0024				
$11_{1,10}$ - $11_{1,11}$			32610.1880[a]	0.0030	33248.5458[a]	0.0070		
$2_{1,2}$ - $1_{1,1}$	31957.4908	0.0041	32609.8498	-0.0019	33248.3063	-0.0055	33898.4742[ab]	-0.0103
$3_{1,2}$ - $2_{1,1}$	31958.1944	-0.0006	32610.5490	-0.0040	33248.9988	0.0016	33899.1606	-0.0078
$4_{1,4}$ - $3_{1,3}$	31958.1710	-0.0068	32610.4590	0.0035	33248.9988	0.0018	33899.1606	-0.0046
$5_{1,4}$ - $4_{1,3}$	31959.0830	-0.0060			33249.8632	0.0034	33900.0173	-0.0065
$6_{1,6}$ - $5_{1,5}$	31958.6646	0.0053	32611.0346	0.0017	33249.4729	-0.0011	33899.6412	0.0070
$7_{1,6}$ - $6_{1,5}$	31959.6806	0.0032	32612.0214	-0.0078			33900.5754	0.0037
$8_{1,8}$ - $7_{1,7}$			32611.2900	-0.0065	33249.7256	-0.0004	33899.8789	0.0042
$9_{1,8}$ - $8_{1,7}$			32612.1628	-0.0051				
$10_{1,10}$ - $9_{1,9}$			32611.3420	-0.0022	33249.7590	-0.0019		
$11_{1,10}$ - $10_{1,9}$			32611.9122	0.0015			33900.3646[a]	0.0005
$12_{1,12}$ - $11_{1,11}$			32611.1826[a]	-0.0091	33249.5964	0.0023		
$13_{1,12}$ - $12_{1,11}$			32611.4116	-0.0002				
$14_{1,14}$ - $13_{1,13}$							33899.3380[a]	0.0020

Table A.2 cont'd.

	Band X		(1,0,0)		(2,0,0)		(3,0,0)	
$J'_{KaKc} - J''_{KaKc}$	ν / cm^{-1}	o-c	ν / cm^{-1}	o-c	ν / cm^{-1}	o-c	ν / cm^{-1}	o-c
			$\Delta K = 0, K''_a = 2$					
$2_{2,1}$ - $3_{2,2}$	31954.2632	0.0010	32606.4658	0.0001			33895.0733[a]	-0.0003
$3_{2,1}$ - $4_{2,2}$			32605.8918	-0.0003	33244.3406	0.0008	33894.4911	0.0017
$4_{2,3}$ - $5_{2,4}$	31953.0756	-0.0005			33243.7338	0.0023	33893.8820	0.0046
$5_{2,3}$ - $6_{2,4}$	31952.5554	-0.0001	32604.7674	-0.0014	33243.1898	0.0062	33893.3378	0.0059
$6_{2,5}$ - $7_{2,6}$			32603.9838	0.0000	33242.4084	0.0055		
$7_{2,5}$ - $8_{2,6}$							33892.1096	0.0020
$8_{2,7}$ - $9_{2,8}$					33240.8956	0.0063		
$9_{2,7}$ - $10_{2,8}$							33890.6598[a]	-0.0009
$2_{2,1}$ - $2_{2,0}$	31955.7980	0.0055	32607.9987	0.0027	33246.4516	-0.0025	33896.6042	0.0003
$3_{2,1}$ - $3_{2,2}$	31955.7980	-0.0006	32607.9987	-0.0060	33246.4516	-0.0008	33896.6042	0.0023
$4_{2,3}$ - $4_{2,2}$			32607.7606	-0.0076	33246.2101	0.0003	33896.3564	0.0007
$5_{2,3}$ - $5_{2,4}$	31955.9094	0.0028	32608.1280	0.0081			33896.6808	-0.0022
$7_{2,5}$ - $7_{2,6}$			32608.4246	-0.0011			33896.9416	0.0034
$8_{2,7}$ - $8_{2,6}$			32606.2228	0.0005				
$9_{2,7}$ - $9_{2,8}$			32608.7834[a]	0.0069			33897.2312	0.0041
$10_{2,9}$ - $10_{2,8}$			32604.6854[a]	-0.0071			33893.1717	0.0026
$3_{2,1}$ - $2_{2,0}$	31957.3206	-0.0083	32609.5316[a]	-0.0034	33247.9812	-0.0015	33898.1332	0.0009
$4_{2,3}$ - $3_{2,2}$	31957.6678	0.0009	32609.8799	-0.0009	33248.3210	-0.0014	33898.4742	0.0059
$5_{2,3}$ - $4_{2,2}$	31958.3842	-0.0007	32610.5932	-0.0050	33249.0200	0.0070	33899.1606[a]	-0.0007
$6_{2,5}$ - $5_{2,4}$			32610.5740	-0.0036	33248.9988[a]	0.0021	33899.1328	-0.0021
$7_{2,5}$ - $6_{2,4}$			32611.6654	-0.0030			33900.1822	0.0013
$8_{2,7}$ - $7_{2,6}$					33249.4500	0.0028		
$9_{2,7}$ - $8_{2,6}$			32612.5040	0.0002	33250.8216	-0.0070		
$10_{2,9}$ - $9_{2,8}$			32611.2556	-0.0033	33249.6268[a]	-0.0013		
$11_{2,9}$ - $10_{2,8}$			32612.8455	-0.0044				
$12_{2,11}$ - $11_{2,10}$			32611.1826[a]	-0.0010	33249.5236	-0.0039		
$13_{2,11}$ - $12_{2,10}$			32612.5918	0-0007				

Table A.2 cont'd.

	Band X		(1,0,0)		(2,0,0)		(3,0,0)	
$J'_{KaKc} - J''_{KaKc}$	ν / cm^{-1}	o-c	ν / cm^{-1}	o-c	ν / cm^{-1}	o-c	ν / cm^{-1}	o-c
			$\Delta K = 0, K''_a = 3$					
$3_{3,0}$ - $4_{3,1}$			32604.3364	-0.0018	33242.7876	-0.0027	33892.9090	0.0085
$4_{3,2}$ - $5_{3,3}$							33892.3012[a]	0.0026
$5_{3,2}$ - $6_{3,3}$					33241.5894	-0.0010	33891.6938[a]	-0.0043
$6_{3,4}$ - $7_{3,5}$					33240.9296	0.0028	33891.0248[a]	-0.0054
$8_{3,6}$ - $9_{3,7}$							33889.6406	-0.0057
$3_{3,0}$ - $3_{3,1}$			32606.3964	0.0010	33244.8438	-0.0036	33894.9608	0.0032
$4_{3,2}$ - $4_{3,1}$			32606.3187	-0.0013	33244.7602	-0.0011	33894.8732	0.0034
$5_{3,2}$ - $5_{3,3}$			32606.2704[a]	-0.0029	33244.6909[a]	-0.0074	33894.8084	0.0024
$6_{3,4}$ - $6_{3,3}$			32606.1038	-0.0032			33894.6195	-0.0025
$7_{3,4}$ - $7_{3,5}$					33244.6242	-0.0052	33894.7330	-0.0042
$8_{3,6}$ - $8_{3,5}$			32605.7360	0.0064	33244.0980	-0.0056		
$9_{3,6}$ - $9_{3,7}$							33894.8732[a]	0.0000
$10_{3,8}$ - $10_{3,7}$			32605.0214[a]	-0.0051				
$4_{3,2}$ - $3_{3,1}$			32608.3826	0.0054	33246.8192	0.0007		
$5_{3,2}$ - $4_{3,1}$					33247.2650[a]	-0.0041	33897.3764	-0.0008
$6_{3,4}$ - $5_{3,3}$			32609.2160	0.0011			33897.7283	-0.0017
$7_{3,4}$ - $6_{3,3}$			32609.8497[a]	0.0065	33248.2208	-0.0004	33898.3234	-0.0056
$8_{3,6}$ - $7_{3,5}$			32609.9498[a]	0.0019	33248.3210	-0.0008	33898.4216[a]	0.0051
$9_{3,6}$ - $8_{3,5}$			32611.0044	-0.0016				
$10_{3,8}$ - $9_{3,7}$			32610.4960	0.0016				
$11_{3,8}$ - $10_{3,7}$			32612.1628[a]	0.0008	33250.4053	0.0021		

Table A.2 cont'd.

Band X			(1,0,0)		(2,0,0)		(3,0,0)	
$J'_{KaKc} - J''_{KaKc}$	ν / cm^{-1}	o-c	ν / cm^{-1}	o-c	ν / cm^{-1}	o-c	ν / cm^{-1}	o-c
			$\Delta K = 0, K''_a = 4$					
$4_{4,1}$ - $4_{4,0}$			32604.1412	-0.0018			33892.6371	-0.0050
$5_{4,1}$ - $5_{4,2}$			32604.0504	-0.0047	33242.4864	0.0004		
$7_{4,3}$ - $7_{4,4}$							33892.3012[a]	-0.0022
$9_{4,5}$ - $9_{4,6}$							33892.1096[a]	0.0029
$5_{4,1}$ - $4_{4,0}$			32606.6264	0.0022	33245.0492[a]	-0.0059	33895.1032[a]	-0.0045
$6_{4,3}$ - $5_{4,2}$			32607.0432	0.0038			33895.5011[a]	-0.0027
$7_{4,3}$ - $6_{4,2}$			32607.4668[a]	-0.0002				
$8_{4,5}$ - $7_{4,4}$			32607.8438	-0.0017	33246.2140[a]	-0.0029	33896.2614	0.0001
$11_{4,7}$ - $10_{4,6}$							33897.7661	-0.0007
$12_{4,9}$ - $11_{4,8}$			32609.2368	0.0050				
$13_{4,9}$ - $12_{4,8}$			32610.7744[a]	0.0075				
$14_{4,11}$ - $13_{4,10}$			32609.6446	0.0040				
			$\Delta K = 0, K''_a = 5$					
$5_{5,0}$ - $5_{5,1}$					33239.6898	0.0032		
$7_{5,2}$ - $6_{5,1}$			32604.6198	-0.0032				

Table A.2 cont'd.

	Band X		(1,0,0)		(2,0,0)		(3,0,0)	
$J'_{KaKc} - J''_{KaKc}$	ν / cm^{-1}	o-c	ν / cm^{-1}	o-c	ν / cm^{-1}	o-c	ν / cm^{-1}	o-c
			$\Delta K = 2, K''_a = 0$					
$8_{2,7}$ - $8_{0,8}$					33248.9304	-0.0011		
$9_{2,7}$ - $8_{0,8}$			32616.8216	0.0027				
			$\Delta K = 2, K''_a = 1$					
$5_{3,2}$ - $6_{1,5}$			32608.3034	-0.0019				
$6_{3,4}$ - $5_{1,5}$			32615.4826	0.0068				
$8_{3,6}$ - $7_{1,7}$			32616.7798	0.0037				
$9_{3,6}$ - $8_{1,7}$			32615.9702	-0.0037				
$11_{3,8}$ - $10_{1,9}$			32617.2350	0.0031				
			$\Delta K = 2, K''_a = 2$					
$5_{0,5}$ - $5_{2,4}$					33244.1600	-0.0022		
$7_{0,7}$ - $6_{2,4}$			32607.9987[a]	-0.0034				
$9_{4,5}$ - $10_{2,8}$			32606.0456	-0.0036				
$9_{4,5}$ - $8_{2,6}$			32616.3380	-0.0050				
$10_{4,7}$ - $9_{2,8}$			32617.4962	0.0067				
$11_{4,7}$ - $10_{2,8}$			32616.9820	-0.0013				
			$\Delta K = 2, K''_a = 3$					
$5_{1,4}$ - $4_{3,1}$			32606.0456	-0.0040				
$6_{1,6}$ - $5_{3,3}$			32604.7674[a]	-0.0046				
$7_{5,2}$ - $6_{3,3}$			32615.9702[a]	0.0002				
$10_{5,6}$ - $9_{3,7}$			32617.1124	0.0003				
			$\Delta K = 2, K''_a = 4$					
$11_{2,9}$ - $10_{4,6}$			32605.3248	-0.0067				

Table A.3: Assigned lines in the $^1B_2(v_1,0,0) \leftarrow {}^1A_1(0,0,0)$ transitions of $^{80}SeO_2$

	Band X		(1,0,0)		(2,0,0)		(3,0,0)	
$J'_{KaKc} - J''_{KaKc}$	ν / cm^{-1}	o-c	ν / cm^{-1}	o-c	ν / cm^{-1}	o-c	ν / cm^{-1}	o-c
			$\Delta K = 0, \quad K''_a = 0$					
$1_{0,1}$ - $2_{0,2}$	31955.9584	-0.0034	32607.1648	0.0053	33244.1200	-0.0006	33892.8484	0.0035
$3_{0,3}$ - $4_{0,4}$	31954.8153	-0.0008	32606.0206	0.0001	33242.9738	-0.0003	33891.6938	0.0022
$5_{0,5}$ - $6_{0,6}$	31953.4736	0.0016	32604.6861	0.0000	33241.6320	0.0007	33890.3398	0.0030
$7_{0,7}$ - $8_{0,8}$					33240.0776	0.0018	33888.7706	0.0010
$9_{0,9}$ - $10_{0,10}$					33238.3568	0.0013	33887.0310	0.0029
$1_{0,1}$ - $0_{0,0}$	31957.4908	-0.0001	32608.6892	0.0006	33245.6540	0.0044	33894.3710	-0.0030
$3_{0,3}$ - $2_{0,2}$	31958.3354	0.0063	32609.5316	-0.0018	33246.4875	0.0005	33895.2036	-0.0009
$5_{0,5}$ - $4_{0,4}$	31958.8552	-0.0036	32610.0754	0.0026	33247.0187	0.0006	33895.7198	-0.0037
$7_{0,7}$ - $6_{0,6}$			32610.3083	-0.0017	33247.2456	-0.0001	33895.9342	-0.0017
$9_{0,9}$ - $8_{0,8}$			32610.3414	-0.0061	33247.2654[a]	-0.0058	33895.9510	0.0072
$11_{0,11}$ - $10_{0,10}$			32610.2320	0.0030			33895.7961[a]	0.0057

[a] These transitions are overlapped, and make up less than 25 % of the total line intensity, and so were given a weight of zero in the fit

Table A.3 cont'd.

	Band X		(1,0,0)		(2,0,0)		(3,0,0)	
$J'_{KaKc} - J''_{KaKc}$	ν / cm^{-1}	o-c	ν / cm^{-1}	o-c	ν / cm^{-1}	o-c	ν / cm^{-1}	o-c
			$\Delta K = 0, K''_a = 1$					
$1_{1,0}$ - $2_{1,1}$			32606.7904	-0.0006	33243.7500	-0.0015	33892.4710	0.0022
$2_{1,2}$ - $3_{1,3}$	31955.5717	0.0063	32606.3644	0.0007	33243.3232	0.0001	33892.0413	0.0024
$3_{1,2}$ - $4_{1,3}$	31954.8641	-0.0015	32605.6478	0.0003	33242.5950	-0.0004	33891.3604	0.0019
$4_{1,4}$ - $5_{1,5}$	31954.3953	0.0013	32605.1702	-0.0010	33242.1206	-0.0025	33890.8329	0.0015
$5_{1,4}$ - $6_{1,5}$	31953.6599	-0.0018	32604.4096	0.0023	33241.3338	-0.0019	33890.0328	0.0032
$6_{1,6}$ - $7_{1,7}$	31953.0616	0.0040			33240.7430	-0.0020	33889.4422	0.0005
$7_{1,6}$ - $8_{1,7}$	31952.2422	0.0009			33239.8495	0.0009	33888.5181	-0.0012
$8_{1,8}$ - $9_{1,9}$					33239.1744	0.0026	33887.8542	0.0011
$9_{1,8}$ - $10_{1,9}$					33238.0314	0.0016	33886.6744	0.0029
$10_{1,10}$ - $11_{1,11}$					33237.4058	0.0014	33886.0668	0.0001
$1_{1,0}$ - $1_{1,1}$			32607.9472	-0.0015	33244.9100	0.0008	33893.6292	0.0027
$2_{1,2}$ - $2_{1,1}$	31956.7858	-0.0067	32607.5960	0.0052	33244.5494	-0.0008	33893.2686	0.0027
$3_{1,2}$ - $3_{1,3}$			32608.2240	0.0016	33245.1730	0.0028	33893.8820	0.0026
$4_{1,4}$ - $4_{1,3}$	31956.0982	0.0093						
$5_{1,4}$ - $5_{1,5}$	31957.8959	0.0020	32608.6416	0.0020			33894.2618	-0.0000
$6_{1,6}$ - $6_{1,5}$	31954.9453	-0.0037	32605.6938	-0.0005				
$2_{1,2}$ - $1_{1,1}$	31957.9437	-0.0065	32608.7522	0.0038	33245.7118	0.0039	33894.4144	-0.0092
$3_{1,2}$ - $2_{1,1}$	31958.6646	-0.0029	32609.4462	-0.0033	33246.3978	0.0005	33895.1032	-0.0033
$4_{1,4}$ - $3_{1,3}$	31958.6646	0.0009	32609.4462	0.0053	33246.3978	0.0050	33895.1032	0.0021
$5_{1,4}$ - $4_{1,3}$	31959.5950	0.0063	32610.3414	0.0070	33247.2654	0.0027	33895.9510	-0.0057
$6_{1,6}$ - $5_{1,5}$	31959.1778	-0.0034	32609.9290	0.0024	33246.8684	-0.0002	33895.5615	-0.0038
$7_{1,6}$ - $6_{1,5}$	31960.2114	-0.0046	32610.9175	0.0028	33247.8222	-0.0010	33896.4925	-0.0015
$8_{1,8}$ - $7_{1,7}$			32610.1880	-0.0004	33247.1180	-0.0007	33895.7961	-0.0040
$9_{1,8}$ - $8_{1,7}$			32611.0357	-0.0074	33247.9296	-0.0044	33896.5749	-0.0008
$10_{1,10}$ - $9_{1,9}$			32610.2320	-0.0028	33247.1500	-0.0017		
$11_{1,10}$ - $10_{1,9}$			32610.7744	-0.0051			33896.2614	-0.0001
$12_{1,12}$ - $11_{1,11}$			32610.0754[a]	-0.0065	33246.9840	0.0008		
$14_{1,14}$ - $13_{1,13}$			32609.7436	0.0018				

Table A.3 cont'd.

	Band X		(1,0,0)		(2,0,0)		(3,0,0)	
$J'_{KaKc} - J''_{KaKc}$	ν / cm^{-1}	o-c	ν / cm^{-1}	o-c	ν / cm^{-1}	o-c	ν / cm^{-1}	o-c
				$\Delta K = 0, K''_a = 2$				
$2_{2,1}$ - $3_{2,2}$	31954.6106	-0.0049	32605.3746	0.0036	33242.3282	-0.0008	33891.0248	0.0015
$3_{2,1}$ - $4_{2,2}$			32604.7972	-0.0004	33241.7467	-0.0010	33890.4392	0.0009
$4_{2,3}$ - $5_{2,4}$			32604.1958	-0.0002	33241.1395	-0.0015	33889.8266	0.0007
$5_{2,3}$ - $6_{2,4}$	31952.8351	0.0006			33240.5986	-0.0014	33889.2794	0.0008
$6_{2,5}$ - $7_{2,6}$					33239.8154	-0.0015	33888.4769	-0.0100
$7_{2,5}$ - $8_{2,6}$					33239.3943	0.0043	33888.0500	0.0019
$8_{2,7}$ - $9_{2,8}$					33238.3114	0.0048	33886.9580	0.0021
$9_{2,7}$ - $10_{2,8}$					33237.9650	0.0030	33886.5928	0.0034
$11_{2,9}$ - $12_{2,10}$							33884.7120	-0.0051
$2_{2,1}$ - $2_{2,0}$	31956.1440	-0.0006	32606.9079	0.0078	33243.8586	0.0005	33892.5520	-0.0004
$3_{2,1}$ - $3_{2,2}$	31956.1440	0.0065	32606.9079	-0.0021	33243.8586	-0.0016	33892.5520	0.0013
$4_{2,3}$ - $4_{2,2}$	31955.9426	0.0041	32606.6706	-0.0002	33243.6148	-0.0010	33892.3012	0.0005
$5_{2,3}$ - $5_{2,4}$	31956.1850	-0.0035			33243.9516	-0.0025	33892.6371	0.0045
$6_{2,5}$ - $6_{2,4}$			32606.1182	-0.0054	33243.0480	-0.0026	33891.7232	0.0026
$7_{2,5}$ - $7_{2,6}$							33892.8888[a]	0.0016
$8_{2,7}$ - $8_{2,6}$			32605.1112	0.0012			33890.6598	-0.0059
$3_{2,1}$ - $2_{2,0}$	31957.6678	0.0012	32608.4374	-0.0017	33245.3920	0.0027	33894.0788	-0.0010
$4_{2,3}$ - $3_{2,2}$	31958.0462	-0.0047	32608.7834	0.0002	33245.7306	0.0024	33894.4144	0.0012
$5_{2,3}$ - $4_{2,2}$	31958.6646	0.0013	32609.5064	0.0030	33246.4293	0.0004	33895.1032[a]	-0.0042
$6_{2,5}$ - $5_{2,4}$			32609.4772	-0.0005	33246.3987[a]	-0.0060	33895.0733	-0.0013
$7_{2,5}$ - $6_{2,4}$			32610.5740[a]	0.0030	33247.4644	0.0016	33896.1186	-0.0023
$8_{2,7}$ - $7_{2,6}$			32609.9498	0.0008	33246.8522	-0.0032	33895.5011	-0.0036
$9_{2,7}$ - $8_{2,6}$					33248.2507	-0.0020	33896.8798	-0.0003
$10_{2,9}$ - $9_{2,8}$			32610.1512	0.0016			33895.6550	-0.0026
$11_{2,9}$ - $10_{2,8}$			32611.7194	-0.0029	33248.5458	-0.0048		
$12_{2,11}$ - $11_{2,10}$			32610.0754[a]	0.0065				

Table A.3 cont'd.

	Band X		(1,0,0)		(2,0,0)		(3,0,0)	
$J'_{KaKc} - J''_{KaKc}$	ν / cm^{-1}	o-c	ν / cm^{-1}	o-c	ν / cm^{-1}	o-c	ν / cm^{-1}	o-c
				$\Delta K = 0, K''_a = 3$				
$3_{3,0}$ - $4_{3,1}$					33240.2072	-0.0006	33888.8606	-0.0033
$4_{3,2}$ - $5_{3,3}$					33239.6116	0.0011	33888.2592	-0.0021
$5_{3,2}$ - $6_{3,3}$					33239.0192	0.0037	33887.6574	-0.0029
$6_{3,4}$ - $7_{3,5}$					33238.3568	0.0024	33886.9922	0.0017
$7_{3,4}$ - $8_{3,5}$					33237.8550	0.0041	33886.4814	0.0012
$8_{3,6}$ - $9_{3,7}$					33236.9894	0.0027	33885.6044	0.0024
$9_{3,6}$ - $10_{3,7}$					33236.7572	0.0017		
$11_{3,9}$ - $12_{3,9}$							33884.1377	0.0026
$3_{3,0}$ - $3_{3,1}$			32605.3056	-0.0050	33242.2614	-0.0023	33890.9188	-0.0010
$4_{3,2}$ - $4_{3,1}$			32605.2352	-0.0001	33242.1796	-0.0004	33890.8329	0.0021
$5_{3,2}$ - $5_{3,3}$			32605.1854	-0.0045	33242.1206[a]	-0.0016	33890.7698	0.0028
$6_{3,4}$ - $6_{3,3}$			32605.0214	-0.0002	33241.9412	-0.0022	33890.5816	0.0021
$7_{3,4}$ - $7_{3,5}$			32605.1704[a]	-0.0026	33242.0646	-0.0052		
$8_{3,6}$ - $8_{3,5}$			32604.6377	-0.0024				
$9_{3,6}$ - $9_{3,7}$							33890.8329[a]	-0.0037
$4_{3,2}$ - $3_{3,1}$			32607.2980	0.0068	33244.2316	-0.0043	33892.8888	0.0021
$5_{3,2}$ - $4_{3,1}$			32607.7606	0.0012	33244.6914	-0.0004	33893.3378	0.0013
$6_{3,4}$ - $5_{3,3}$			32608.1280	-0.0003	33245.0492	-0.0009	33893.6876	0.0014
$7_{3,4}$ - $6_{3,3}$			32608.7626	0.0006	33245.6540	-0.0048	33894.2876	-0.0004
$8_{3,6}$ - $7_{3,5}$			32608.8628	0.0038	33245.7530	0.0017	33894.3710[a]	0.0045
$9_{3,6}$ - $8_{3,5}$			32609.9290[a]	0.0011	33246.7814	0.0059	33895.3778	-0.0046
$10_{3,8}$ - $9_{3,7}$			32609.4074	0.0071	33246.2596	-0.0003	33894.8486	0.0014
$11_{3,8}$ - $10_{3,7}$			32611.0732	-0.0038			33896.4448	0.0007
$12_{3,10}$ - $11_{3,9}$			32609.6696	0.0053	33246.4890[a]	-0.0015		
$13_{3,10}$ - $12_{3,9}$			32611.8584	0.0027	33248.6032	-0.0010		

Table A.3 cont'd.

	Band X		(1,0,0)		(2,0,0)		(3,0,0)	
$J'_{KaKc} - J''_{KaKc}$	ν / cm^{-1}	o-c	ν	/ cm^{-1} o-c	ν	/ cm^{-1} o-c	ν / cm^{-1}	o-c
				$\Delta K = 0, K''_a = 4$				
$4_{4,1}$ - $5_{4,2}$							33886.0562	0.0005
$5_{4,1}$ - $6_{4,2}$							33885.4320	-0.0017
$4_{4,1}$ - $4_{4,0}$					33240.0190	-0.0014	33888.6210	-0.0022
$5_{4,1}$ - $5_{4,2}$					33239.9221	-0.0000	33888.5181	-0.0003
$6_{4,3}$ - $6_{4,2}$							33888.3896	-0.0060
$5_{4,1}$ - $4_{4,0}$			32605.5508	-0.0026	33242.4864	-0.0032	33891.0872	0.0013
$6_{4,3}$ - $5_{4,2}$			32605.9697	0.0012	33242.8904	-0.0015	33891.4859	0.0055
$7_{4,3}$ - $6_{4,2}$			32606.3964	-0.0008	33243.3054	0.0015	33891.8812	-0.0026
$9_{4,5}$ - $8_{4,4}$			32607.2980	-0.0059			33892.7300	0.0039
$10_{4,7}$ - $9_{4,6}$			32607.5304	0.0034	33244.3750[a]	-0.0012		
$12_{4,9}$ - $11_{4,8}$			32608.1566	0.0009				
				$\Delta K = 0, K''_a = 5$				
$5_{5,0}$ - $5_{5,1}$							33885.6742	-0.0007
$6_{5,2}$ - $6_{5,1}$							33885.5454	-0.0013
$6_{5,2}$ - $5_{5,1}$							33888.6210[a]	-0.0061
$7_{5,2}$ - $6_{5,1}$					33240.4890	0.0060		
$8_{5,4}$ - $7_{5,3}$							33889.3648	0.0035
$9_{5,4}$ - $8_{5,3}$			32604.3582	0.0040				

Table A.3 cont'd.

	Band X		(1,0,0)		(2,0,0)		(3,0,0)	
$J'_{KaKc} - J''_{KaKc}$	ν / cm^{-1}	o-c	ν / cm^{-1}	o-c	ν / cm^{-1}	o-c	ν / cm^{-1}	o-c
			$\Delta K = 2, K''_a = 0$					
$5_{2,3}$ - $6_{0,6}$					33244.0000	-0.0037	33892.6840	0.0017
$9_{2,7}$ - $10_{0,10}$			32606.7904[a]	0.0002				
$2_{2,1}$ - $2_{0,2}$			32609.7308	-0.0023				
$5_{2,3}$ - $4_{0,4}$			32612.4580	-0.0070			33898.0648	-0.0042
$7_{2,5}$ - $6_{0,6}$			32613.9680	-0.0067	33250.8626	-0.0039	33899.5244	-0.0002
			$\Delta K = 2, K''_a = 1$					
$9_{3,6}$ - $10_{1,9}$			32604.9478	0.0065				
$5_{3,2}$ - $4_{1,3}$			32613.0874	-0.0072	33250.0252	-0.0018	33898.6694[a]	-0.0023
$7_{3,4}$ - $6_{1,5}$			32613.8398	-0.0066	33250.7432	0.0001		
$9_{3,6}$ - $8_{1,7}$			32614.8430	-0.0025				
			$\Delta K = 2, K''_a = 2$					
$5_{0,5}$ - $5_{2,4}$			32604.6382	0.0018				
$5_{0,5}$ - $4_{2,2}$			32607.1040	-0.0072				

Table A.4: Assigned lines in the $^1B_2(v_1,0,0) \leftarrow ^1A_1(0,0,0)$ transitions of $^{82}SeO_2$

	Band X		(1,0,0)		(2,0,0)		(3,0,0)	
$J'_{KaKc} - J''_{KaKc}$	ν / cm^{-1}	o-c	ν / cm^{-1}	o-c	ν / cm^{-1}	o-c	ν / cm^{-1}	o-c
				$\Delta K = 0, K''_a = 0$				
$1_{0,1}$ - $2_{0,2}$	31956.3899	0.0062			33241.6320[a]	-0.0048	33888.9654	0.0010
$3_{0,3}$ - $4_{0,4}$	31955.2278	0.0089			33240.4902	-0.0006	33887.8102	-0.0030
$5_{0,5}$ - $6_{0,6}$	31953.8932	0.0018			33239.1518	0.0042	33886.4600	-0.0007
$9_{0,9}$ - $10_{0,10}$							33883.1632	0.0015
$1_{0,1}$ - $0_{0,0}$	31957.9123	0.0007			33243.1658	0.0011	33890.4982	0.0059
$3_{0,3}$ - $2_{0,2}$	31958.7440	-0.0018			33244.0000	0.0001	33891.3217	-0.0006
$5_{0,5}$ - $4_{0,4}$	31959.2721	0.0020			33244.5258	-0.0005	33891.8400	0.0006
$7_{0,7}$ - $6_{0,6}$					33244.7530[a]	0.0032		

[a] These transitions are overlapped, and make up less than 25 % of the total line intensity, and so were given a weight of zero in the fit.

Table A.4 cont'd.

	Band X		(1,0,0)		(2,0,0)		(3,0,0)	
$J'_{KaKc} - J''_{KaKc}$	ν / cm^{-1}	o-c	ν / cm^{-1}	o-c	ν / cm^{-1}	o-c	ν / cm^{-1}	o-c
				$\Delta K = 0, K''_a = 1$				
$1_{1,0}$ - $2_{1,1}$					33241.2682	-0.0012	33888.5809	-0.0089
$2_{1,2}$ - $3_{1,3}$	31955.8764	-0.0027			33240.8426	0.0004	33888.1604	-0.0013
$3_{1,2}$ - $4_{1,3}$	31955.1668	-0.0090			33240.1118	-0.0017	33887.4279	0.0002
$4_{1,4}$ - $5_{1,5}$	31954.7074	0.0035			33239.6462	0.0034	33886.9580	0.0009
$5_{1,4}$ - $6_{1,5}$	31953.9674	0.0018			33238.8574	0.0046	33886.1542	-0.0008
$6_{1,6}$ - $7_{1,7}$					33238.2660	0.0014	33885.5670	-0.0037
$7_{1,6}$ - $8_{1,7}$	31952.5296	-0.0076						
$8_{1,8}$ - $9_{1,9}$							33883.9891	0.0029
$1_{1,0}$ - $1_{1,1}$					33242.4282	0.0011	33889.7513	0.0038
$3_{1,2}$ - $3_{1,3}$					33242.6798	-0.0098		
$4_{1,4}$ - $4_{1,3}$	31956.3899	-0.0022					33888.6382	-0.0071
$5_{1,4}$ - $5_{1,5}$							33890.3972	0.0069
$7_{1,6}$ - $7_{1,7}$	31958.6240	-0.0009						
$2_{1,2}$ - $1_{1,1}$	31958.5658	0.0047			33243.2238	-0.0004	33890.5414	-0.0023
$3_{1,2}$ - $2_{1,1}$	31958.9708	-0.0054			33243.9118	-0.0021	33891.2264	-0.0017
$4_{1,4}$ - $3_{1,3}$	31958.9708	0.0025			33243.9118	0.0047	33891.2264	0.0049
$5_{1,4}$ - $4_{1,3}$	31959.9032	0.0140					33892.0774	-0.0012
$6_{1,6}$ - $5_{1,5}$					33244.3750	-0.0048		
$7_{1,6}$ - $6_{1,5}$	31960.5062	0.0015					33892.6102	-0.0015
$8_{1,8}$ - $7_{1,7}$					33244.6242	-0.0018	33891.9210	-0.0003

Table A.4 cont'd.

	Band X		(1,0,0)		(2,0,0)		(3,0,0)	
$J'_{KaKc} - J''_{KaKc}$	ν / cm^{-1}	o-c	ν / cm^{-1}	o-c	ν / cm^{-1}	o-c	ν / cm^{-1}	o-c
				$\Delta K = 0, K''_a = 2$				
$2_{2,1}$ - $3_{2,2}$	31955.0554	0.0038					33887.1550	0.0034
$3_{2,1}$ - $4_{2,2}$	31954.4610	-0.0070					33886.5693	0.0013
$4_{2,3}$ - $5_{2,4}$							33885.9560	-0.0011
$5_{2,3}$ - $6_{2,4}$							33885.4118	-0.0008
$6_{2,5}$ - $7_{2,6}$							33884.6280	-0.0005
$7_{2,5}$ - $8_{2,6}$							33884.1892	0.0041
$9_{2,7}$ - $10_{2,8}$							33882.7214	-0.0028
$2_{2,1}$ - $2_{2,0}$	31956.5796	0.0001			33241.3828	0.0012	33888.6802	0.0007
$3_{2,1}$ - $3_{2,2}$	31956.5796	-0.0007			33241.3828	-0.0021	33888.6802	-0.0001
$4_{2,3}$ - $4_{2,2}$	31956.3899	-0.0036			33241.1395	0.0020		
$5_{2,3}$ - $5_{2,4}$	31956.6554	0.0021						
$3_{2,1}$ - $2_{2,0}$	31958.1104	0.0022			33242.9140	0.0011	33890.2106	0.0024
$4_{2,3}$ - $3_{2,2}$	31958.5099	0.0041			33243.2506	0.0008	33890.5414	0.0006
$5_{2,3}$ - $4_{2,2}$	31959.1238	-0.0009			33243.9516[a]	-0.0025		
$7_{2,5}$ - $6_{2,4}$							33892.2560	-0.0013
$9_{2,7}$ - $8_{2,6}$							33893.0105	-0.0013

Table A.4 cont'd.

	Band X		(1,0,0)		(2,0,0)		(3,0,0)	
$J'_{KaKc} - J''_{KaKc}$	ν / cm^{-1}	o-c	ν / cm^{-1}	o-c	ν / cm^{-1}	o-c	ν / cm^{-1}	o-c
				$\Delta K = 0, K''_a = 3$				
$6_{3,4}$ - $7_{3,5}$							33883.1322	-0.0039
$7_{3,4}$ - $8_{3,5}$							33882.6400	0.0068
$3_{3,0}$ - $3_{3,1}$					33239.7784^a	-0.0191	33887.0606	0.0026
$5_{3,2}$ - $5_{3,3}$					33239.6462^s	-0.0113	33886.9119	0.0019
$6_{3,4}$ - $6_{3,3}$							33886.7203	-0.0021
$4_{3,2}$ - $3_{3,1}$					33241.7676	-0.0009	33889.0234	-0.0017
$5_{3,2}$ - $4_{3,1}$							33889.4744	-0.0036
$6_{3,4}$ - $5_{3,3}$							33889.8178^a	-0.0101
$7_{3,4}$ - $6_{3,3}$							33890.4392^a	0.0002